THE EFFECT OF SCREENING PARAMETERS ON MISCIBLE AND IMMISCIBLE CO_2 EOR APPLICATIONS

A THESIS SUBMITTED TO
THE GRADUATE SCHOOL OF NATURAL AND APPLIED SCIENCES
OF
MIDDLE EAST TECHNICAL UNIVERSITY

BY

UMUT EFE ARSLAN

IN PARTIAL FULFILLMENT OF THE REQUIREMENTS
FOR
THE DEGREE OF MASTER OF SCIENCE
IN
PETROLEUM AND NATURAL GAS ENGINEERING

DECEMBER 2024

Approval of the thesis:

THE EFFECT OF SCREENING PARAMETERS ON MISCIBLE AND IMMISCIBLE CO_2 EOR APPLICATIONS

submitted by **UMUT EFE ARSLAN** in partial fulfillment of the requirements for the degree of **Master of Science** i**n Petroleum and Natural Gas Engineering, Middle East Technical University** by,

Prof. Dr. Naci Emre Altun
Dean, **Graduate School of Natural and Applied Sciences** _____

Assoc. Prof. Dr. İsmail Durgut
Head of the Department, **Petroleum and Natural Gas Eng.** _____

Assist. Prof. Dr. Mehmet Onur Doğan
Supervisor, **Petroleum and Natural Gas Eng., METU** _____

Examining Committee Members:

Assoc. Prof. Dr. Çağlar Sınayuç
Petroleum and Natural Gas Eng., METU _____

Assist. Prof. Dr. Mehmet Onur Doğan
Petroleum and Natural Gas Eng., METU _____

Assist. Prof. Dr. Selçuk Erol
Energy Systems Engineering, IZTECH _____

Date: 02.12.2024

I hereby declare that all information in this document has been obtained and presented in accordance with academic rules and ethical conduct. I also declare that, as required by these rules and conduct, I have fully cited and referenced all material and results that are not original to this work.

Name Last name : Umut Efe Arslan

Signature :

ABSTRACT

THE EFFECT OF SCREENING PARAMETERS ON MISCIBLE AND IMMISCIBLE CO_2 EOR APPLICATIONS

Arslan, Umut Efe
Master of Science, Petroleum and Natural Gas Engineering
Supervisor : Assist. Prof. Dr. Mehmet Onur Doğan

December 2024, 205 pages

CO_2 injection has been employed as an enhanced oil recovery (EOR) method for over 50 years and is classified into two types: miscible and immiscible. In miscible injection, CO_2 and reservoir fluid mix to form a single-phase fluid, whereas in immiscible injection, they do not. Achieving miscibility depends on the minimum miscibility pressure (MMP), the lowest pressure at which CO_2 completely mixes with reservoir oil at a given temperature. MMP is a critical design parameter for CO_2 injection, alongside API gravity, reservoir temperature, reservoir pressure, permeability, and porosity, which also play significant roles in determining the success of the process.

To evaluate the combined effects of these parameters, black oil simulations were conducted using five distinct oil samples with varying API gravities. MMP values were calculated through slim tube simulations and empirical correlations. Porosity and permeability effects were analyzed using Petrel's Uncertainty and Optimization tool for both miscible and immiscible scenarios. Pearson and Chatterjee correlations were implemented to porosity, permeability, and recovery factor data. Results indicated that both porosity and permeability negatively affect recovery factors, with porosity having a greater influence in miscible runs, while permeability is more

significant in immiscible runs. Furthermore, sensitivity analyses were performed on reservoir temperature and pressure for one fluid sample. These analyses revealed that pressure negatively impacts recovery factors in immiscible cases and positively impacts miscible cases, while temperature has the opposite effect, showing positive influence in immiscible runs and negative influence in miscible runs.

Keywords: Carbon Dioxide, Screening, Minimum Miscibility Pressure (MMP), Miscible, Immiscible

ÖZ

GELİŞTİRİLMİŞ PETROL KURTARIM YÖNTEMLERİNDEN OLAN KARIŞABİLİR VE KARIŞAMAYAN CO_2 UYGULAMALARINDA FİLTRELEME PARAMETRELERİNİN ETKİLERİ

Arslan, Umut Efe
Yüksek Lisans, Petrol ve Doğal gaz Mühendisliği
Tez Yöneticisi: Dr. Ögr. Üyesi Mehmet Onur Doğan

Aralık 2024, 205 sayfa

CO_2 enjeksiyonu, 50 yılı aşkın süredir geliştirilmiş petrol kurtarımı (EOR) yöntemi olarak uygulanmaktadır. CO_2 enjeksiyonu karışabilir (miscible) ve karışamayan (immiscible) olarak ikiye ayrılmaktadır. Karışabilir enjeksiyonlarda, CO_2 ve rezervuar sıvısı birlikte tek fazlı bir akışkan oluştururlar; lakin, karışamayan enjeksiyonlarda bu gerçekleşmez. Karışımın oluşumu en düşük karışabilirlik basıncına (EDKB) bağlıdır. Belirli bir rezervuar sıcaklığında karbon dioksitin rezervuar petrolü ile tamamen karışabildiği en düşük basınca, en düşük karışabilirlik basıncı denir. Bu sebeple EDKB, CO_2 enjeksiyonu metodu tasarımlarında kritik bir değişkendir. EDKB'nin yanı sıra, petrolün API cinsinden ağırlığı, rezervuarın sıcaklığı, petrolün viskozitesi, geçirgenlik ve gözeneklilik değerleri de CO_2 enjeksiyonu projelerinde önemli rol oynayan faktörlerdir.

Bu parametrelerin birleşik etkilerini değerlendirmek için farklı API gravitesine sahip beş petrol örneği kullanılarak kompozisyonel olmayan rezervuar simülasyonları yapılmıştır. EDKB değerleri ince tüp (slim tube) simulasyonları ve ampirik korelasyonlarla hesaplanmıştır. Gözeneklilik ve geçirgenlik etkileri her bir sıvı örneği ve her iki enjeksiyon senaryosu için Petrel programının "Uncertainty and

Optimization" aracı ile analiz edilmiştir. Sonrasında Pearson ve Chatterjee korelasyon hesaplama yaklaşımları gözeneklilik, geçirgenlik ve kurtarım faktörü verilerine uygulanmıştır. Hem gözeneklilik hem de geçirgenlik iki senaryoda da negatif etki göstermiştir. Bunun yanında gözeneklilik karışabilen senaryoda daha baskın etki gösterirken geçirgenlik karışamayan senaryoda daha çok etki eden değişken olmuştur.

Bunlara ek olarak bir sıvı örneğinde rezervuar sıcaklığı ve basıncı için hassasiyet analizi yapılmıştır. Bu analizler, rezervuar basıncının karışamayan durumlarda kurtarım faktörünü olumsuz, karışabilen senaryoda ise olumlu etkiledğini; rezervuar sıcaklığının ise bunun tam tersi olacak şekilde karışamayan durumda pozitif, karışabilen durumda negatif etkiye sahip olduğunu göstermiştir.

Anahtar Kelimeler: Karbon Dioksit, Filtreleme, En Düşük Karışabilirlik Basıncı, Karışabilen, Karışamayan

All that is gold does not glitter

ACKNOWLEDGMENTS

I would like to thank my supervisor Assist. Prof. Dr. Mehmet Onur Doğan for his support, advice, and guidance throughout this study.

I would also like to thank Assoc. Prof. Dr. Çağlar Sınayuç and Assist. Prof. Dr. Selçuk Erol for their valuable recommendations and their involvement in my examining committee.

I extend my deepest gratitude to my beloved parents, Feriha and Orhan Arslan, who unwaveringly supported me in every step of this research and believed in me; without their great support, I would not be here today.

TABLE OF CONTENTS

LIST OF TABLES

TABLES

LIST OF FIGURES

FIGURES

LIST OF ABBREVIATIONS

ABBREVIATIONS

EOR	Enhanced Oil Recovery
FCM	First Contact Miscibility
MCM	Multi Contact Miscibility
ASP	Alkali-Surfactant-Polymer Flooding
SAGD	Steam-Assisted Gravity Drainage
IFT	Interfacial Tension
MMP	Minimum Miscibility Pressure
WAG	Water Alternating Gas
E300	Eclipse 300
E100	Eclipse 100
EVP	Extrapolated Vapor Pressure
GA	Genetic Algorithm
MW	Molecular Weight
ACE	Alternating Conditional Expectations
SWFN	Water Saturation Functions
SGFN	Gas saturation functions
SOF3	Oil saturation functions (three-phase)
SOF2	Oil saturation functions (two-phase)
SDENSITY	Miscible gas density at surface conditions

PMISC	Pressure-dependent miscibility tables
TLMIXPAR	Todd-Longstaff mixing parameter
U & O	Uncertainty and Optimization Tool
RF	Recovery Factor

CHAPTER 1

INTRODUCTION

The global demand for oil and natural gas continues to rise (BP, 2024) (Energy Institute, 2024). Additionally, many of the major oil fields are aging. Therefore, enhanced oil recovery (EOR) is a hot topic in the petroleum industry, now. One of the primary methods of EOR is CO_2 flooding in miscible or immiscible conditions. The first immiscible CO_2 flooding test was conducted in the Ritchie Field, USA, in 1968, followed by the first commercial production in the Kelly-Snyder Oilfield, Texas, in 1972 (Liu, et al., 2020). In 1973, the first miscible CO_2 injection test was carried out in Little Creek Oilfield in United States (Liu, et al., 2020) (Koottungal, 2014). Following these pioneering applications in the United States, other countries, including Brazil, Canada, Malasia and Türkiye, adopted carbon dioxide injection to enhance and maintain production (Koottungal, 2014) (Zhang, Wei, & Bai, 2017). Today, carbon dioxide injection is the leading enhanced oil recovery technique in the world.

In the miscible CO_2 injection case, carbon dioxide can create a mixing with reservoir oil, which improves the effect of CO_2 injection since oil viscosity and interfacial tension (IFT) will reduce. Moreover, the dissolution of carbon dioxide within reservoir oil causes the oil swelling (Zhang, Yin, Wei, & Bai, 2019a). In the immiscible CO_2 injection case, carbon dioxide cannot form a mixture with reservoir oil. However, oil viscosity and interfacial tension reduction have occurred but not as high as in miscible condition (Zhang, Wei, & Bai, 2018a).

Since the 70s, “go” or “no-go” type screening criteria have been developed and widely implemented for various enhanced oil recovery (EOR) techniques. Some of the best-known screening criteria are for carbon dioxide flooding: (National Petroleum Council (NPC), 1976), (Geffen, 1977) (Brashear & Kuuskra, 1978)

(Iyoho, 1978), (OTA, 1978), (Carcoana, 1982), (Taber & Martin, 1983), (Taber, Martin, & Seright, 1997a), (Taber, Martin, & Seright, 1997b), (Al Adasani & Bai, 2011), (Bourdarot & Ghedan, 2011), (Zhang, Wei, & Bai, 2018a), (Zhang, Yin, Wei, & Bai, 2019a). According to these studies, API gravity, oil viscosity, oil composition, oil saturation before the treatment, formation type, porosity, net thickness, average permeability, depth, reservoir temperature and reservoir pressure were introduced as screening criteria for an enhance oil recovery projects.

From the mid-1980s onward, machine learning techniques were also utilized in the development of EOR screening criteria. Guerillot (1988) introduced an Expert System (ES) using fuzzy logic for EOR screening. Similarly, Gharbi (2000) and Moreno, Gürpınar, Liu, Al-Kinani, & Çakır (2014) put forward an Expert System for selecting and designing EOR processes. Surguchev and Li (2000) proposed an EOR screening method based on artificial neural networks (ANN), while Parada and Ertekin (2012) utilized ANN algorithms to identify suitable EOR methods. Alvarado et al. (2002) employed clustering and rule extraction techniques for EOR screening. Zhang et al. (2019b) combining conventional screening methods and the random forest algorithm for EOR screening. Additionally, Sun and Ertekin (2020) developed a polymer flooding screening and optimization method with help of ANN and particle swarm optimization.

Minimum Miscibility Pressure (MMP) is the lowest pressure at which a gas, such as CO_2, becomes completely miscible with the reservoir oil, allowing them to mix without forming an interface and continuing to flow as one-phase (Alston, Kokolis, & James, 1985) (Zhang, Wei, & Bai, 2018a) (Dindoruk, Johns, & Orr Jr., 2020). At this pressure, the injected gas effectively reduces oil viscosity, swells the oil, and mobilizes it for improved recovery (Gao, Towler, & Pan, 2010). Achieving MMP is crucial for the success of miscible gas injection in enhanced oil recovery (EOR). If the reservoir pressure is higher than the MMP, the injection case continues as miscible. Otherwise, injection is immiscible. Thus, minimum miscibility pressure is the key factor when designing a CO_2 injection project.

Miscibility can occur as either First Contact Miscibility (FCM) or Multi-Contact Miscibility (MCM) (Hamdi & Awang, 2014) (Dindoruk, Johns, & Orr Jr., 2020). FCM takes place when gas and oil become miscible immediately upon contact at the Minimum Miscibility Pressure (MMP); however, this is rare in real reservoirs due to the presence of heavy oil components. In contrast, MCM occurs through repeated interactions between the injected gas and reservoir oil (Dindoruk, Johns, & Orr Jr., 2020). This process can involve either a condensing gas drive, where heavy hydrocarbons condense from the gas into the oil phase to enrich the oil, or a vaporizing gas drive, where the gas vaporizes intermediate hydrocarbons from the oil phase to enrich itself (Stalkup Jr, 1983) (Neau, Avaullée, & Jaubert, 1996) (Saini, 2019). Most commercially viable miscible CO_2 EOR projects utilize MCM conditions (Alston, Kokolis, & James, 1985).

Experimental and computational methods are used in the literature to obtain the MMP (Delforouz, Movaghar, & Shariaty, 2019). For instance, the slim tube experiment is one of the experimental methods, and slim tube simulation and empirical correlations are some typical computational methods (Amao, Siddiqui, Menouar, & L., 2012).

The slim tube experiment is frequently used method to find minimum miscibility pressure. It is a synthetic apparatus designed to mimic the porous media of a reservoir. The length of a conventional slim tube is 80 ft (Adel, Tovar, & Schechter, 2016). With a small diameter, typically up to 0.6 inches, it is filled with glass beads or sand to simulate porous and permeable zones. This testing method is commonly conducted under conditions of high porosity and permeability (Dindoruk, Johns, & Orr Jr., 2020). The standard procedure involves injecting 1.2 pore volumes of gas into the slim tube and measuring the recovery factor. This process is repeated at various pressures, and the resulting recovery factors are plotted against the pressures to generate two curves. The intersection point of these two curves are labeled as minimum miscibility pressure (Aleidan & Mamora, 2011) (Jaferi, Ashoori, & MK, 2019). However, the slim tube test needed to much time to do the test properly. To shorten the time, Adel, Tovar, & Schechter (2016) reduced the length of the slim

tube to 20 ft. They said that a test with four pressure values took 481 hours with a normal slim tube; moreover, four points are not enough to control the test reliability. When they did the test using a 20 ft long slim tube, the test approximately takes half the time (234 hours) with six pressure values. The obtained MMP value was not significantly different from the 80 ft slim tube test. Moreover, the authors also utilized slim tube simulation, where the length is 40 ft, to control at 12 pressure points the outcomes of experiments and they found out that the results are close each other (Adel, Tovar, & Schechter, 2016). Consequently, the physical slim tube experiment is time and money consuming because it takes too much time and required apparatus; however, slim tube simulation does the same calculation within seconds. In addition, Vulin, Gaćina, & Biličić (2018) compared their slim tube experiment and slim tube simulation results with real field data, which is in Croatia, and they obtained approximate values. Therefore, slim tube simulations could be used instead of physical tests.

Slim tube simulations should be performed on compositional simulators as a 1-D flow and applied following the procedure, which is suggested by Stalkup Jr (1984). The author posits that 1.2 pore volume gas should be injected into the simulated slim tube, then extrapolating the simulation results, which are recovery factors at pressure values, to where the grid numbers are infinite for dispersion-free results because dispersion may affect outcomes, such as, obtaining higher recovery factors as a result. Therefore, the slim tube simulation should be executed at various grid numbers in order to extrapolate their outputs to infinite grid numbers (Stalkup Jr., 1984). Stalkup proposed using $1/N^{0.5}$ for extrapolation of recovery factors, where N is number of grid blocks (Orr Jr. & Jessen, 2007). After that, Høier and Whitson (1998) utilized the same procedure in their calculation. Moreover, Jaubert, Wolff, Neau, & Avaullee (1998) were also used the same procedure during comparing 1-D simulation with other methods in their articles. Yan, Michlesen, & Stenby (2012) were recommended a simulation run with N grid blocks inherently provides results for any M grid blocks ($M<N$) by scaling appropriately. For instance, recovery at 1.2 pore volume injection (PVI) for M blocks can be calculated using the first M blocks

at 1.2M/N PVI. Thus, a single simulation can yield recoveries for different grid block counts for extrapolation.

Empirical correlations are other computational methods to decide MMP value. Benham, Dowden, & Kunzman (1960) created early foundation for subsequent work in empirical miscibility correlations. Afterward, Holm and Josendal (1974) used Benham, Dowden, & Kunzman findings to plot a graph for temperature, pressure and molecular weight as correlations. Cronquist (1978) posits one of the first formulation type emperical correlation to obtain MMP as an function of mole fraction of CH_4, temperature and molecular weight of C_{5+}. Then, Mungan (1981) extended Holm and Josendal's graph with more molecular weight curves. Lee (1979) calculated MMP solely as a function of temperature. Like Lee, Yellig – Metcalfe (1980) and Orr – Jensen (1984) used temperature only to computed MMP. Moreover, Yellig – Metcalfe (1980) suggested that when the result is lower than the bubble point pressure, the bubble point pressure accepted as MMP. Subsequent, Glasø (1985) were utilised reservoir temperature, the molecular weight of the C7+ fraction of reservoir oil, and the mole fraction of intermediate components (C2–C6) into the correlation equations. In addition, Glasø applied a correction for the molecular weight of C7+ using the Watson characterization factor (K factor). The K factor, which ranges from 10 (indicating highly aromatic oil) to 13 (indicating highly paraffinic oil), was adjusted for values of 11.95 or higher to account for the paraffinicity of the oil. Later, Alston, Kokolis, and James (1985), firstly, determined that which parametres have effects on MMP value. Subsequently, reservoir temperature, C_{5+} molecular weight, mole fraction of volatile and intermediate components are used as parameters in their equation. Furthermore, they proposed that when the bubble point pressure is less than 50 psi (0.35 MPa), mole fraction of volatile and intermediate components should not be considered in calculations. Emera and Sarma (2004) practiced genetic algorithms, which is an artificial intelligence technique. They modified the correlation of Alston, Kokolis, and James with new data. Next, Yuan, Johns, Egwuenu, & Dindoruk (2004) created a correlation took into account the analytical solution results. Afterwards, Shokir

(2007) performed alternating conditional expectations (ACE) algorithm to found empirical correlation. Further, Shokir practiced sensitivity analysis to figure out the influence of the parameters on MMP values. Similar to Emera and Sarma (2004), Li, Qin, and Yang (2012) rewrite the correlation of Alston, Kokolis, and James using new data.

The purpose of this thesis is to conduct black oil simulations for both miscible and immiscible CO_2 injection scenarios. Through uncertainty runs, the study aims to evaluate the impact of various screening parameters on the recovery factor. To represent a wide range of API gravities, five distinct fluid samples were selected. Reservoir temperature, pressure, oil viscosity, and API gravity were varied for each sample. Minimum miscibility pressure of each samples were computed aformentioned methods. Additionally, porosity and permeability were identified as uncertain screening parameters. The combined effects of these parameters on the recovery factor were evaluated through uncertainty analyses. Sensitivity analyses were performed on reservoir pressure and temperature using one of the fluid samples to evaluate their impact on the recovery factor. Subsequently, Pearson, Spearman Rank, and Chatterjee Rank Correlations were applied to determine the relationships between the parameters and the recovery factor for both miscible and immiscible cases. During this study, PVTi, Eclipse 300, Eclipse 100, Petrel, Uncertainty & Optimization Tool (U&O) of Petrel and MATLAB were used.

CHAPTER 2

LITERATURE REVIEW

2.1 Hydrocarbon Recovery Mechanisms

The hydrocarbon recovery process could be subdivided into three phases, which are named primary, secondary, and tertiary recovery. The primary recovery period starts with the first day of production. During the primary recovery period, oil production depends on natural energy of the reservoir itself. The natural energy of the reservoir is named drive, and there are five different drive mechanisms exist, which are gas cap, solution gas, water, rock and fluid expansion and gravity drive. Artificial lifts may help production during primary recovery. The reservoir pressure (natural energy) will be depleted because of continuous production. To maintain reservoir pressure, water or gas is injected into the reservoir as an additional energy source. The secondary recovery process begins after injecting water or gas into the reservoir.

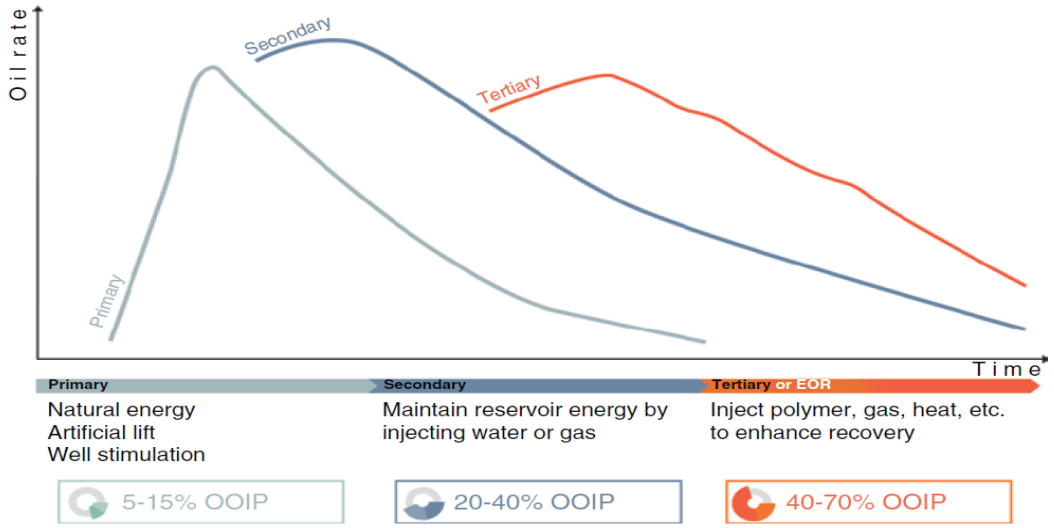

Figure 2.1. Hydrocarbon recovery mechanism (Thomas, 2019)

Tertiary recovery starts when secondary recovery is not economically feasible. It covers every other supplemental method. Tertiary recovery is also referred to as enhanced oil recovery and is divided into four main categories: thermal, chemical, gas flooding, and microbial.

2.2 Enhanced Oil Recovery (EOR)

Enhanced oil recovery is intended to change the overall displacement efficiency of fluid in the reservoir in a positive way. Overall displacement efficiency represents the ratio of the amount of oil displaced and amount of oil in initial state. Displacement efficiency can also be represented as the product of microscopic, areal, and vertical displacement efficiencies. Furthermore, the multiplication of areal and vertical displacement efficiencies is volumetric displacement efficiency, also known as macroscopic displacement efficiency.

$$E = \frac{Amount\ of\ oil\ displaced}{Amount\ of\ oil\ in\ initial\ state} \tag{2.1}$$

$$E = E_D E_A E_I \tag{2.2}$$

$$E_V = E_A E_I \tag{2.3}$$

where:

E = Overall displacement efficiency,

E_D = Microscopic displacement efficiency,

E_A = Areal displacement efficiency,

E_I = Vertical displacement efficiency,

E_V = Volumetric (macroscopic) displacement efficiency (Sehbi, Frailey, & Lawal, 2001).

The effectiveness of displacing fluids contacting the reservoir both vertically and areally represents macroscopic displacement efficiency. It is affected by the

geometry of injection and production well pattern, reservoir heterogeneities and fluid properties differences of the displacing and reservoir fluids (Ghedan, 2009) (Green & Willhite, 2018).

Microscopic displacement efficiency is a measure of effectiveness of injectant to transportation the oil from porous media. It is affected by reservoir pressure, reservoir temperature, oil composition, phase behavior, fluid properties, saturation history of rock-fluid system, diffusion, solvent flow rate slug size, dispersion, dead-end pore volume, rock pore geometry and pore structure (Sehbi, Frailey, & Lawal, 2001).

Enhanced oil recovery (EOR) is often mentioned as tertiary recovery, but it does not always utilize as the third scenario to produce oil from the reservoir. In heavy oil reservoirs, for example, oil is highly viscous, and primary production may not be applicable since the natural energy of the reservoir is not powerful enough to support production. Moreover, secondary recovery methods, such as waterflooding, might not be effective to produce heavy oil. Thus, thermal methods, which are reckoned as enhanced oil recovery methods, may be used in the first place in order to produce heavy oil with feasible conditions (Green & Willhite, 2018). Consequently, the EOR methods may be used on the first day of production.

2.3 Types of EOR

Enhanced oil recovery is sectionalized into four categories: chemical, thermal, microbial and gas flooding, which can be seen in Figure 2.2. Likewise, these categories are divided into themselves.

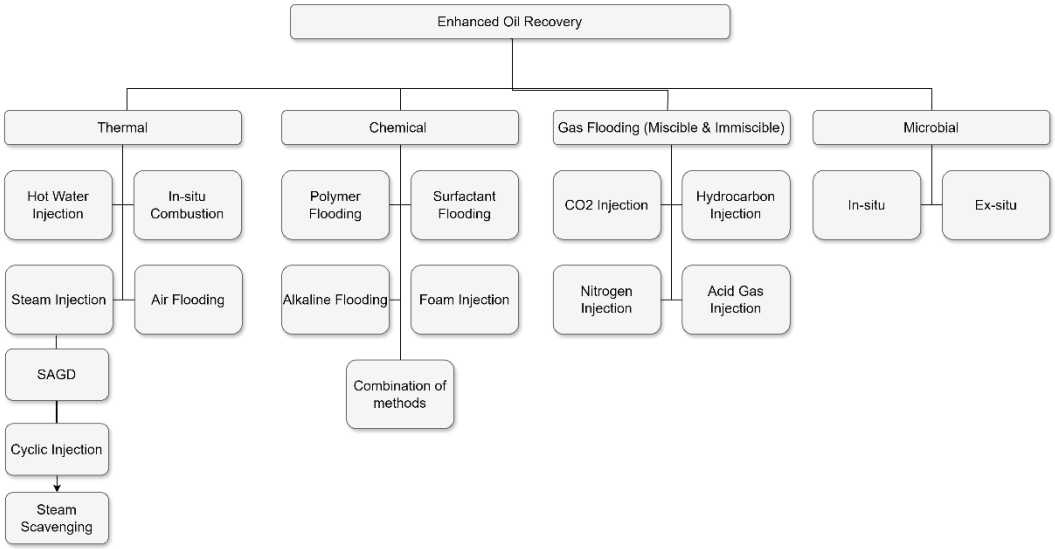

Figure 2.2. EOR method's classification

2.3.1 Chemical EOR

Polymer, surfactant, alkaline flooding, foam, and their combinations are grouped as chemical methods. These chemicals are generally used with water except foams. It is practiced with gas. Polymer flooding is targeted to increase the viscosity of water and improve the sweep efficiency. Surfactant flooding aims to reduce interfacial tension (IFT) between oil and water. Alkaline flooding is used for creating a chemical reaction with oil, water, and reservoir rocks in order to reduce the IFT. Surfactants are formed in-situ as a result of these reactions. Foams are utilized to reduce gas mobility in gas flooding process (Sheng, 2013a) (Thomas, 2019) (Green & Willhite, 2018).

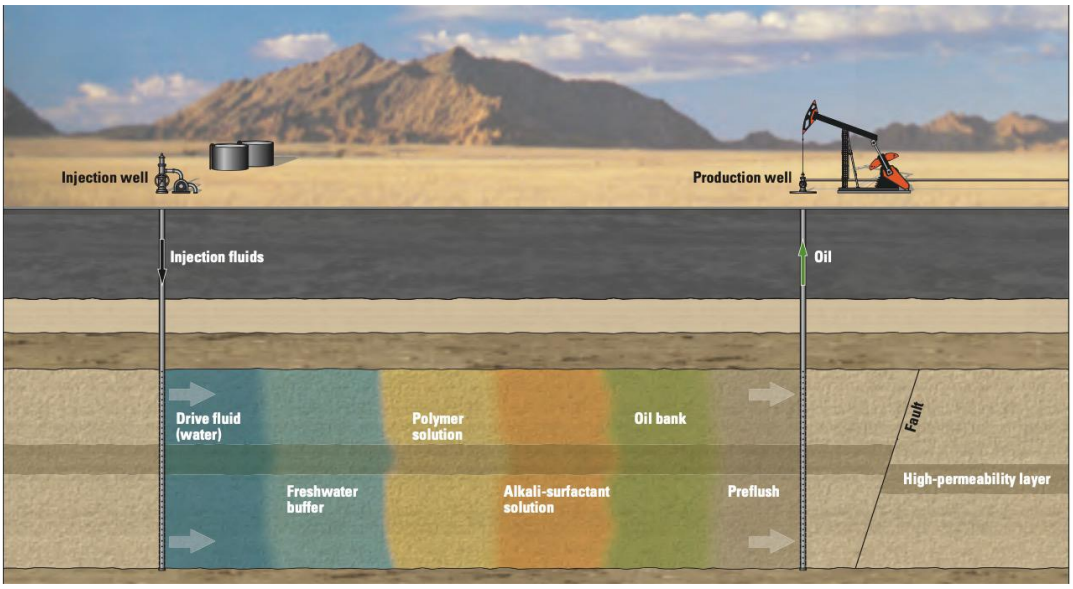

Figure 2.3. Example chemical method diagram: alkali-surfactant-polymer (ASP) flooding (Al-Mjeni, et al., 2010)

2.3.2 Thermal EOR

The main objective of thermal EOR techniques is to increase the temperature inside the reservoir in order to reduce oil viscosity and density. This method is mainly practiced in heavy oil reservoirs. Thermal methods include steam injection, hot water injection, air flooding and in situ combustion. According to data at Koottungal (2014), nearly %90 of the thermal EOR applications is steam injection. The steam injection reduced the oil viscosity but also boosted the reservoir pressure. Hot water injection also decreases the oil viscosity; nevertheless, it is rarely applied because of high heat loss during the injection. Some part of the oil in the reservoir is burned near to the injected well to create thermal energy. Afterward, this energy propagates inside the reservoir, and air or oxygen is injected into the reservoir to continue to combustion and displace combustion zone. Furthermore, air injection helps pressure maintenance (Dai, You, Zhao, Zhao, & Zhao, 2023) (Turta, 2013). These processes are called in situ combustion method. In consequence of in situ combustion, oil viscosity is reduced, and some light oil is generated in reservoir. In this study, steam-

assisted gravity drainage (SAGD), cyclic steam injection (CSI), and steam scavenging techniques are considered as steam injection.

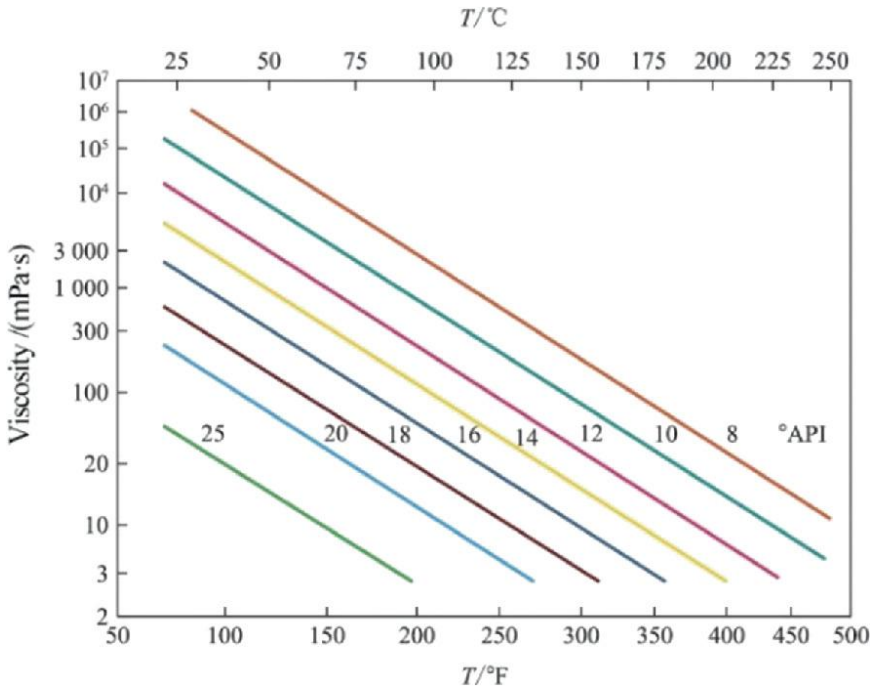

Figure 2.4. Relationship between viscosity, crude oil API, and temperature (Dai, You, Zhao, Zhao, & Zhao, 2023)

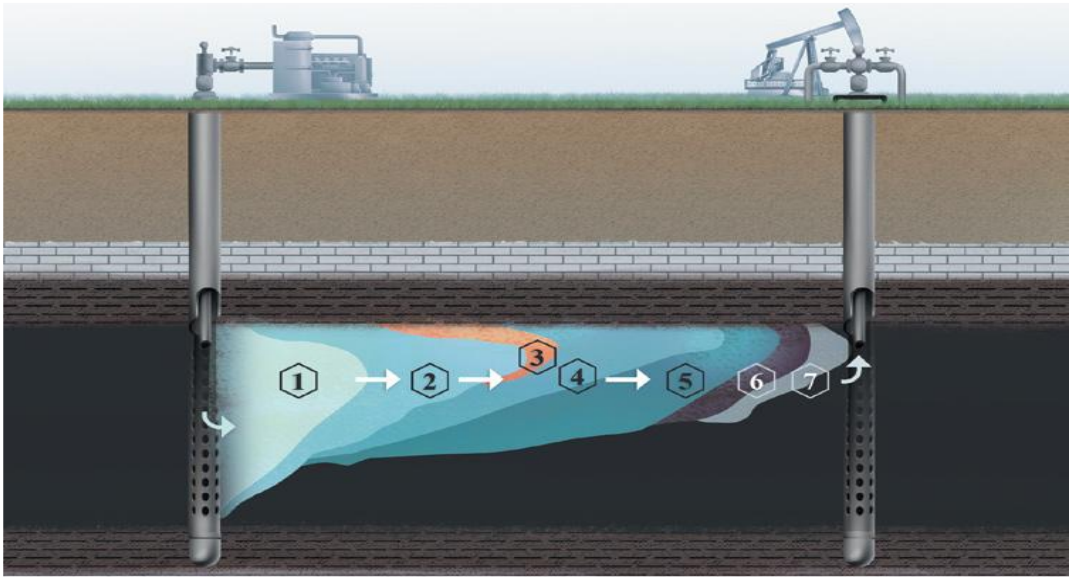

Figure 2.5. Example thermal method diagram: in situ combustion (Thomas, 2019)

2.3.3 Microbial EOR

The microbial EOR (MEOR) can be divided into two sections based on the preparation place of microbial products, which are in-situ and ex-situ of the reservoir. The ex-situ MEOR process is akin to chemical EOR. On the other hand, the reactions occur in the reservoir in the in-situ MEOR process. According to the type of microbial products, such effects may happen during MEOR, increasing reservoir pressure, reducing oil viscosity, improving permeability by dissolving carbonate precipitates, and reducing IFT (Sheng, 2013b).

2.3.4 Gas Flooding

Gas flooding involves the injection of acid gas, carbon dioxide, nitrogen, and hydrocarbon. Acid gas is a mixture of CO_2 and H_2S. The favorable effect of injecting acid gas is assisting in disposal of H_2S and CO_2. In addition, H_2S can reduce the MMP because of forming an impurity (Alston, Kokolis, & James, 1985). It also helps to reduce viscosity of oil and boosting the mobility (Kanakaki, et al., 2023).

Nitrogen is one of the most abundant gases in the world because of that it is cheaper than the other injected gases. Therefore, it can be injected in large volumes. Additionally, N_2 has no corrosive effect on tubing. Nitrogen assists the recovery via reducing viscosity and oil swelling. On the other side, nitrogen requires high pressure to achieve miscible conditions due to the inert nature of N_2. Nitrogen injection to the deep reservoir may reach a miscible state (Hassan, Azad, & Mahmoud, 2023). Nitrogen flooding forms a gas drive in the reservoir to support production (Taber, Martin, & Seright, 1997b).

Hydrocarbon injection means that light hydrocarbon gases flooding into the reservoir. LPG injection is also considered as hydrocarbon injection method. The main aims of the hydrocarbon injection are oil swelling, decreasing oil viscosity (Dai, You, Zhao, Zhao, & Zhao, 2023).

Gas injection methods can be miscible or immiscible. The miscibility condition of a gas injection process can be checked by calculating minimum miscibility pressure (MMP) before implementing the injection. If the reservoir pressure is higher than the MMP, the flooding will be miscible if not it will be immiscible. In miscible gas injection cases, the injected gas forms a mixing with reservoir oil, then they act as one phase fluid. On the other hand, the gas in immiscible injection cases cannot create a mixing with reservoir crude oil.

2.3.4.1 Carbon Dioxide Flooding

As mentioned above, gas injections can be divided into immiscible and miscible injections. Carbon dioxide could be used in both types of injection as EOR methods. To reach miscible condition, CO_2 required less pressure than other gas flooding methods. The main objectives of miscible CO_2 injection are that oil viscosity and interfacial tension (IFT) reduction because of dissolution of carbon dioxide within reservoir oil, which cause oil swelling (Zhang, Yin, Wei, & Bai, 2019a). Then again, oil swelling occurs during the immiscible CO_2 injection, which causes a decrease in oil viscosity, but not as high as miscible flooding one. Moreover, CO_2 aids to pressure maintenance in immiscible flooding (Zhang, Wei, & Bai, 2018a). Hence, miscible carbon dioxide injection is more beneficial than the immiscible one. However, the benefit of the immiscible injection should not be underestimated.

Three different CO_2 injection methods are mainly used in industry. These are continuous injection, cyclic injection (huff ‘n’ puff), water alternating gas injection (WAG). In the continuous injection method, as its name signifies, the injection well continuously injects CO_2 into the reservoir. During the injection, the oil production continues from production wells.

The cyclic injection (huff ‘n’ puff) method is applied with single well. Firstly, the well injected CO_2 into the formations. Then, the well is shut in to wait soaking of the CO_2 into the formations. After the soaking period, the well starts producing. The

injection, soaking and production process may be repeated (National Petroleum Council (NPC), 2021).

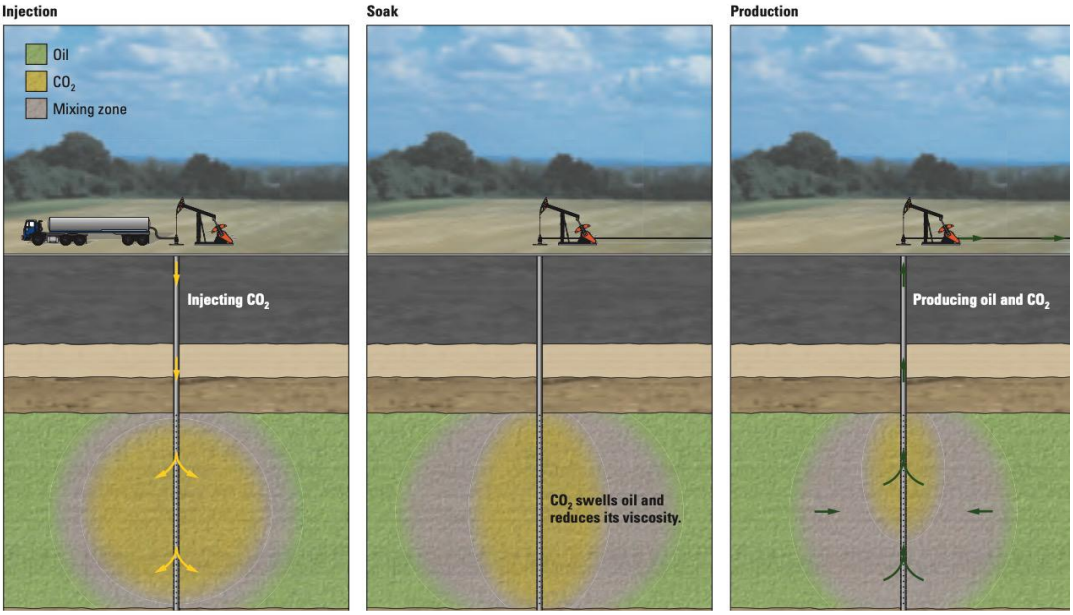

Figure 2.6. Cyclic gas injection (huff ‘n’ puff) (Al-Mjeni, et al., 2010)

In the water alternating gas (WAG) injection method, water and gas injected in turn. This method synthesizes the power of water injection and gas injection. Water is injected to avert early gas breakthrough and viscous fingering. Plus, water boosts sweep efficiency in the reservoir (Johns & Dindoruk, 2013).

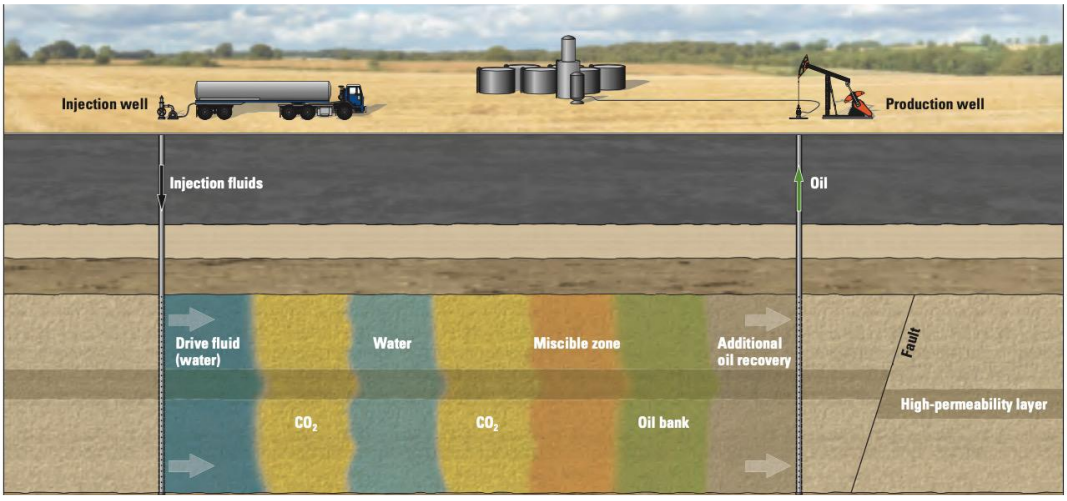

Figure 2.7. Miscible water alternating gas injection (WAG) (Al-Mjeni, et al., 2010)

2.4 Current Situation of EOR

Oil and Gas Journal (OGJ) had been reporting biennial surveys, Worldwide EOR Survey, in order to track current EOR projects. The journal published these surveys from 1974 through 2014. It incorporates country, operator, and field name, start date of the treatment, number of wells, fundamental reservoir and fluid data, scope of the project and evaluation of it.

After 2014, OGJ did not publish any surveys. When OGJ did not print one survey in last 10 years, SPE or other petroleum organizations and journals have not perpetuated these lists instead of OGJ. Thus, the most recent EOR database is the 2014 Worldwide EOR Survey. The 2014 Worldwide EOR Survey are published 346 different EOR project data. Table 2.1, which is derived from Koottungal (2014), illustrates the main types of EOR and subdivisions of them and the number of projects of each subdivision.

Nonetheless, some countries' data was not listed in the last survey. For instance, OGJ did not include data from China in 2010, 2012 and 2014's Surveys, so that in 2018, Chinese researchers published a survey about EOR projects in China. The article mentioned 375 projects. However, the only information about mentioned projects is what type of EOR methods implemented and their numbers. These data are tabulated in Table 2.2. At the third and fourth columns in the Table 2.2, previous and ongoing projects in 2016 are listed, respectively (Guo, et al., 2018). Again, the table just illustrates the main types of EOR and subdivisions and the number of projects of each subdivision. The list does not say anything about miscibility condition of gas flooding projects, except CO_2 injections. On the other hand, the 2014 Survey does not touch on foam method. In the light of these, Table 2.1 and Table 2.2 statistics were plotted on pie charts (Figure 2.8 and Figure 2.9) to indicate main EOR categories and percentages of it in total number of projects.

Table 2.1 Number of EOR Projects in 2014 OGJ EOR Survey derived from Koottungal (2014)

EOR Type		Number of EOR Project
Thermal	Steam	123
	SAGD	2
	Combustion	13
	Cyclic steam	1
	Hot water	2
	Water (Steam Scavenging)	2
Chemical	Polymer	6
	Surfactant	1
Gas Flooding	CO_2 miscible	135
	CO_2 immiscible	16
	Acid gas miscible	1
	Hydrocarbon immiscible	2
	Hydrocarbon miscible	37
	Nitrogen immiscible	4
Microbial	Microbial	1
Total		**346**

Table 2.2 Numbers of EOR Projects in China derived from (Guo, et al., 2018)

EOR Type		2016	To 2016
Thermal	Steam	3	20
	Combustion in situ	3	3
	Hot water	2	4
Chemical	Polymer	160	170
	Surfactant–Polymer	27	30
	Alkali–Surfactant–Polymer	28	34
	B-PPG+SP	3	5
	Foam	5	30
Gas Flooding	CO_2 miscible	1	1
	CO_2 immiscible	4	28
	Hydrocarbon	2	13
	Nitrogen	1	5
	Flue gas	0	1
	Air	6	2
Microbial	Microbial	4	29
Total		**249**	**375**

Both surveys together demonstrate the most up-to-date condition of EOR projects in the World. Nevertheless, they were considered separately for now because the 2018 EOR Survey in China solely printed eighty-two projects that have detailed data like the OGJ survey (Table 2.3), but they were not mentioned miscibility conditions of gas flooding projects. If elaborating the Figure 2.8 and Figure 2.9, the most common EOR method in China is chemical EOR while gas injection is the most widely used EOR technique in rest of the world. The number of gas injection applications is high because of miscible and immiscible CO_2 injection. Carbon dioxide injections have had a growing trend among in the EOR application in the last 20 years (Figure 2.10 and 2.11) (Zhang, Wei, & Bai, 2018a) (Zhang, Yin, Wei, & Bai, 2019a).

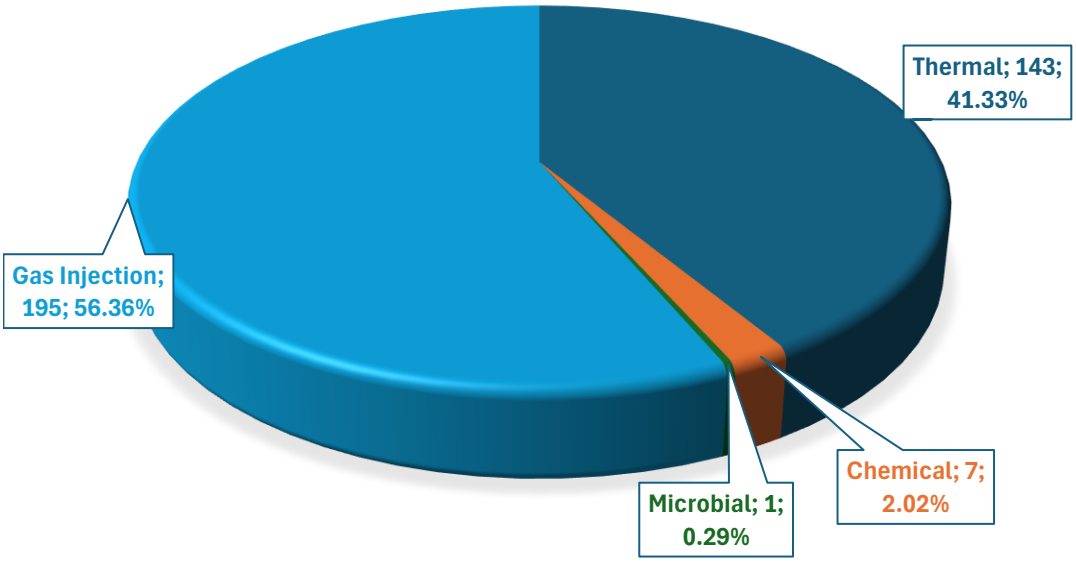

Figure 2.8. The 2014 World EOR Project Categories derived from (Koottungal, 2014)

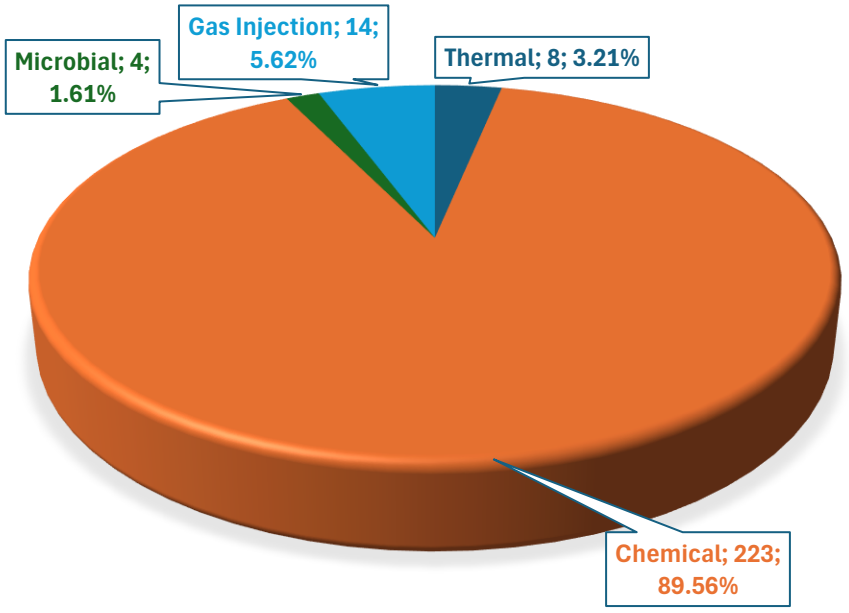

Figure 2.9. EOR Methods in China (2016) derived from (Guo, et al., 2018)

Table 2.3 EOR methods in China which has detailed data (Guo, et al., 2018)

	EOR Type	Number of EOR Project
Thermal	Steam	5
	Combustion	7
	Air flooding	5
Chemical	Polymer	11
	Surfactant–Polymer	8
	Alkali–Surfactant–Polymer	7
	Air foaming	4
	Surfactant	5
Gas Flooding	Carbon dioxide	8
	Hydrocarbon	7
Microbial	Microbial	15
Total		**82**

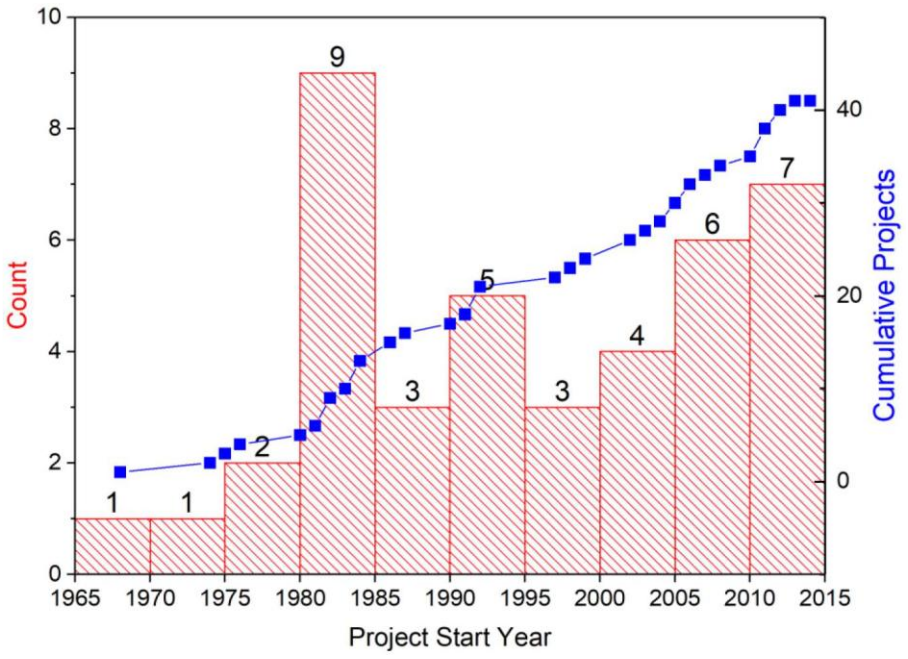

Figure 2.10. Number of immiscible CO_2 applications in worldwide (Zhang, Wei, & Bai, 2018b)

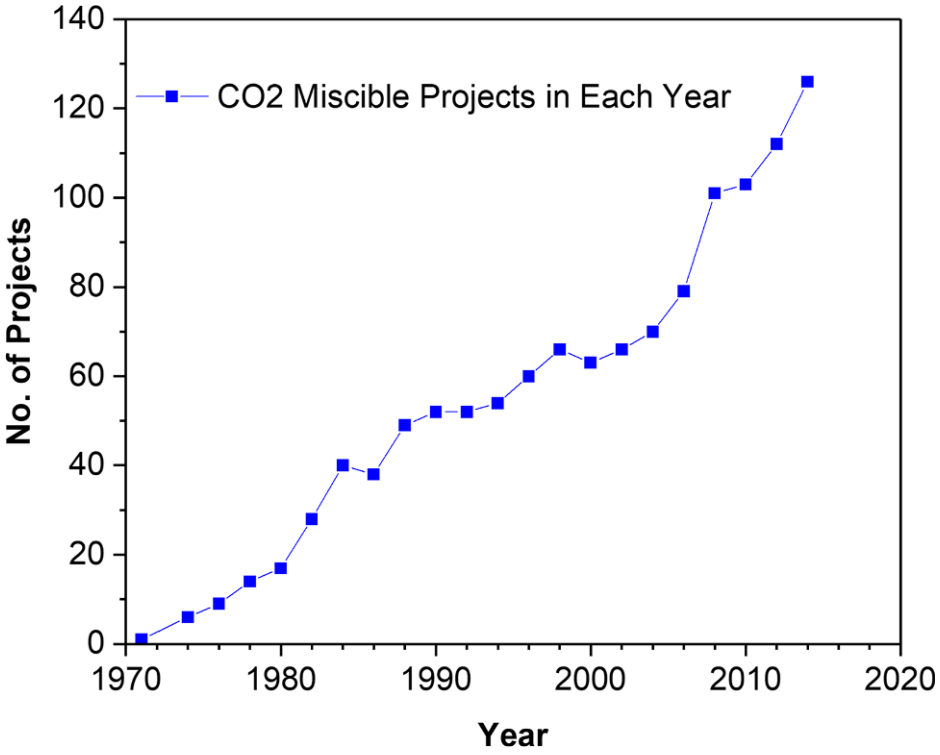

Figure 2.11. Number of miscible CO_2 projects in the US (Zhang, Yin, Wei, & Bai, 2019a)

Both surveys evaluated the projects in five categories, which are promising, successful, to early to tell (TETT), discouraging, and not evaluated. After extracting the not evaluated and blank data, the 2014 Survey and the 2018 China Survey have 335 and 58 evaluation data, respectively. The data of the surveys are graphed by author of the thesis in Figure 2.12 and 2.13 that also betrays evaluation of the project for each subcategory, as well. The 2014 data have 241 successful and forty-eight promising projects. There are only twelve projects categorized as discouraging. Figure 2.12 indicates that steam and miscible CO_2 injection are leading types of EOR with 124 and 132 activities, respectively. In addition, their success rates are more meaningful than other types of EOR due to high project numbers. Promising ones have also been treated as accomplished. Hence, the success rates for steam and CO_2 injection are 87.1% and 80.3%, in that order. If applying for the same things to Figure 2.13, almost all projects are evaluated as successful. There are only five surfactant-polymer flooding projects, which are labeled as discouraging.

Some subgroups are considered as one, such as SAGD is counted as steam injection. These kinds of aggregation issues are aforementioned in previous topics.

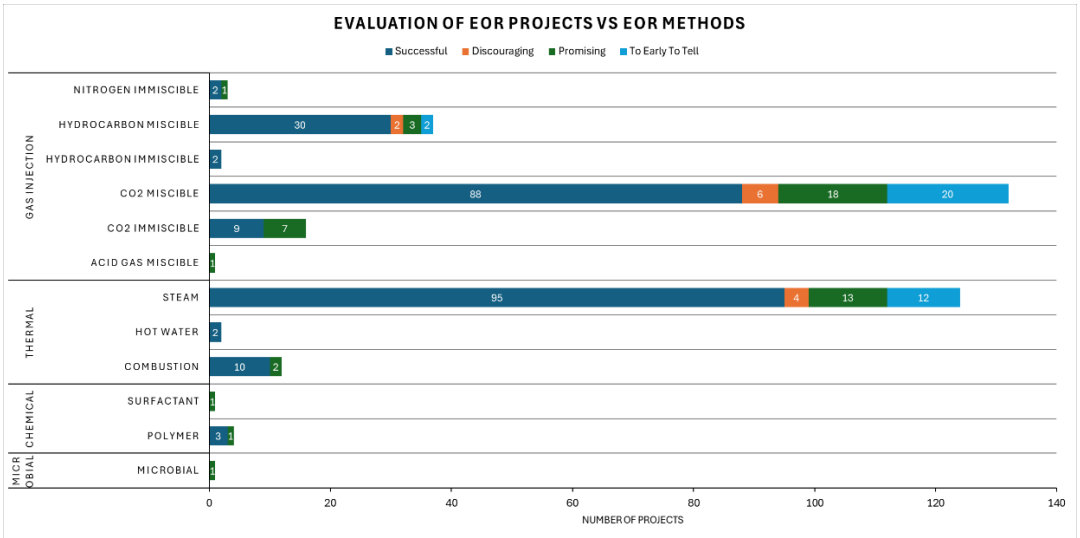

Figure 2.12. Evaluation of the 2014 World EOR Project Categories is derived from (Koottungal, 2014)

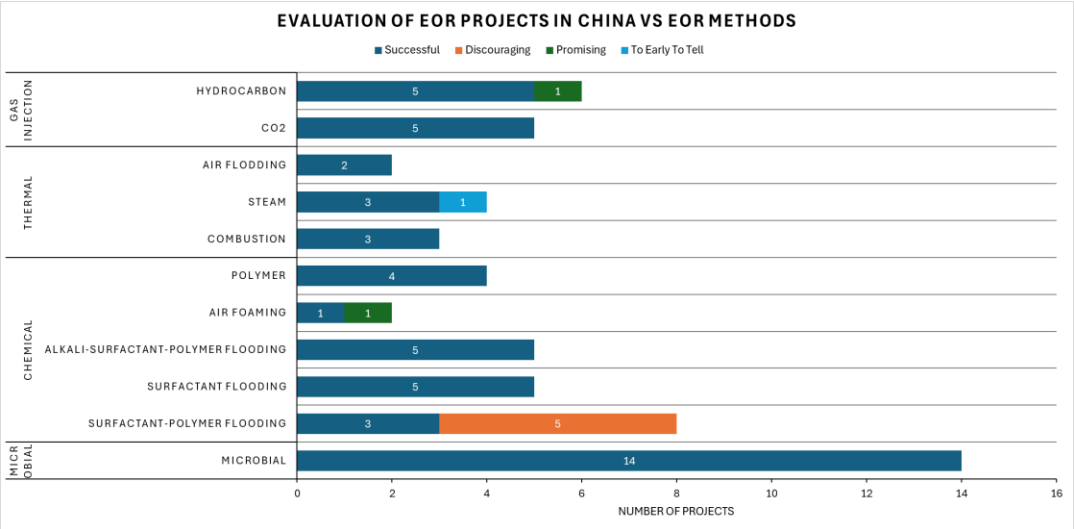

Figure 2.13. Evaluation of EOR Methods in China (2016) is derived from (Guo, et al., 2018)

Afterward, both surveys data were collected and united by author of the thesis in order to reveal the porosity, API gravity, reservoir temperature, reservoir depth, oil

viscosity and permeability values of each project according to EOR types on graphs. Nonetheless, not all the projects in surveys have these parameters, so that in such a case, that project will not be considered. These graphs are visible at Figure 2.14 through Figure 2.22.

Figure 2.14 demonstrates the number of EOR projects by porosity values. The X-axis shows the number of EOR projects, and Y-axis represents porosity ranges, which are between 0 – 65% and increasing with 5, and types of the EOR project in that range. According to Figure 2.14, steam injection is usually implemented on moderate to high porosity (20 – 65%) valued reservoir, yet gas injections (carbon dioxide, hydrocarbon, air, and acid gas) are applied on low to moderate porosity (0 – 30%) reservoirs regardless of miscibility condition. However, many of the gas injections were done at low porosity values (5 – 10%). Moreover, only gas injection methods were used where porosity is lower than 10%. On the other hand, chemical and microbial methods were just utilized at intervals of porosity higher than %10 and lower than 35%. The porosity range where the most EOR projects, which is sixty-five, are applied is between 25-30%. In other respects, EOR projects regardless of their types are almost divided equally to each range except where porosity is between 0 – 5%.

In Figure 2.15, the number of EOR projects by API values are plotted. The X-axis shows the number of EOR projects, and Y-axis represents API gravity ranges, which are between 8 – 50 and increasing with 5 except the first range is 8 to 10, and types of the EOR project in that range. When the graph is elaborated, steam injections are mainly practiced at low to moderate (8– 25) API gravity ranges and mostly utilized between 10 – 15 API gravity range. On the other side, gas injections are commonly performed in which at moderate to high API gravity (25 – 50). Chemical methods were applied in a wide range of API gravity, which is 10 – 40. Microbial methods practiced between 20 – 30 API gravity. The API gravity range where the most EOR projects, which is eighty-seven, are applied is between 10-15. In that range, eighty steam injection projects were done. On the other side, EOR projects regardless of

their types are essentially practiced between 30 – 35, 35 – 40 and 40 – 45 °F, 73, 62 and 47 EOR projects were used in these ranges, respectively.

Figure 2.16 represents the number of EOR projects by temperature (°F). The X-axis shows the number of EOR projects, and Y-axis represents temperature ranges, which are between 50 – 300 °F and increasing with 25 °F, and types of the EOR project in that range. Gas flooding methods were applied in nearly all the temperature range except 50 – 75 °F. The gas flooding mostly applied between 100 – 125 °F, which is 72 projects and all of them are CO_2 injections. Miscible hydrocarbon injections are dominant in the range of 175 – 200 °F. Steam injection was practiced at lower than 175 °F and predominantly performed in the range of 75 – 100 °F. Microbial and chemical methods were utilized in every temperature range till 200 °F. The temperature range where the most EOR projects, which is 133, are applied is between 100-125. In that range, 72 carbon dioxide (67 miscible + 5 immiscible) and 63 steam injection projects were carried out. On the other hand, EOR projects regardless of their types are primarily practiced between 75 – 100 °F, 100 – 125 °F and 125 – 150 °F, 71, 133 and 56 EOR projects were used in these ranges, respectively.

In Figure 2.17 and 2.18, the number of EOR projects by depth (ft) values are graphed. The X-axis shows the number of EOR projects, and Y-axis represents depth ranges, which are between 0 – 14500 ft and increasing with 500 ft, and types of the EOR project in that range. Gas injection methods were utilized except shallow reservoirs, which are shallow than 1000 ft. Especially, immiscible carbon dioxide injection applications were used till 8500 ft, yet miscible CO_2 injection were practiced until 12000 ft. Hydrocarbon injection method was generally utilized deeper reservoir than CO_2 injection because it is normally required more pressure to overcome minimum miscibility pressure. In shallow reservoirs (lower than 3000 ft), steam injection is the predominant technique. In the range between 4000 – 8500 ft carbon dioxide injection are prevalent regardless of miscibility conditions. The microbial method was performed between 1500 – 6000 ft reservoir depth. The chemical methods were mostly conducted in the range of 2500 – 5500 ft. The depth range where the most EOR projects, which is 46, are applied is between 1000-1500 because of 41 steam

injection projects. On the other side, EOR projects regardless of their types are mainly practiced between 4000 – 4500 ft, 4500 – 5000 ft and 5000 – 5500 ft, 25, 36 and 35 EOR projects were used in these ranges, respectively.

Figure 2.19 and 2.20 demonstrated the number of EOR projects by oil viscosity on the basis of 10^3 cP. The X-axis shows the number of EOR projects, and Y-axis represents oil viscosity (10^3 cP) ranges, which are between 0 – >20000 10^3 cP types of the EOR project in that range. The increment of ranges in this figure was not evenly distributed. Firstly, starting with a 1 cP increment between 0 – 10 cP; then, continuing with 10 points increasing between 10 – 100 cP. Afterward, oil viscosity increased with 100 cP at each range between 100 – 1000 cP. Later, the incrimination values of viscosity proceeded 500 and 1000 cP between 1000 – 5000 cP and 5000 – 20000 cP, respectively. Lastly, there is a group in which oil viscosity is higher than 20000 cP. To elaborate the graph, more than half of the EOR methods, which is 198, were applied where oil viscosity below 10 cP and most of them -156- implemented lower than 1 and between 1 to 2 cP, which are 84 and 72 in that order. Almost all of these are gas injection methods, which are dominated by CO_2 injection. Thermal methods are predominantly practiced -136- where oil viscosity higher than 70 cP. Only 21 projects were not a thermal method above 70 cP. Chemical techniques are generally utilized at oil viscosity below 50 cP. Microbial EOR was principally done at moderate to high viscosity areas.

In Figure 2.21 and 2.22, the number of EOR projects by permeability (mD) values are graphed. The X-axis shows the number of EOR projects, and Y-axis represents permeability (mD) ranges, which are between 0 – >40000 mD types of the EOR project in that range. Again, the increment of ranges in this figure was not evenly distributed. Firstly, starting with a 1 mD increment between 0 – 10 mD; then, continuing with 10 mD increasing between 10 – 100 mD. After, permeability increased with 100 mD at each range between 100 – 1000 mD. Later, the incrementation values of permeability proceeded 500 and 1000 cP between 1000 – 5000 mD and 5000 – 20000 mD, respectively. Lastly, there is a group in which permeability is higher than 40000 mD. Steam injections were mainly applied to high

permeability areas. The reservoirs which have low permeability values (<10 mD), carbon dioxide injections were utilized. Chemical methods were practiced no higher than 3500 mD. Microbial EOR approaches were performed at low to moderate intervals. The permeability range where the most EOR projects, which is 33, were applied is between 1000 – 1500 and 18 of them are steam injection projects. Almost all intervals have a similar number of projects.

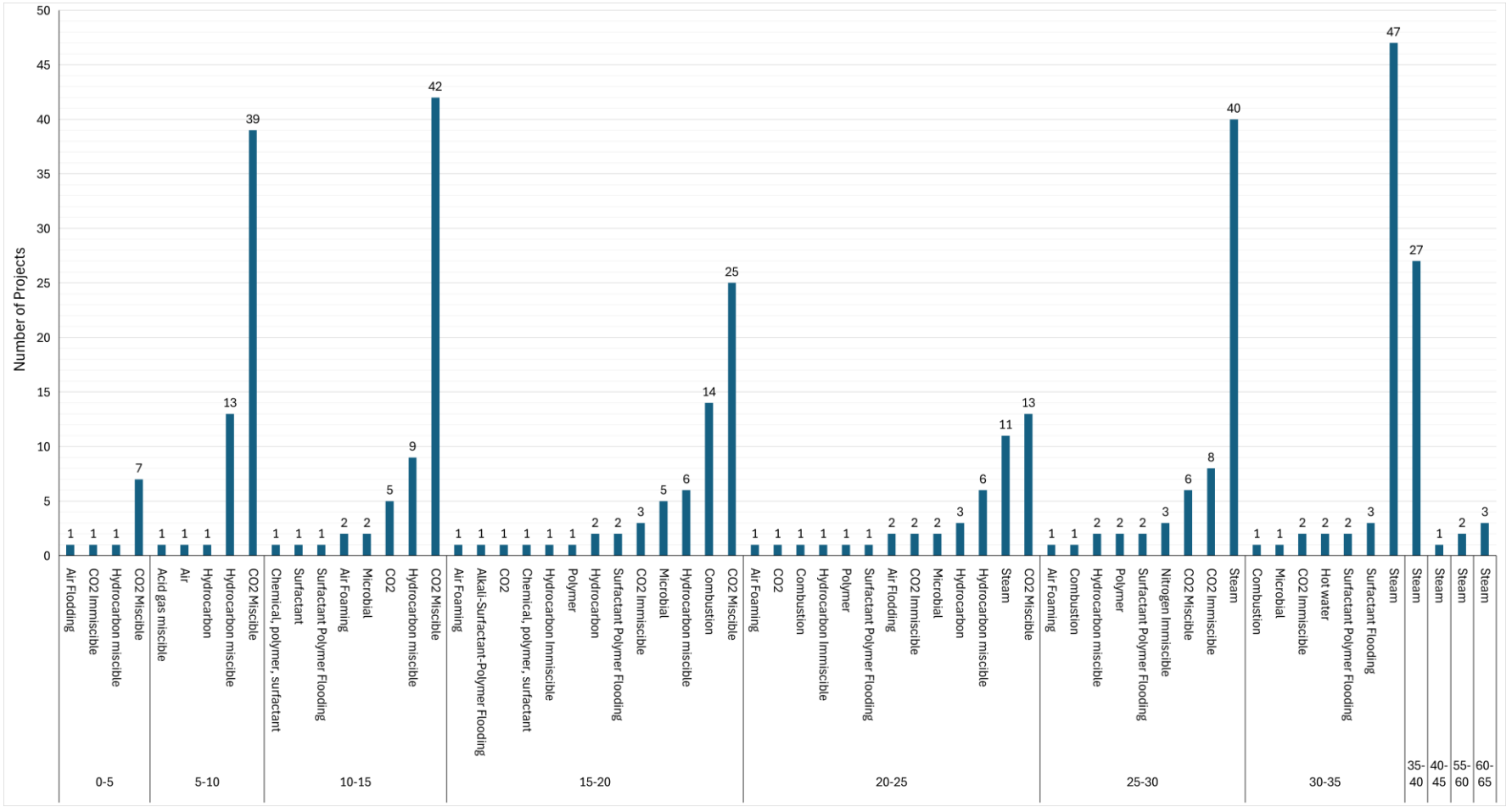

Figure 2.14. Number of EOR projects by porosity (%) values derived from (Koottungal, 2014) (Guo, et al., 2018)

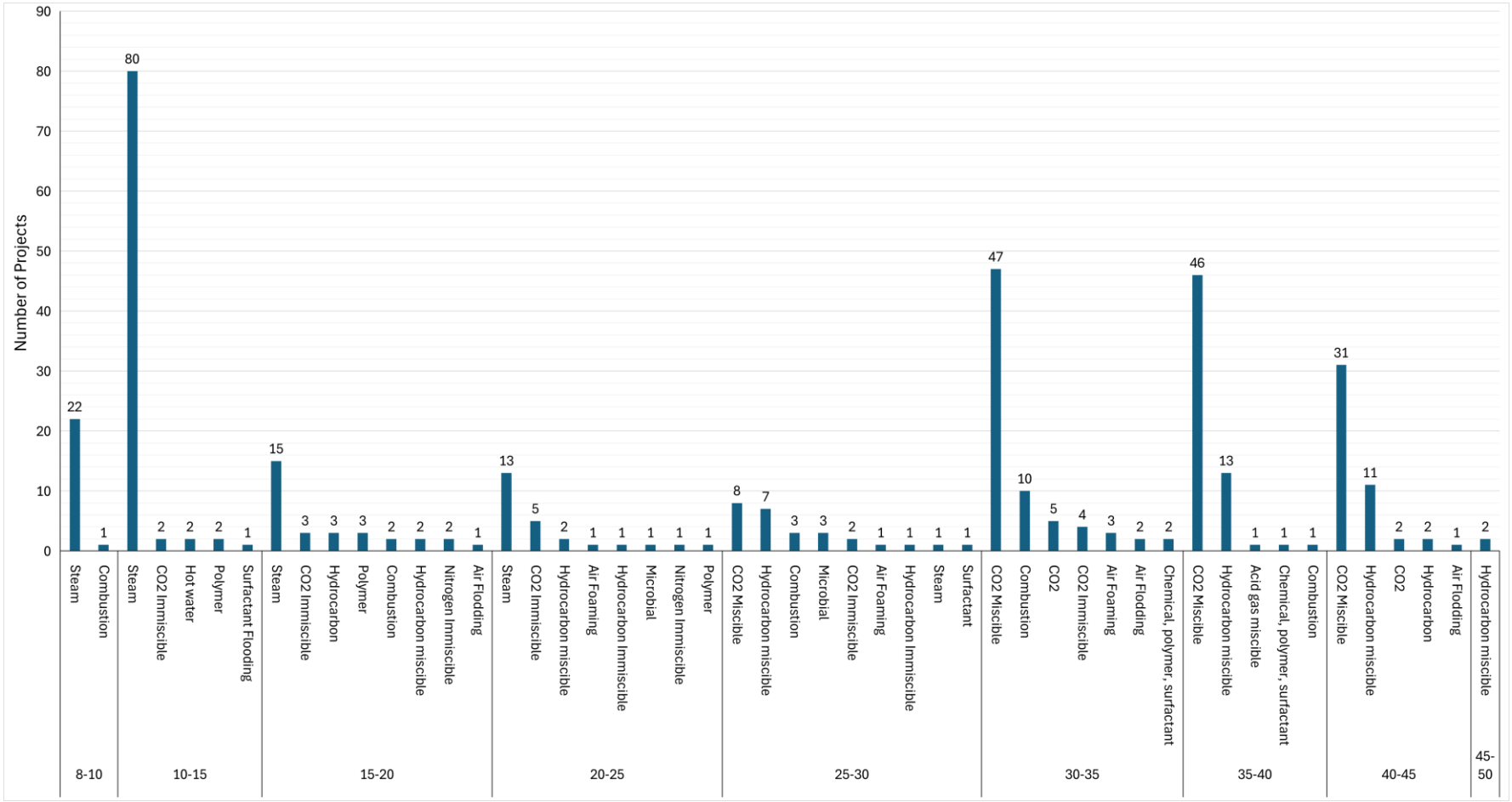

Figure 2.15. Number of EOR projects by API gravity values derived from (Koottungal, 2014) (Guo, et al., 2018)

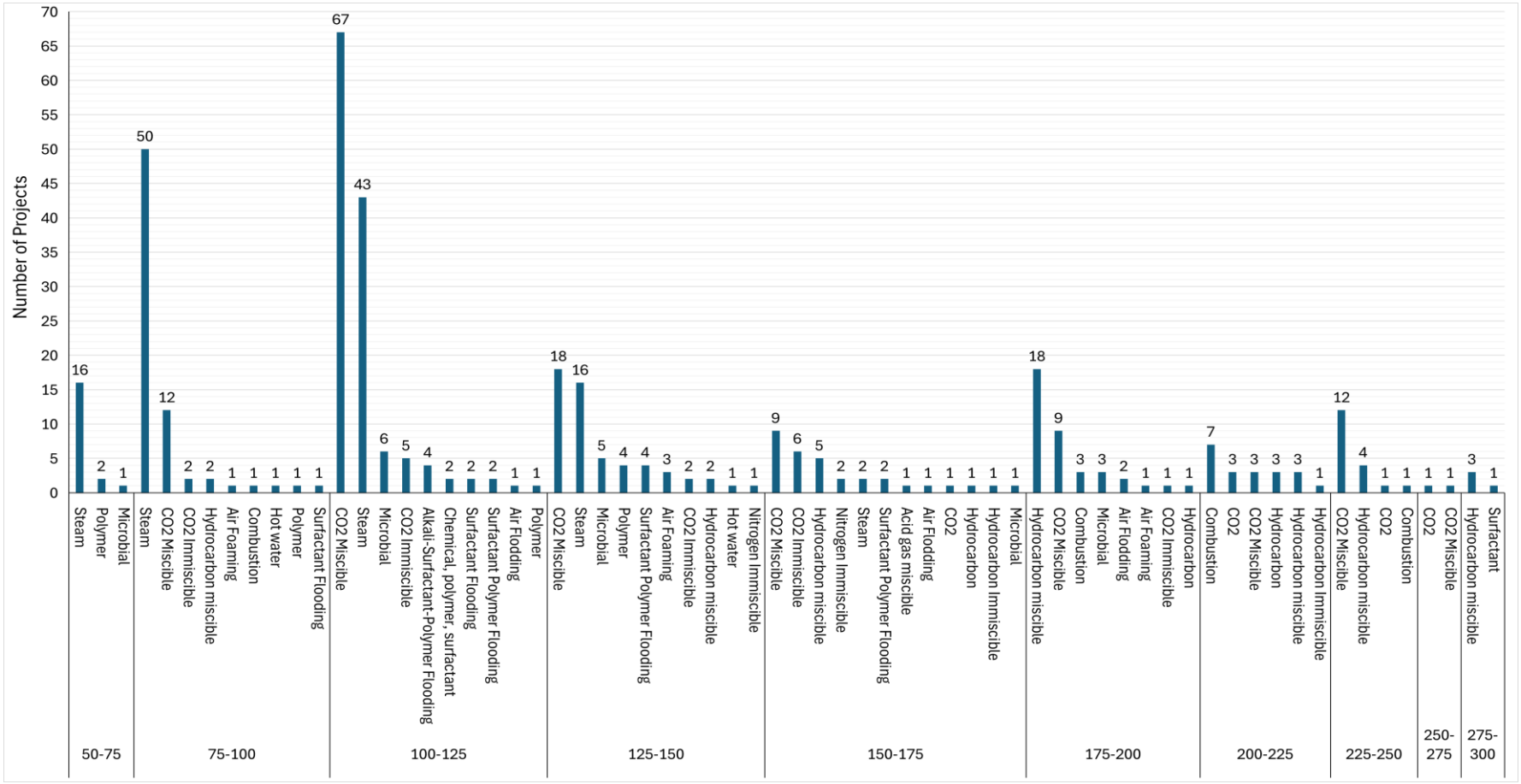

Figure 2.16. Number of EOR projects by temperature (°F) values derived from (Koottungal, 2014) (Guo, et al., 2018)

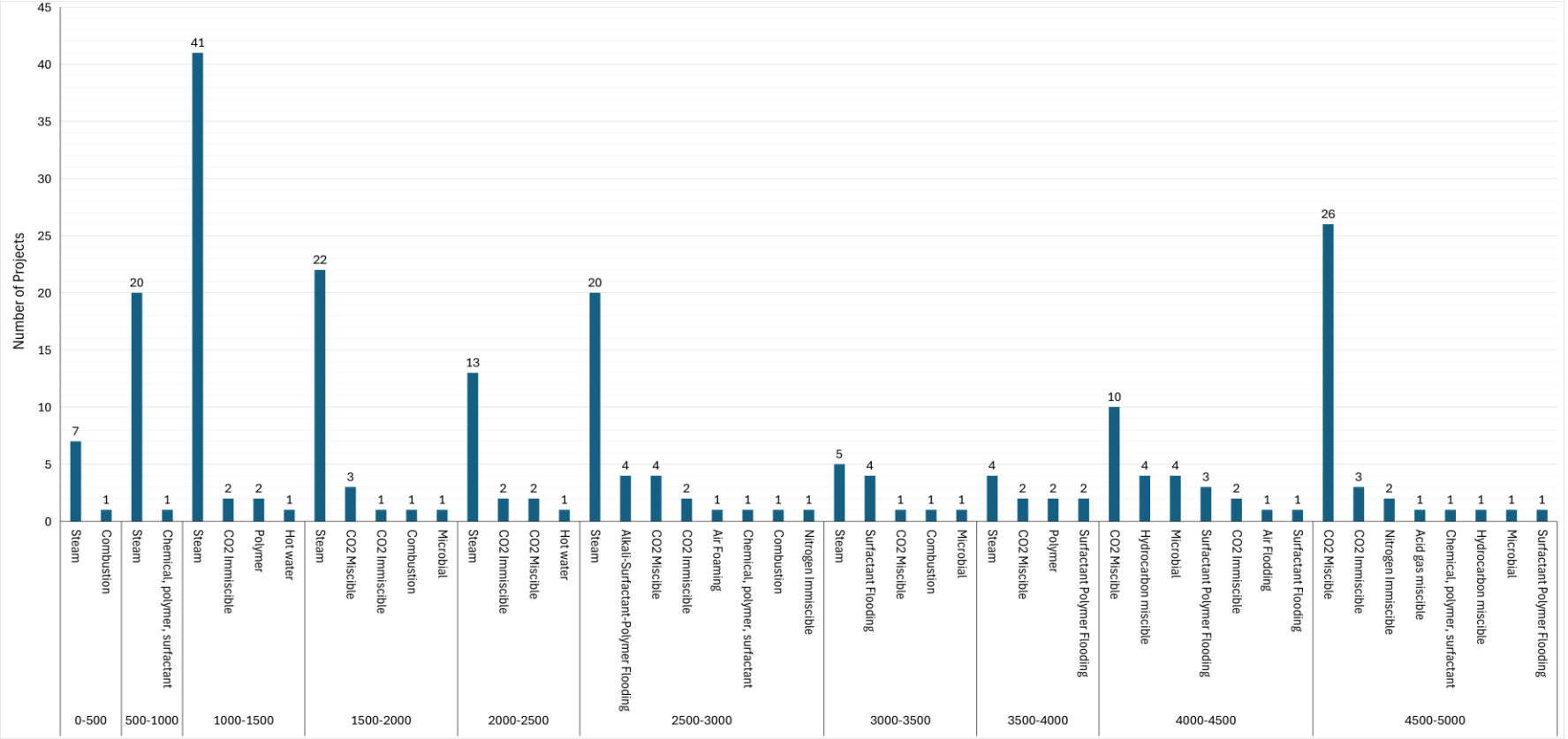

Figure 2.17. Number of EOR projects by depth (ft) values Part-1 derived from (Koottungal, 2014) (Guo, et al., 2018)

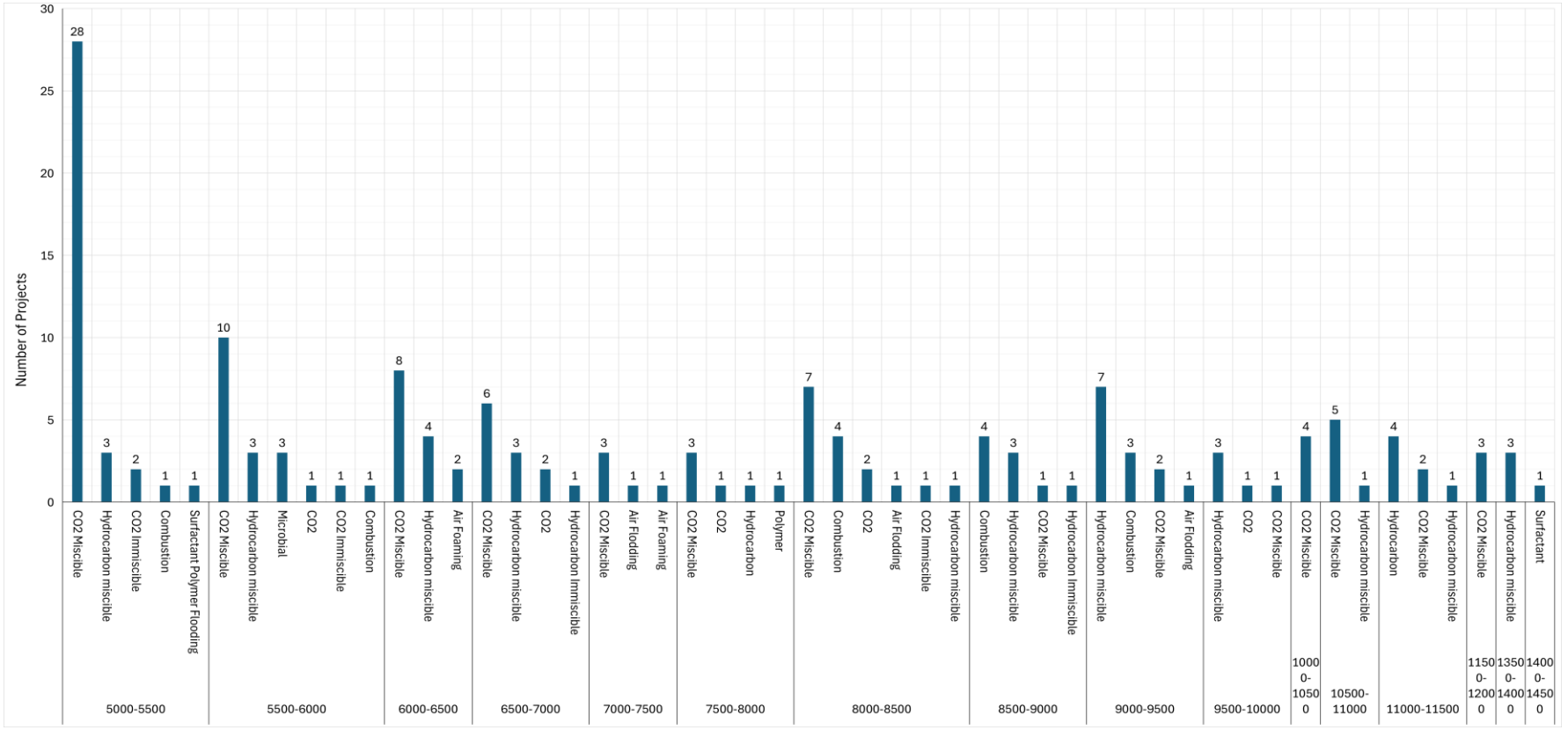

Figure 2.18. Number of EOR projects by depth (ft) values Part-2 derived from (Koottungal, 2014) (Guo, et al., 2018)

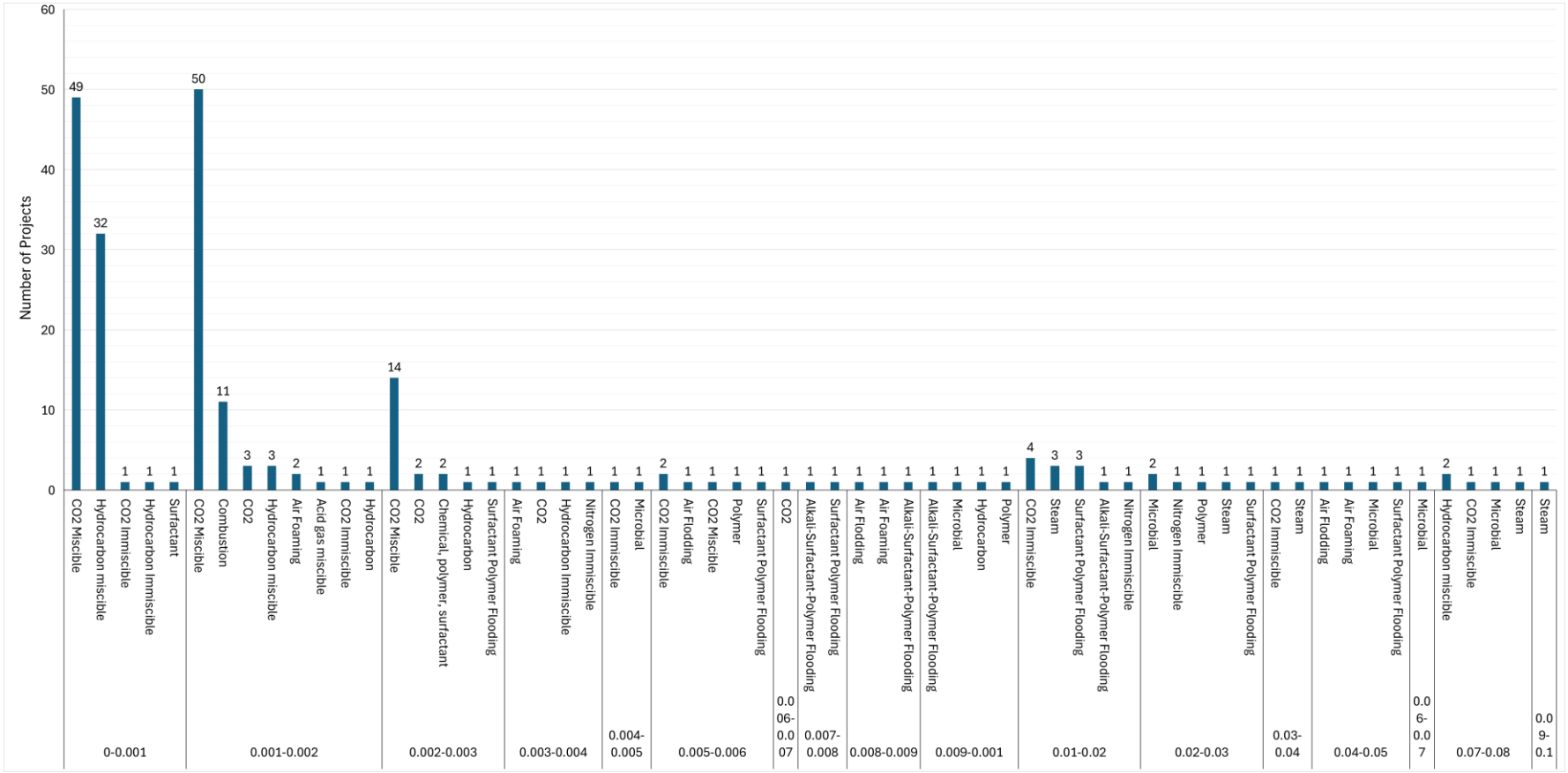

Figure 2.19. Number of EOR projects by oil viscosity (10^3 cP) values Part-1 derived from (Koottungal, 2014) (Guo, et al., 2018)

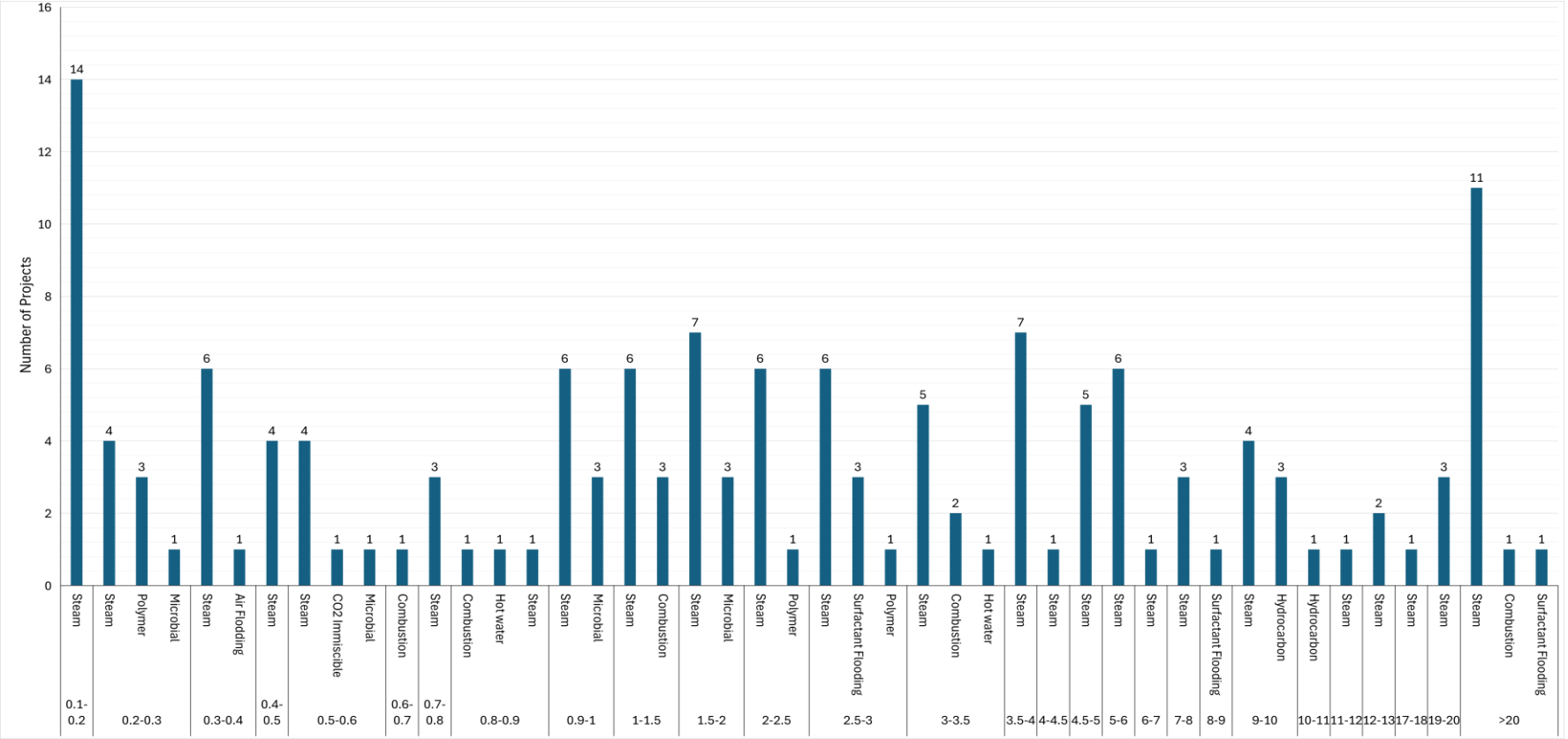

Figure 2.20. Number of EOR projects by oil viscosity (10^3 cP) values Part-2 derived from (Koottungal, 2014) (Guo, et al., 2018)

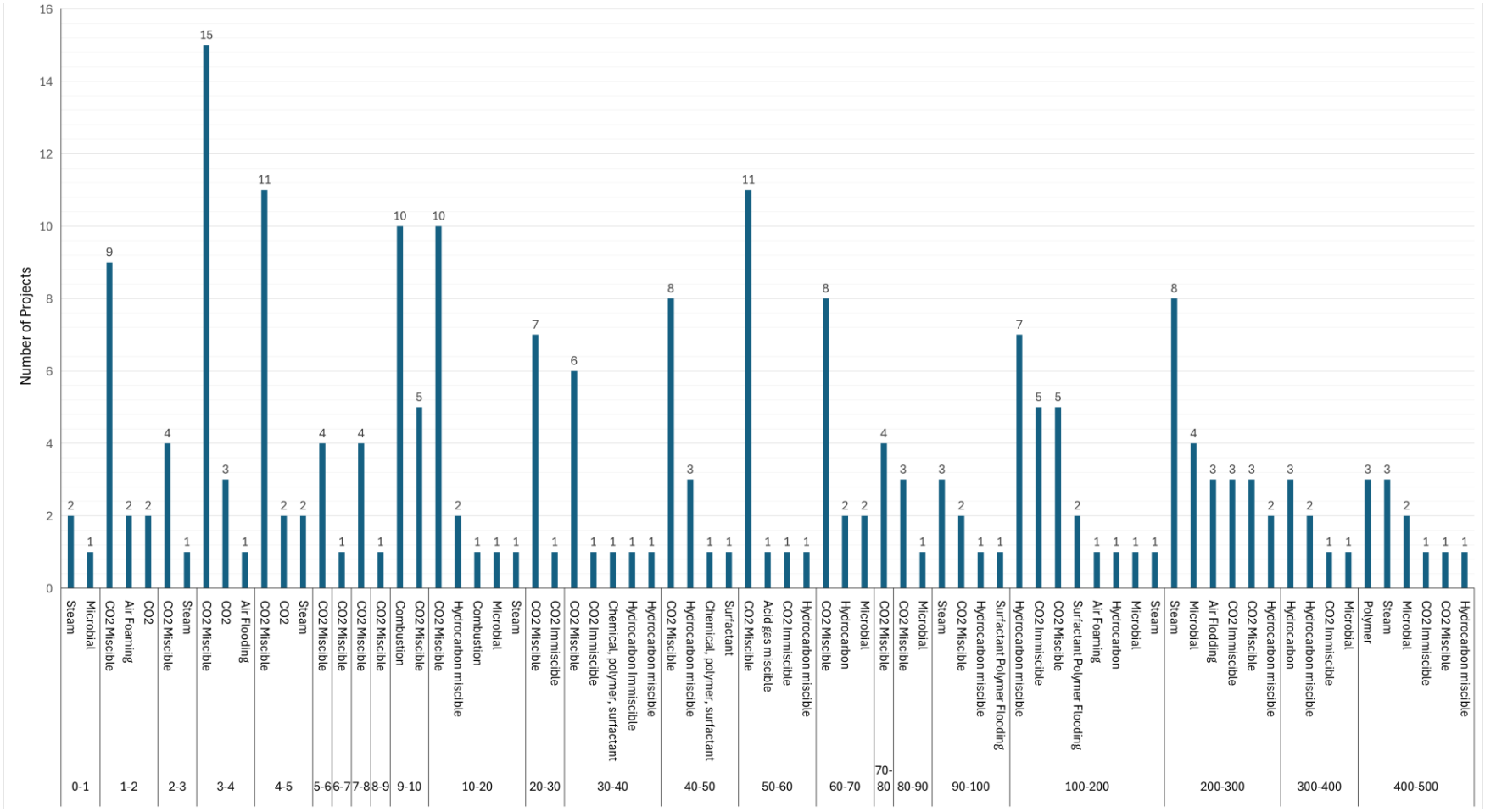

Figure 2.21. Number of EOR projects by permeability values (mD) Part 1 derived from (Koottungal, 2014) (Guo, et al., 2018)

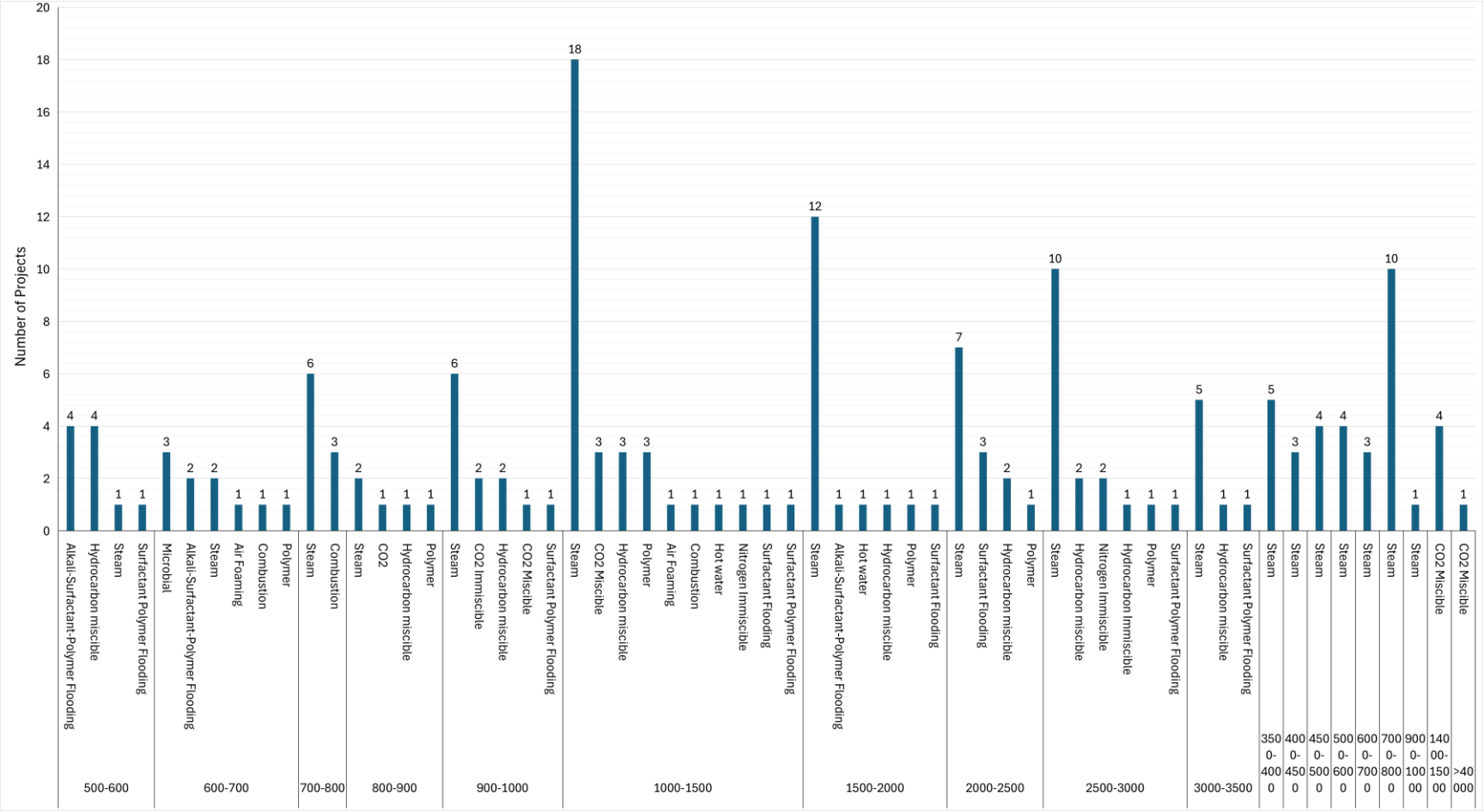

Figure 2.22. Number of EOR projects by permeability values (mD) Part 2 derived from (Koottungal, 2014) (Guo, et al., 2018)

2.5 EOR Screening

Many EOR projects have been conducted since 1959. Some of these projects have achieved success, some of them not. Each venture's data is unique, and one project's data tells little about how EOR could be succeed or not, so that this data is not sufficient, intrinsically. However, when whole projects information is collected for creating a database, these data can be utilized to generate filters, ranges, means and boundaries. EOR screening is formed with determining these entities.

EOR screening is not a new topic; researchers have worked on it since the 70s in order to obtain the most inclusive rules. Hence, there are various EOR screening in literature (National Petroleum Council (NPC), 1976), (Geffen, 1977) (Brashear & Kuuskra, 1978) (Iyoho, 1978), (OTA, 1978), (Carcoana, 1982), (Taber & Martin, 1983), (Taber, Martin, & Seright, 1997a), (Taber, Martin, & Seright, 1997b), (Al Adasani & Bai, 2011), (Bourdarot & Ghedan, 2011), (Zhang, Wei, & Bai, 2018a), (Zhang, Yin, Wei, & Bai, 2019a).

This study is utilized data from (Taber & Martin, 1983), (Taber, Martin, & Seright, 1997a), (Taber, Martin, & Seright, 1997b), (Al Adasani & Bai, 2011), (Zhang, Wei, & Bai, 2018a), (Zhang, Yin, Wei, & Bai, 2019a). In 1983, Taber & Martin took into account eight EOR methods, which are miscible hydrocarbon, carbon dioxide, nitrogen and flue gas injection as gas injection methods, surfactant/polymer, polymer, and alkaline as chemical flooding and lastly, combustion and steam flooding as thermal methods. The authors created a screening table, which contains three oil properties (oil gravity, oil viscosity and oil composition) and six reservoir properties (oil saturation, formation type, net thickness, average permeability, depth, and reservoir temperature). They set boundaries of the properties for each method. Taber and Martin did not differentiate miscible and immiscible injections for CO_2, nitrogen, and flue gas flooding, in their work.

14 years later, they revisited their screening criteria and published two articles (Taber, Martin, & Seright, 1997a) (Taber, Martin, & Seright, 1997b). This time, they used the 1994 Worldwide EOR Surveys of Oil and Gas Journal's as database to set screening boundaries. The writers utilized the same oil and reservoir properties, but this time they combined alkaline and surfactant flooding method because there was no pure alkaline flooding performed to a field; however, there are alkaline surfactant polymer flooding methods performed in industry. In addition to that, Taber et. al. (1997a) considered all gas injections as miscible, and they delivered a separate immiscible gas injections criteria for whole gas injection methods. Further, the authors put in surface mining in screening table, they added it because of tar sand productions. Nevertheless, they were not considered it as EOR method (Taber, Martin, & Seright, 1997a). In part-2, they considered the oil prices and advanced some screening criteria, such as miscible and immiscible CO_2. These two articles are regarded as cornerstones of the EOR screening literature.

In 2011, Al Adasani and Bai updated the EOR screening criteria, which are claimed by Taber, Martin, & Seright in 1997. They built a database based on Oil and Gas Journal's EOR survey reports from 1998 through 2010 and SPE publications. The authors used surveys from 1998 because Taber, Martin, & Seright already used previous surveys in their publications, so that these surveys are included newsworthy data. Their database comprises 652 EOR projects. Similar to Taber's Table, they employed API gravity, and viscosity as crude oil parameters, and oil saturation, formation type, permeability, net thickness, depth, and temperature as reservoir parameters. Moreover, porosity is included as a reservoir parameter; yet oil composition is discarded. Additionally, limits are enforced for temperature and permeability. Temperature is an important parameter for minimum miscibility pressure (MMP) since MMP is a function of temperature. Al Adasani and Bai listed 16 EOR methods in their table. The writers allocated to miscible and immiscible gas injections. Then, water alternating gas (WAG) method inserted to miscible gas injection categories. Plus, hydrocarbon + WAG method added to immiscible gas

injection topic. Unlike Taber's Table, the authors separated surfactant flooding as a chemical method. Hot water injection is adjoined to thermal methods, as well.

In 2018, Zhang, Wei, & Bai (2018a) analyzed forty-one immiscible CO_2 injection applications. The purpose of the article is to update screening criteria for only immiscible CO_2 injection, so that other EOR methods data and screening results are out of scope. The main difference in their screening table is that they deliberated reservoir net thickness as a criterion, unlike the screening tables in literature. They decided that because net thickness is vital for success of injection in economic way (Zhang, Wei, & Bai, 2018a).

In the same manner, the scope of (Zhang, Yin, Wei, & Bai, 2019a) is just miscible CO_2 injection; therefore, other EOR methods are not considered. The surveys generally did not report minimum miscibility pressure (MMP). However, MMP is the key factor of miscible injections since when MMP is higher than reservoir pressure, there is no miscible solution that could be possible. Hence, it is easy to decide to go/no go for miscible CO_2 injection by just checking MMP and reservoir pressure relation. Consequently, the authors inserted reservoir pressure as a criterion for screening. The writers collected thirty-three entries for MMP and utilized them to set boundaries.

Since the scope of this thesis is CO_2 injection, immiscible and miscible CO_2 injection method screening ranges are tabulated in Table 2.4 and 2.5. For miscible CO_2 injection, (Taber & Martin, 1983), (Taber, Martin, & Seright, 1997a), (Al Adasani & Bai, 2011), and (Zhang, Yin, Wei, & Bai, 2019a) tables are summarized in Table 2.4. For immiscible CO_2 injection, (Taber, Martin, & Seright, 1997a), (Taber, Martin, & Seright, 1997b) (Al Adasani & Bai, 2011), and (Zhang, Wei, & Bai, 2018a) tables are summarized in Table 2.5.

Table 2.4 Miscible CO_2 Injection Screening Criteria

	Taber & Martin (1983)	Taber, Martin, & Seright (1997a)	Al Adasani & Bai (2011)	Zhang, Yin, Wei, & Bai (2019)
Oil Gravity, API	> 26	> 22	> 22	> 25
Oil Viscosity, cP	< 15	< 10	< 35	< 4
Oil Composition	High % of C5 - C12	High % of C5 - C12	-	-
Oil Saturation	> 30	> 20	> 15	> 15
Formation Type	Sandstone or Carbonate	Sandstone or Carbonate	Sandstone or Carbonate	-
Porosity, %	-	-	> 3	> 3
Net Thickness, ft	Thin unless dipping	Thin unless dipping	Wide Range	> 15
Average Permeability, mD	Not Critical	Not Critical	> 1.5	> 0.1
Depth, ft	> 2000	> 2500	> 1500	> 1150
Temperature, °F	Not Critical	Not Critical	< 257	< 260
Reservoir Pressure, psia	-	-	-	> 1020

Table 2.5 Immiscible CO_2 Injection Screening Criteria

	Taber, Martin, & Seright (1997a, b)	Al Adasani & Bai (2011)	Zhang, Wei, & Bai (2018)
Oil Gravity, API	> 12	> 11	> 10.8
Oil viscosity, cP	< 600	< 592	< 936
Oil Composition	Not Critical	-	-
Oil Saturation	> 35	> 42	> 30
Formation Type	Not Critical	Sandstone or Carbonate	Sandstone or Carbonate
Porosity, %	-	> 17	> 11.5
Net Thickness, ft	Not Critical	-	> 5.215
Average Permeability, mD	Not Critical	> 30	> 1.4
Depth, ft	> 1800	> 1150	> 1400
Temperature, °F	Not Critical	< 198	< 235.4
Reservoir Pressure, psia	-	-	-

2.6 Minimum Miscibility Pressure

The minimum miscibility pressure (MMP) is the lowest pressure at which injected gas becomes fully miscible with the reservoir oil at the reservoir temperature. The fully miscible means that at this pressure, the gas and oil mix and create a one-phase fluid in the reservoir. It is the most crucial property of any gas injection project in order to detect miscibility condition of the injection. Miscibility can occur in two different types, which are First Contact Miscibility (FCM) and Multi Contact Miscibility (MCM) (Hamdi & Awang, 2014) (Dindoruk, Johns, & Orr Jr., 2020).

The First Contact Miscibility refers to gas and oil become miscible as soon as they come into contact at the MMP (Stalkup Jr, 1983) (Hamdi & Awang, 2014). It is not

common to witness a FCM under real reservoir conditions due to heavy components of oil (Dindoruk, Johns, & Orr Jr., 2020).

In most cases, the injected gas and crude oil of the reservoir are not directly miscible. However, the gas and oil can reach miscibility under proper conditions of pressure and gas composition (Stalkup Jr, 1983). This kind of miscibility is called Multi Contact Miscibility (MCM). It refers that injected gas and petroleum mix in repeated contacts (Dindoruk, Johns, & Orr Jr., 2020). Moreover, MCM could be divided into vaporizing gas drive and condensing gas drive or their combination, which is called condensing/vaporizing gas drive (Saini, 2019).

In a condensing gas drive, the injected gas mixes with the reservoir oil, causing heavier hydrocarbons from the gas phase to condense into the oil phase. The oil is enriched with these hydrocarbons until miscibility occurs (Saini, 2019) (Yan, Michlesen, & Stenby, 2012).

In a vaporizing gas drive, the injected gas vaporizes intermediate hydrocarbon components from the reservoir oil into the gas phase over multiple contacts, enriching the gas phase with these components until miscibility is achieved (National Petroleum Council (NPC), 2021) (Saini, 2019) (Yan, Michlesen, & Stenby, 2012). Most of the commercially viable miscible CO_2 EOR projects are Multi-Contact Miscibility (MCM) type of miscibility (Alston, Kokolis, & James, 1985).

In literature, minimum miscibility pressure is obtained by experimental and computational methods. The experimental methods include slim tube experiment, vanishing interfacial tension (VIT), and rising bubble apparatus (RBA). VIT and RBA methods are still utilized for calculation to MMP while they have crucial uncertainties. However, they may provide functional data. Computational methods contain slim tube simulation, multiple-mixing-cell calculation, method of characteristics (MOC) and empirical correlations. There are various empirical MMP correlations to calculate the pressure. In these correlations, MMP calculated as function of reservoir temperature, molecular weight, and mole fraction of reservoir fluids (Dindoruk, Johns, & Orr Jr., 2020).

The slim tube experiment is the most commonly applied method of determining the MMP (Yan, Michlesen, & Stenby, 2012). Nevertheless, it is time and money consuming and not every company or research organization has this experiment set up in their laboratory (Vulin, Gaćina, & Biličić, 2018) (Dindoruk, Johns, & Orr Jr., 2020). For these reasons, slim tube simulations could be substituted instead of real experiments for saving time and money. Moreover, plenty of correlations are implemented in literature since they do not need complex algorithms.

Hence, in this study, slim tube simulations and MMP correlations are utilized to obtain minimum miscibility pressure.

2.6.1 Slim Tube Simulations

In slim tube experiments, slim tube is synthetically created in order to act as a porous media in reservoir. The tube has a small diameter between 0.15 to 0.6 inch. Glass beads or sands are used to represent porous and permeable areas. The test is commonly practiced with high porosity and permeability values (Dindoruk, Johns, & Orr Jr., 2020). Figure 2.23 shows a slim tube experiment chart. The experiment tube has to be a long length because of forming a transition zone to stabilize the flow. Slim tube test should be run in different pressures. The most common application is injecting 1.2 pore volume (PV) of gas into the slim tube and recording the recovery factor. This process should be practiced at various pressures. After that, each run's pressures and recovery factors are plotted to obtain the curves. Minimum miscibility pressure value could be determined visually via extrapolating the curves forward and backward, and then the pressure value of the intersection point of the curves is minimum miscibility pressure (Figure 2.24). In addition, slope equation of two curves can be solved together to calculate MMP value. If the oil samples, which is utilized in slim tube experiment, has low API, heavily biodegraded or particularly aromatic, the intersection of the two curves (MMP point) may not be determined. (Dindoruk, Johns, & Orr Jr., 2020) (Jaferi, Ashoori, & MK, 2019) (Karamnia & Ashoori, 2021).

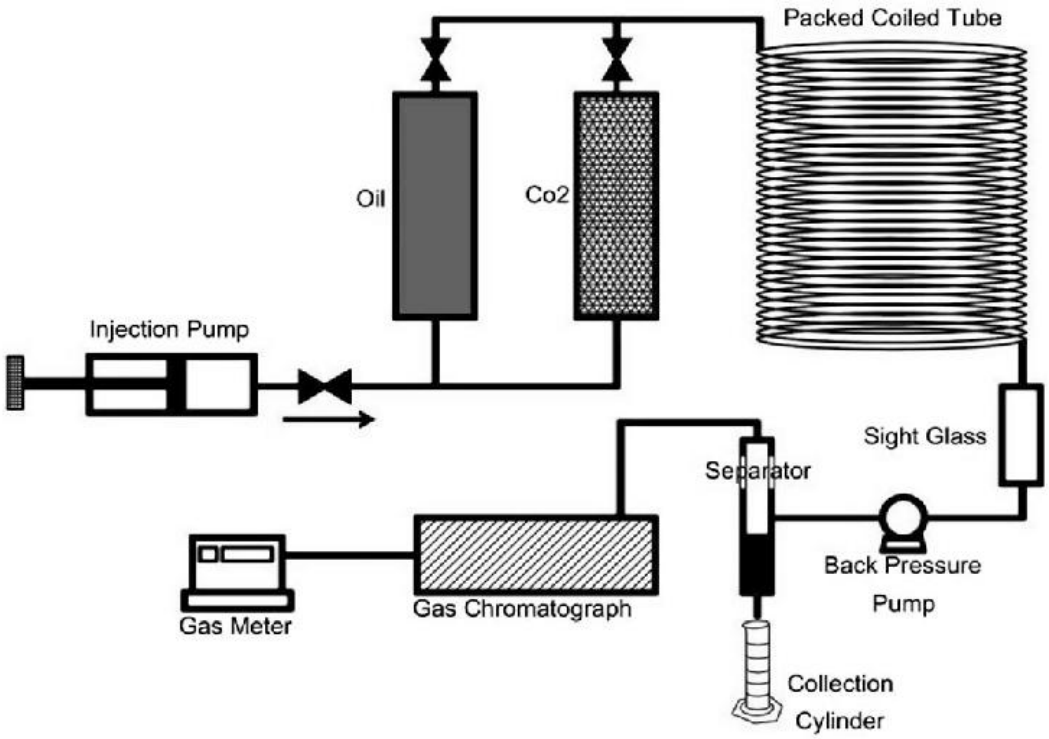

Figure 2.23. Schematic of slim-tube apparatus (Delforouz, Movaghar, & Shariaty, 2019)

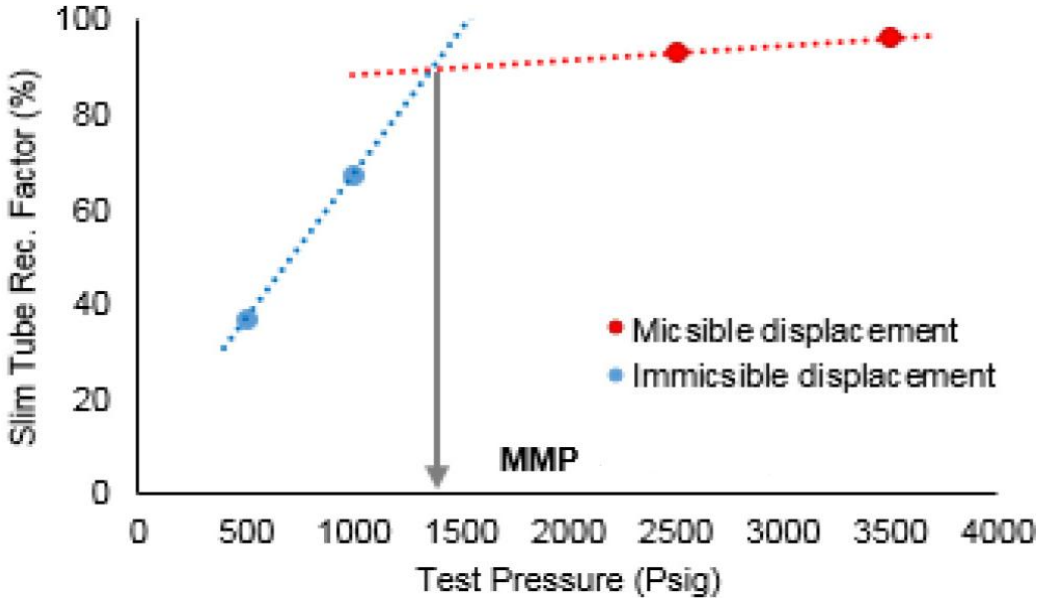

Figure 2.24. Recovery factor vs pressure graph example (Adel, Tovar, & Schechter, 2016)

The relative permeabilities, which is used in the slim tube simulation, do not require to be the correct ones since all of the oil in the slim tube will be produced in the end of the simulation independently from the relative permeabilities and saturations (Karamnia & Ashoori, 2021) (Dindoruk, Johns, & Orr Jr., 2020).

When the reservoir fluid and the injected fluid form a mixed fluid, the dispersion occurs in the reservoir. A transient flow region can be created because of the dispersion. This flow region may cause miscalculation of minimum miscibility pressure. To solve this problem, the plot of the recovery factors at 1.2 PV vs. pressures graph should be corrected to zero dispersion situation. The grid sizes of the simulation have substantial impact on the MMP results, in a such case MMP tends to be computed greater than normal value (Stalkup Jr., 1990).

Hence, Stalkup Jr. (1984) suggested that when the number of the grid block increases, the dispersion will decrease, so that transient region will go to zero. Consequently, the following procedures should be applied to find the correct MMP value.

1- Firstly, 200 grid block model created with aforementioned dimension, properties, and time steps.

2- The model is run at various pressures, and at the end of each run the oil recovery factors (RF) are recorded. Afterward, recovery factors vs pressure graph is plotted.

3- The grid number of the model is changed to 100 and 500 grids. Then, the second article is practiced for 100 and 500 grids models.

4- Recovery factors of each grid model are tabulated according to their pressure. By plotting the recovery factor versus $1/\sqrt{N}$, where N is the number of the blocks, and extrapolating it for N (infinite equivalent), the true value of the final recovery factor (RF∞) per each pressure is determined.

5- For each pressure, article four is implemented. The recovery factors at infinite number of grids are plotted against the pressure. The breaking point of the lines represents the minimum miscibility pressure (Stalkup Jr., Miscible Displacement,

1984) (Dindoruk, Johns, & Orr Jr., 2020) (Jaferi, Ashoori, & MK, 2019) (Karamnia & Ashoori, 2021).

2.6.2 MMP Correlations

Many empirical minimum miscibility correlations are presented in literature. Correlations are used because they are easy to apply. In addition to that, correlations do not require too much data. Most of the correlations are functions of reservoir temperature, molecular weight, and mole fraction of reservoir fluids. The correlations are dependent on their database, which is utilized to derive the correlation. Therefore, each correlation covers some point of literature. Hence, in this section, the MMP correlations, which are implemented in this study, are briefly described. The following MMP correlations are used ℃ as temperature unit.

2.6.2.1 Benham, Dowden, and Kunzman Correlation (1960)

In 1960, (Benham, Dowden, & Kunzman) created a correlation, which is the pioneer of MMP literature. They normally determined the miscibility conditions of an injection case by using two-phase ternary diagrams (methane and intermediates). However, reservoir pressures and temperatures are altered during the injection, so that the process requires building many ternary diagrams for different pressure and temperature. To solve this problem, the writers utilized five reservoir fluids and six displacement fluids, and then they used their ternary results to create correlations.

The authors considered the reservoir temperature and pressure, C5+ molecular weight of the reservoir fluid, C2+ molecular weight of the displacing fluid and mole percentage of methane in displacing fluid. Later, they created graphs, which are in range between 1000 to 3000 psi, 70 to 260 ℉, C5+ molecular weights of reservoir fluids from 180 to 240 g/mole and intermediates molecular weights of displacing fluids from 34 to 58.1 g/mole. An example of these graphs can be found in Figure 2.25. The X-axis of the graph shows reservoir temperature. The Y-axis of the graph

represents the mole percentage of methane in the displacing fluid. The curves in the graphical area distinguished according to intermediates (ethane – propane – butane) molecular weight of displacing fluids. Moreover, the curves may be severable according to molecular weight of C5+ of the reservoir fluid. After selecting the right curve, the correct temperature value must be obtained on the curve following the X-axis. Then, the Y-axis should be controlled to determine mole percentage of methane in the displacing fluid. Finally determining the mole percentage of methane, if the displacing fluid used in injection has less mole percentage of methane than determined one, the displacing fluid will be miscible in the reservoir. The graph and curves are plotted for various pressures. (Benham, Dowden, & Kunzman, 1960).

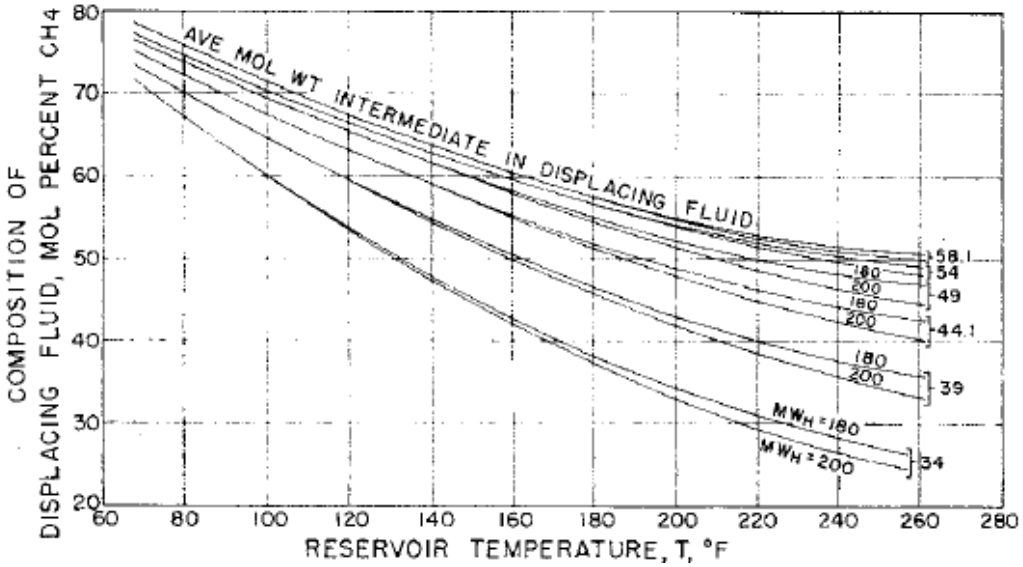

Figure 2.25. Example Benham Correlation Graph (Benham, Dowden, & Kunzman, 1960)

2.6.2.2 Holm and Josendal Correlation (1974)

Holm and Josendal (1974) created a graphical correlation based on (Benham, Dowden, & Kunzman, 1960) technique. In this method, the writers only need to know the reservoir temperature and the molecular weight of the C5+ composition. They drew a graph, where X axis is reservoir temperature and Y axis is pressure.

There are curves in the graph area, which represent different molecular weights of C5+ composition.

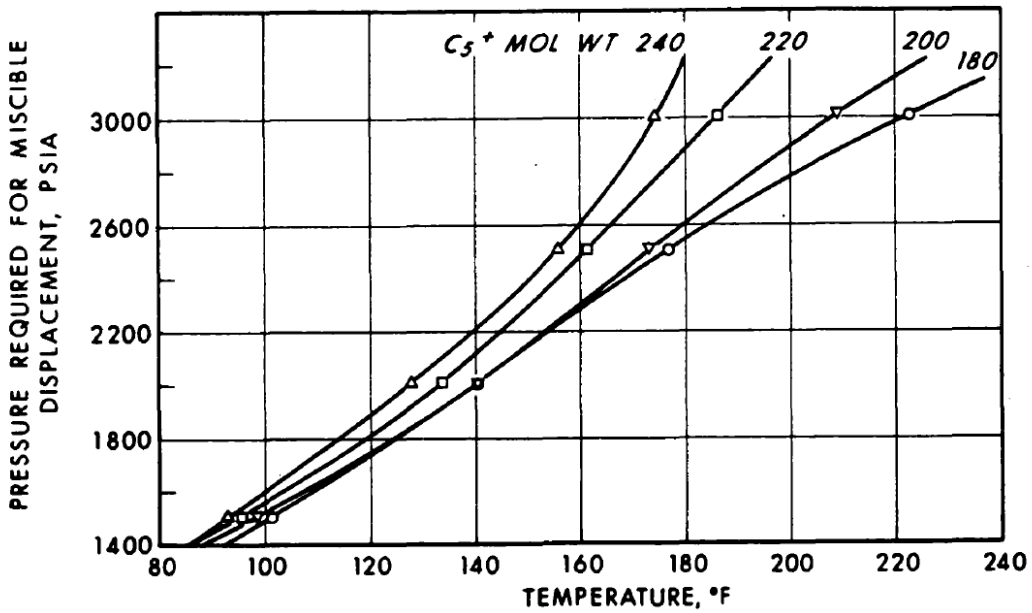

Figure 2.26. Holm and Josendal Graphical Correlation for MMP (Holm & Josendal, 1974)

2.6.2.3 Mungan Correlation (1981)

The Mungan Correlation is an updated form of Holm and Josendal's correlation. Holm and Josendal's (1974) method have limitations where are in the range of molecular weight of C5+. Therefore, it cannot be applied where molecular weight of C5+ is higher than 240. For that reason, Mungan (1981) made new calculations for 260 – 340 molecular weights of C5+ in order to extend the method. Afterwards, Mungan's and Holm – Josendal's curves are plotted together (Figure 2.27). On the other hand, the temperature and pressure limitation of this technique have continued.

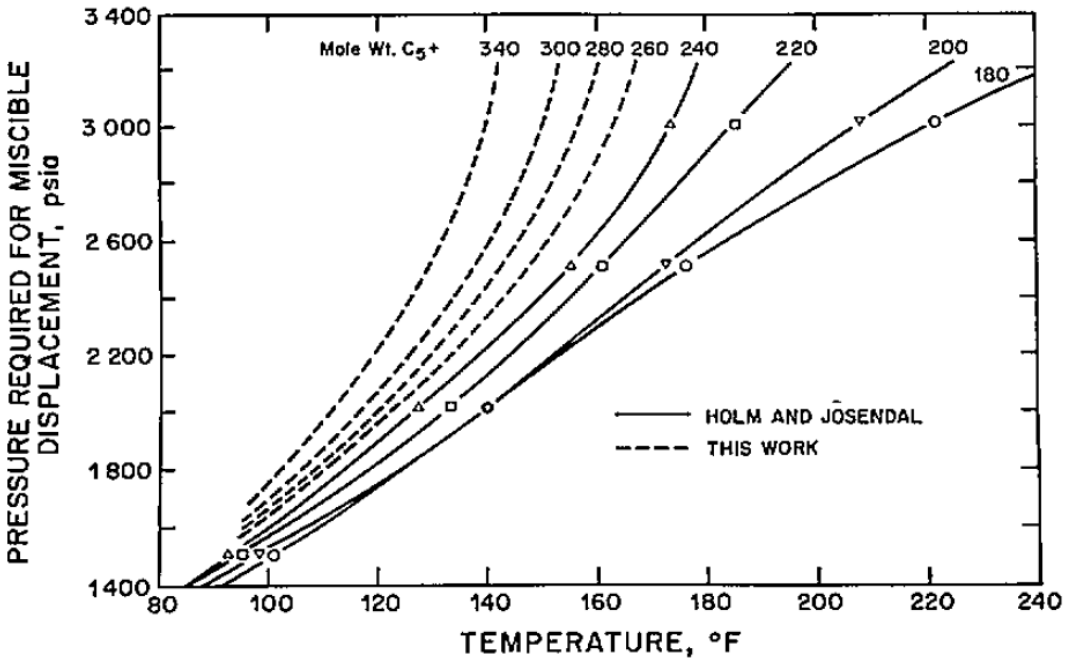

Figure 2.27. Mungan and Holm and Josendal Graphical Correlation for MMP (Mungan, 1981) (Holm & Josendal, 1974)

2.6.2.4 Cronquist Correlation (1978)

Cronquist (1978) posits an equation for determining minimum miscibility pressure. As distinct from the other correlations, the mole fraction of methane is used as a parameter in the correlation. Nevertheless, like other correlations, this method has some limitations because of the dataset that is used for creating the correlation. The dataset is laid in the ranges of 23.7 – 44 API, 21.67 – 120 ℃ and 1073.3 – 4989.3 psia (Emera & Sarma, 2004).

$$MMP = 0.1127 * (1.8T + 32)^{0.744206 + 0.0011038 * MW_{C5+} + 0.0015279 * C_1} \qquad (2.4)$$

where, T denotes Temperature (℃) (Cronquist, 1978) (Li, Qin, & Yang, 2012).

2.6.2.5 Lee Correlation (1979)

Lee (1979) correlation solely uses reservoir temperature as a parameter in the calculation. While reservoir temperature is lower than the CO_2 critical temperature, MMP is equal to vapor pressure of CO_2. If the reservoir temperature is higher or equal to CO_2 critical temperature, the correlation is utilized to obtain MMP (Lee, 1979) (Emera & Sarma, 2004). (Li, Qin, & Yang, 2012).

$$MMP = 7.3924 * 10^{2.772-[1519/(492+1.8*T)]} \quad (2.5)$$

2.6.2.6 Yellig and Metcalfe Correlation (1980)

Likewise Lee correlation, Yellig – Metcalfe (1980) correlation implements only reservoir temperature as parameter in the correlation equation. They performed slim tube experiments in the article with five different oil compositions and various temperatures. Nonetheless, the results of their slim tube experiments showed that altering compositions of oils had insignificant or no effect on the MMP. Thus, the writers created the graphical correlation, which can be seen in Figure 2.28. Furthermore, they controlled that the experimental MMP results where predicted MMP value from the correlation is lower than the bubble point pressure. They realized that in those kinds of situations experimental results are approximating the bubble point pressure. Hence, the authors put forward that if correlation computes a MMP value lower than the bubble point pressure, the bubble point pressure accepted as MMP (Yellig & Metcalfe, 1980).

The limitation of this correlation is the temperature range, which is used in experiments. The experiments were operated at 95, 118, 150 and 192 °F, so that if the reservoir temperature exceed the 192 °F, this correlation may not give correct result. The equation form of the correlation can be seen below.

$$MMP = 12.6472 + 0.01553 * (1.8T + 32) + 1.24192 * 10^{-4}(1.8T + 32)^2 - \frac{716.9427}{(1.8T + 32)} \quad (2.6)$$

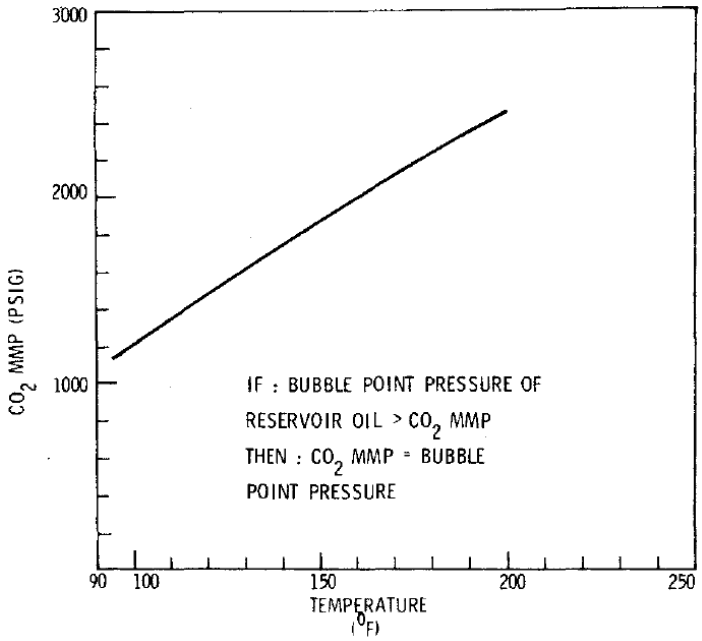

Figure 2.28. Yellig – Metcalfe MMP Correlation Graphical Display (Yellig & Metcalfe, 1980)

2.6.2.7 Orr and Jensen Correlation (1984)

Alike, Orr – Jensen (1984) correlation just utilize reservoir temperature as parameter. They worked on ternary diagram with nine different oil composition at three (32 – 41 – 49 ℃). In the light of the results of the experiments, the writers suggested that in low temperature reservoirs, extrapolated vapor pressure (EVP) of CO_2 could be used as minimum miscibility pressure. Afterwards, they put forward an equation to calculate EVP.

$$MMP = 0.101386 * e^{10.91 - \frac{2015}{255.372 + 0.5556 * (1.8T + 32)}} \quad (2.7)$$

2.6.2.8 Glasø Correlation (1985)

The correlation is derived from Benham, Dowden, & Kunzma (1960) graphical correlations. However, Glasø utilized reservoir temperature, molecular weight of C7+ components of reservoir oil and mole fraction of intermediates (C2 – C6) as parameters in the correlation equations. Moreover, the author used K factor (Watson characterization factor) correction for molecular weight of C7+, where the K factor is 11.95 or higher because this value represents paraffinicity of the oil. The K factor is laid between 10 (highly aromatic) to 13 (highly paraffinic). The equation of the K factor can be seen below (Equation 2.8). Glaso decided that 11.95 is a threshold value for the K factor. If the K factor is less than 11.95, the oil has high content of aromatic compound (Glasø, 1985) (Li, Qin, & Yang, 2012).

$$\mathrm{K}_{\mathrm{C}_{7+}} = 4.5579 * \mathrm{M}_{\mathrm{C}_{7+}}^{0.15178} * \gamma_{\mathrm{C}_{7+}}^{-0.84573} \tag{2.8}$$

$$\text{Corrected MW of } \mathrm{C}_{7+} \text{ in stock tank oil} = \left(\frac{2.622}{\gamma_{\mathrm{o,C}_{7+}}^{-0.846}}\right)^{6.588} \tag{2.9}$$

He posits that there is no effect of the intermediate compounds (C2 – C6) on the MMP value if intermediate compounds (X_{int}) mole percentage higher than %18. In such situations, Equation 2.10 is utilized as Glaso Correlation. Otherwise, Equation 2.11 is performed to predict MMP value (Glasø, 1985).

$$MMP = 5.5848 - 2.3470 * 10^{-2} MW_{C7+} + 1.1721 * 10^{-11} * MW_{C7+}^{3.73} e^{786.8 MW_{C7+}^{-1.058}} (1.8T + 32) \tag{2.10}$$

$$MMP = 20.3251 - 2.3470 * 10^{-2} MW_{C7+} + 1.1721 * 10^{-11} * MW_{C7+}^{3.73} e^{786.8 MW_{C7+}^{-1.058}} (1.8T + 32) - 8.3564 * 10^{-1} * X_{int} \tag{2.11}$$

2.6.2.9 Alston, Kokolis, and James Correlation (1985)

Before creating the empirical correlation, Alston, Kokolis, and James (1985) focused on to determine which parameters may affect MMP value. Therefore, they prepared

seven oil samples. Each oil instance has various component fractions of volatiles (X_{vol}) and intermediates (X_{int}). Because of that, they practiced slim tube experiments at 130 °F and 1500 psia for each oil sample. Then, the results of the experiment were plotted in a graph (Figure 2.29). The graph proves that changing the fraction of volatile and intermediate components has an impact on the recovery factor, so that they have impact on MMP, too (Alston, Kokolis, & James, 1985).

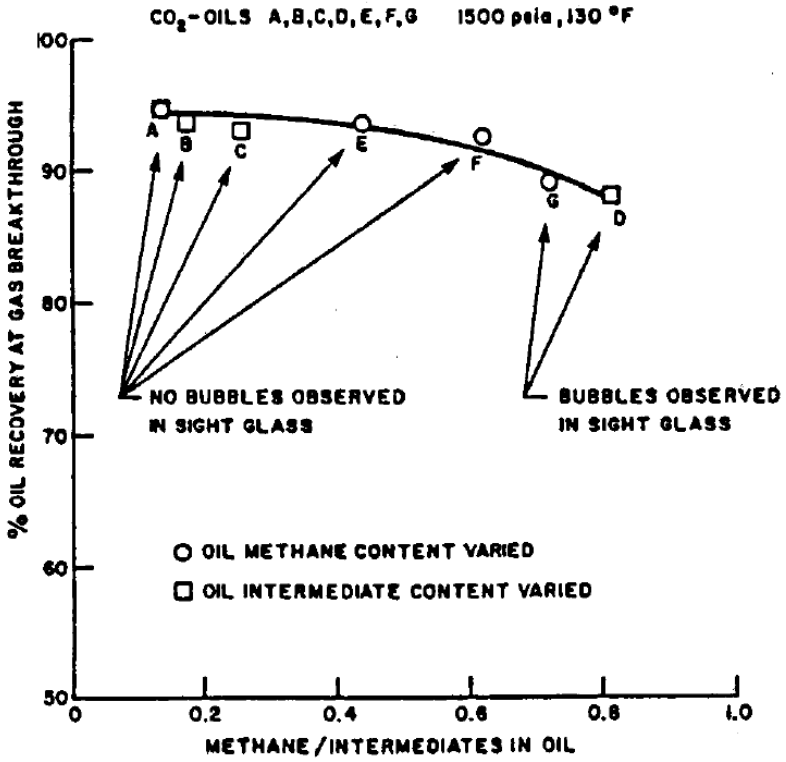

Figure 2.29. The slim tube recovery vs methane/intermediate content in oil (Alston, Kokolis, & James, 1985)

Consequently, reservoir temperature, molecular weight of C5+ components, mole fraction of volatile and intermediate components is accepted as parameters. While the volatile components are CH_4 and N_2, the intermediate components are H_2S, CO_2 and C2 through C6.

$$MMP = 6.0536 * 10^{-6}(1.8T + 32)^{1.06}(MW_{C5+})^{1.78}\left(\frac{X_{Vol}}{X_{Int}}\right)^{0.136} \qquad (2.12)$$

The authors converted their empirical correlation to a graphical method. Two graphs were plotted for graphical method. The first chart obtains MMP value as a function of molecular weight of C5+ oil and reservoir temperature (Figure 2.30). Afterward, the second graph (Figure 2.31) may be used as correction factor where mole fraction of volatile and intermediate components difference is not small (Alston, Kokolis, & James, 1985).

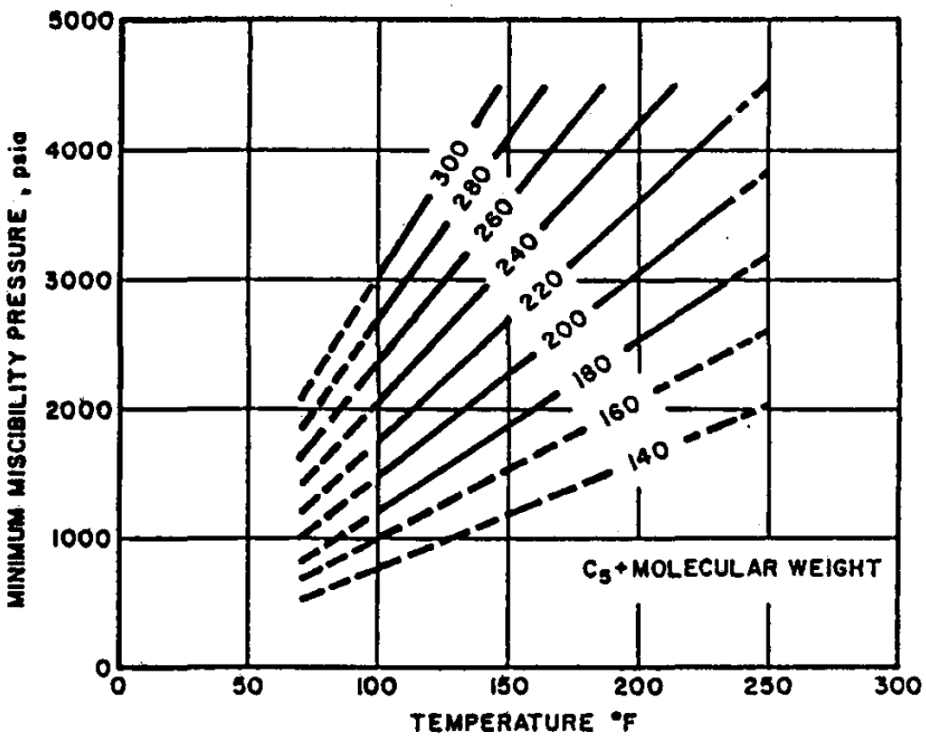

Figure 2.30. MMP vs. temperature and MW of C5+ (Alston, Kokolis, & James, 1985)

Moreover, the writers advised that if bubble point pressure is less than 50 psi (0.35 MPa), mole fraction of volatile and intermediate components might not be utilized in calculation (Equation 2.13). In addition, they suggested that if the computed MMP value is lower than bubble point pressure, bubble point pressure is accepted as MMP, similar to Yellig – Metcalfe (Alston, Kokolis, & James, 1985) (Li, Qin, & Yang, 2012).

$$MMP = 6.0536 * 10^{-6}(1.8T + 32)^{1.06}(MW_{C5+})^{1.78} \qquad (2.13)$$

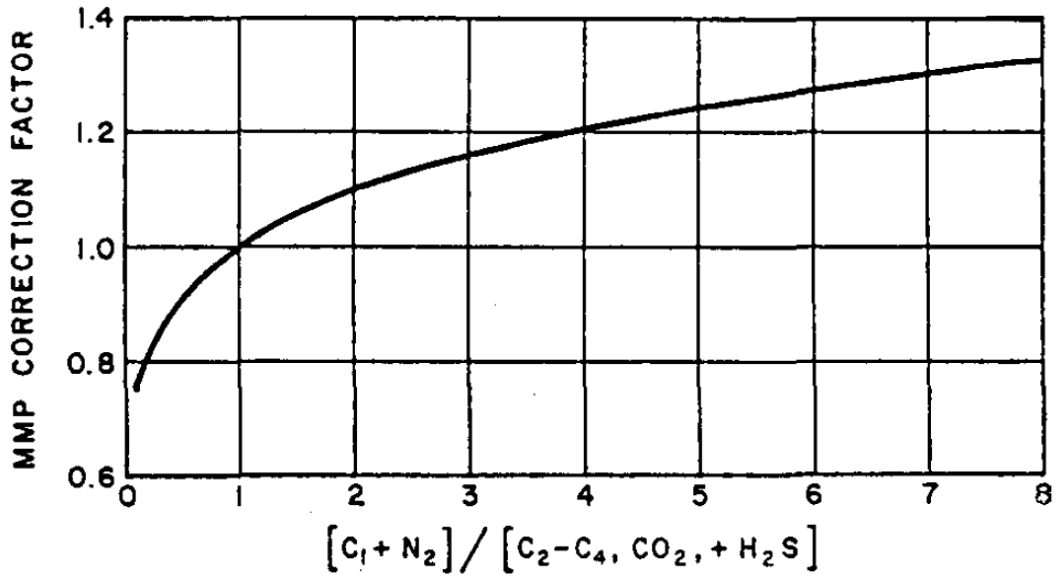

Figure 2.31. MMP correction factor (Alston, Kokolis, & James, 1985)

The test database has some restrictions. The interval of the temperatures data was 90 – 243 °F; moreover, most of pressure data in range between 1000 – 2500 psia. Hence, the correlation is accurate within this ranges (Alston, Kokolis, & James, 1985).

2.6.2.10 Emera and Sarma Correlation (2004)

Emera and Sarma (2004) is utilized genetic algorithm to determine the minimum miscibility pressure. The genetic algorithm (GA) is an artificial intelligence method, which mimicked biological evaluation process; it generates solutions until matching the desired criteria. Their genetic algorithm workflow can be seen in Figure 2.32. However, genetic algorithm is out of the scope of this study, so that there will not be further information about GA.

The writers inspected which factors affected the MMP value from the previous MMP correlations. Furthermore, they revealed their limitations if there are. After that, the authors decided to put reservoir temperature, molecular weight of C5+ oil, volatile components of oil ($CH_4 – N_2$) and intermediate components of oil (H_2S, CO_2 and C2

through C6). With these parameters, they formed the Equation 2.14 in order to obtain MMP.

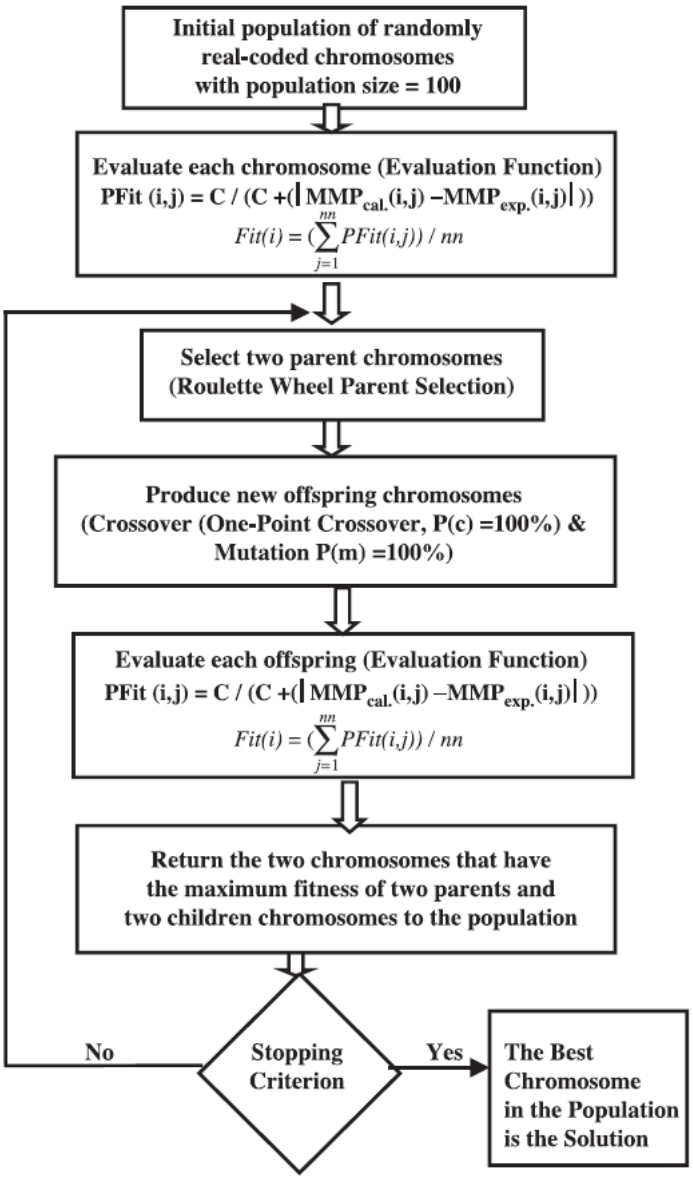

Figure 2.32. Flow chart of the genetic algorithm (Emera & Sarma, 2004)

Similar to Alston, Kokolis, and James (1985), the authors advised that if bubble point pressure is less than 50 psi (0.35 MPa), mole fraction of volatile and intermediate components might not be utilized in calculation (Equation 2.15). Additionally, they suggested that if the computed MMP value is lower than bubble point pressure,

bubble point pressure is accepted as MMP, like Yellig – Metcalfe and Alston, Kokolis and James (Emera & Sarma, 2004).

$$MMP = 5.0093 * 10^{-5}(1.8T + 32)^{1.164}(MW_{C5+})^{1.2785}\left(\frac{X_{Vol}}{X_{Int}}\right)^{0.1073} \quad (2.14)$$

$$MMP = 5.0093 * 10^{-5}(1.8T + 32)^{1.164}(MW_{C5+})^{1.2785} \quad (2.15)$$

2.6.2.11 Yuan, Johns, Egwuenu, and Dindoruk Correlation (2004)

Most of the correlations are developed as regards slim tube experiment results for MMP. However, the authors utilized analytical solutions for creating their MMP correlation. Besides, they said that most of the correlations have a linear relationship with reservoir temperature. They posited that instead of linear relationship between MMP and temperature, in high temperature region the incrementing of MMP should decrease. That decreasing can be seen in analytical solution (Figure 2.32) (Yuan, Johns, Egwuenu, & Dindoruk, 2004).

The writers formed a correlation equation by practicing seventy data, in which MMP values of them are calculated via analytical method. Then, they used 111 known MMP value, where seventy of them are analytical MMP results and the rest of forty-one values are slim tube experiment results, to determine coefficients in the equation. The writers obtained the best fit coefficients of their correlation equation. The parameters of this equation are reservoir temperature, molecular weight of C7+ components and molar fraction of intermediates, which are C2 – C6. The coefficients in the equation are given below (Yuan, Johns, Egwuenu, & Dindoruk, 2004) (Li, Qin, & Yang, 2012).

$$a_1 = -9.8912, a_2 = 4.5588 * 10^{-2}, a_3 = -3.1012 * 10^{-1}, a_4 = 1.4748 * 10^{-2},$$

$$a_5 = 8.0441 * 10^{-4}, a_6 = 5.6303 * 10^{1}, a_7 = -8.4516 * 10^{-4},$$

$$a_8 = 8.8825 * 10^{-6}, a_9 = -2.7684 * 10^{-8}\ and\ a_{10} = -6.6830 * 10^{-6}$$

$$MMP = a_1 + a_2 MW_{C7+} + a_3 X_{Int} + (a_4 + a_5 MW_{C7+} + a_6 \frac{X_{Int}}{MW_{C7+}^2}) * (1.8T + 32) + (a_7 + a_8 MW_{C7+} + a_9 MW_{C7+}^2 + a_{10} X_{Int}) * (1.8T + 32) \quad (2.16)$$

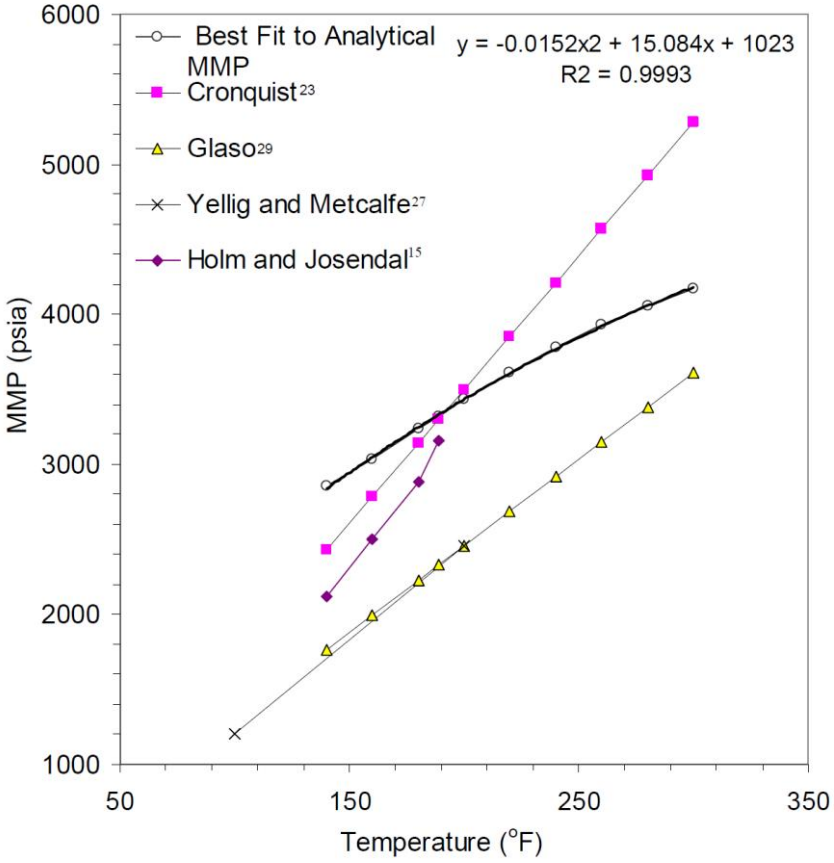

Figure 2.33. Effects of temperature to MMP for different correlations (Yuan, Johns, Egwuenu, & Dindoruk, 2004)

2.6.2.12 Shokir Correlation (2007)

Shokir (2007) practiced alternating conditional expectations (ACE) algorithm, which was developed by Breiman and Friedman (1985). It is used to obtain optimal transformations of variables in multiple regression (Shokir, 2007). There is no further information about alternating conditional expectations will be given, as it is out of scope this work. The author controlled previous MMP correlation, such as

Cronquist, Alston et al., in order to decide which parameters should be used in his correlation. After that, reservoir temperature, molecular weight of C5+ components, mole fractions of volatiles (X_{vol}) and intermediates (X_{int}) hydrocarbons were utilized as parameters. N_2 and C1 are grouped as volatile hydrocarbons; then, CO_2, H_2S, and C2 through C4 grouped as intermediates hydrocarbons. Hence, Equation 2.17 – 2.19 formed and values in Table 2.6 practiced as coefficients of Equation 2.19. Moreover, the writer applied sensitivity analysis via @Risk. Therefore, he determined which parameter has more influence on MMP correlation (Figure 2.34). Consequently, reservoir temperature is the most influential parameter to the MMP value (Shokir, 2007).

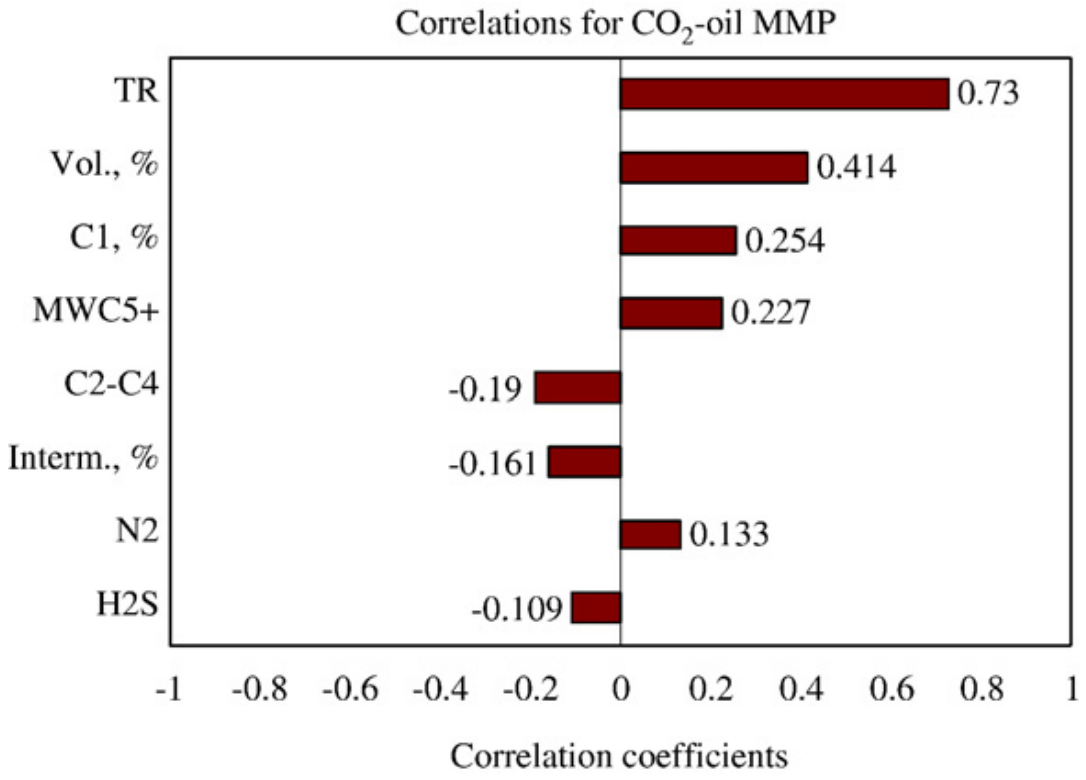

Figure 2.34. Shokir's sensitivity analysis (Shokir, 2007)

Table 2.6 Shokir Correlation coefficients for the input parameters (Shokir, 2007)

n	x	A3	A2	A1	A0
1	T_R	2.3660E-06	-5.5996E-04	7.5340E-02	-2.9182E+00
2	X_{vol}	-1.3721E-05	1.3644E-03	-7.9169E-03	-3.1227E-01
3	X_{int}	3.5551E-05	-2.7853E-03	4.2165E-02	-4.9485E-02
4	MW_{C5+}	-3.1604E-06	1.9860E-03	-3.9750E-01	2.5430E+01

$$MMP = -0.068616z^3 + 0.31733z^2 + 4.9804z + 13.432 \quad (2.17)$$

$$z = \sum_{i=1}^{4} z_i \quad (2.18)$$

$$z_i = A3y_i^3 + A2y_i^2 + A1y_i + A0_i \quad (2.19)$$

2.6.2.13 Li, Qin, and Yang Correlation (2012)

Firstly, Li, Qin, and Yang was controlled other MMP correlations in the literature. Then, they decided to take Alston et al. correlation as a base case since it is widely used in the industry. In addition, they checked Emera – Sarma correlation because it is a modified version of Alston et al. correlation. Normally, Alston et al. and Emera – Sarma correlations were applied up to 240.7 and 247.8 C5+ molecular weight. The authors put both correlation to the test with eight oil samples, which have high C7+ molecular weight. Four of these oil samples were only practiced in this article, so that they did slim tube experiments for these samples. Hence, the results demonstrated that these two correlations do not work for high C7+ molecular weight oil samples (Table 2.7). Therefore, they decided to modify the original Alston et al. correlation (Equation 2.12) with a new database, which includes 10 dead oil and 41 live oil samples and the C7+ molecular weight of this dataset is up to 402.7. Thus, the authors can modify the base correlation to compatible with high C7+ molecular weight samples. They used C7+ molecular weight in their correlation instead of C5+

one since it is a routine measurement, and it represents slightly better performance than C5+. In their calculations, they obtained that their correlation is superior to Alston et al. and Emera – Sarma correlation because of wide C7+ molecular weight range.

Table 2.7 Comparison of MMP correlations for four oil samples (Li, Qin, & Yang, 2012)

Oil	T_R (°C)	EXP (MPa)	Li et al (MPa)	Abs. Error (%)	Emera - Sarma (MPa)	Abs. Error (%)	Alston et al. (MPa)	Abs. Error (%)
A	101.6	31.3	30.55	2.39	46.94	49.97	59.98	91.62
B	99	22.3	23.86	7.01	31.58	41.63	35.65	59.88
C	108.4	27.9	29.7	6.45	43.75	56.82	53.09	90.3
D	101.6	24.1	24.31	0.88	33.39	38.56	38.17	58.38

They utilized reservoir temperature, molecular weight of C7+ oil, volatile components of oil ($CH_4 – N_2$) and intermediate components of oil (H_2S, CO_2 and C2 through C6) as parameters in their equation (Equation 2.20).

$$MMP = 7.30991 * 10^{-5}[\ln(1.8T + 32)]^{5.33647}[ln(MW_{C7+})]^{2.08836} * \left(1 + \frac{X_{Vol}}{X_{Int}}\right)^{0.201658} \quad (2.20)$$

2.7 The Correlation Coefficients

The correlation coefficients stand for relationships between two variables. There are various correlation coefficients calculation methods in literature. They demonstrate the strength of the relationship between the variables, and some techniques also show the direction of the relationship.

2.7.1 Pearson Product Moment Correlation Coefficient

The most predominantly used correlation coefficient method is Pearson Correlation Coefficient (Cohen, 1988) (Göktaş & İşçi, 2011). This method measures the strength and direction of two variables in linear condition (Figure 2.35). The results of the coefficient are in between –1 to +1. The +1 value indicates a perfect positive linear relationship and –1 value indicates a perfect negative linear relationship. If the coefficient number is zero, there is no linear correlation among the variables. The correlation is calculated with following formula, in which "n" is sample size and x_i and y_i are sample points (Fujita, et al., 2009).

$$r_p = \frac{n\sum x_i y_i - \sum x_i \sum y_i}{\sqrt{n\sum x_i^2 - (\sum x_i)^2} * \sqrt{n\sum y_i^2 - (\sum y_i)^2}} \tag{2.21}$$

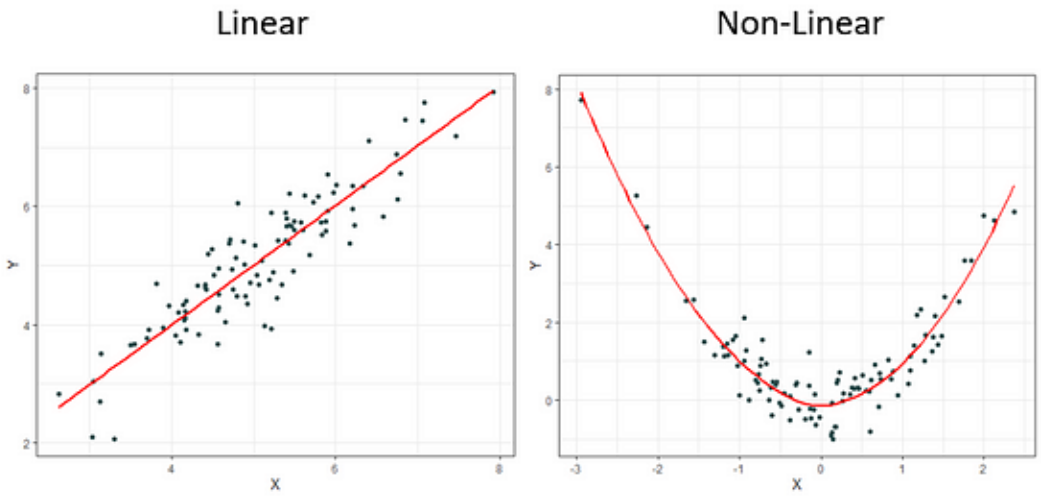

Figure 2.35. Linear and non-linear graph example (Sumner, 2024)

2.7.2 Spearman's Rank Correlation Coefficient

Spearman's method is one of the most commonly utilized correlation coefficients (Göktaş & İşçi, 2011). It is based on rank statistics, which means that the real data are ranked according to their values. Spearman's rank correlation coefficient is

utilized where variables are in monotonic relationship (Figure 2.36). In a similar way of Pearson correlation, the results of the coefficient are in between –1 to +1. The +1 value indicates a perfect positive monotonic relationship and –1 value indicates a perfect negative monotonic relationship. If the coefficient number is zero, which means that there is no correlation there. When the ranks are not tied, which means that there are no repeated values, Equation 2.22 is used to obtain Spearman's rank correlation coefficient, where the "n" is number of pairs of values and d_i is the difference between the ranked values of variables. However, if there are tied values in the ranks, Pearson correlation coefficient is utilized between ranks of the variables (Fujita, et al., 2009).

$$r_s = 1 - \frac{6 \sum d_i^2}{n(n^2 - 1)} \tag{2.22}$$

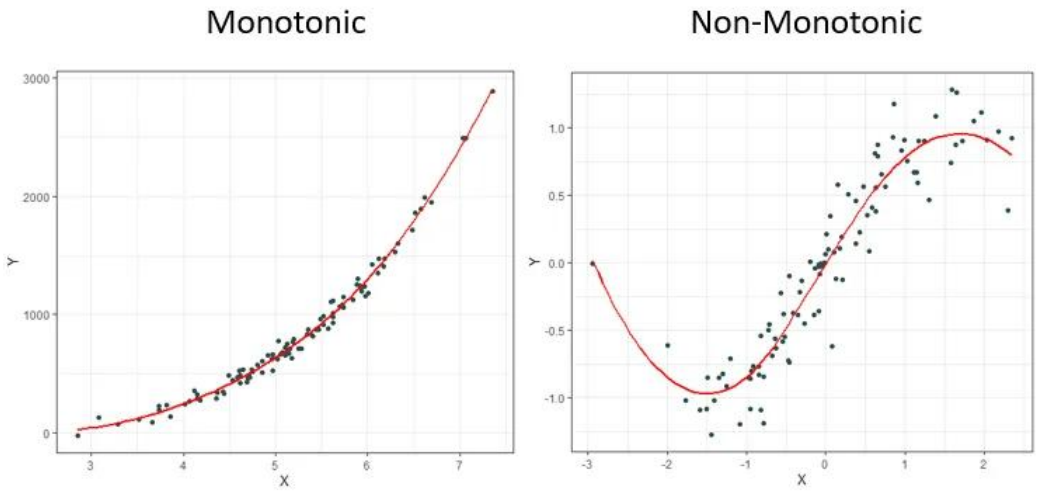

Figure 2.36. Monotonic and non-monotonic graph examples (Sumner, 2024)

2.7.3 Chatterjee's Rank Correlation Coefficient

The Chatterjee's rank correlation coefficient is developed in order to be as simple as Pearson and Spearman correlation coefficient and measure the dependency of variables. The Chatterjee correlation coefficient can also be practiced where two variables are not linear and monotonic. In such cases, Pearson and Spearman

correlation coefficients do not give the correct relationship among the variables. There are three examples to show the difference between Pearson and Chatterjee's correlation results in Figure 2.37. The results of the coefficient are ranging 0 to +1. The +1 value indicates a strong relationship and 0 value indicates a no relationship. This correlation coefficient does not specify the direction of the association of variables. The following formulas are used to determine the correlation coefficient at the presence or absence of ties, respectively. X and Y are variables, and Y is not a constant. Plus, the r_i is the rank of Y_i, that is, the number of j such that $Y_j \leq Y_i$ at Equation 2.23 The l_i is the number of j such that $Y_j \geq Y_i$ (Chatterjee, 2020).

$$\xi_n(X,Y) = 1 - \frac{3\sum_{i=1}^{n-1}|r_{i+1} - r_i|}{n^2 - 1} \tag{2.23}$$

$$\xi_n(X,Y) = 1 - \frac{n\sum_{i=1}^{n-1}|r_{i+1} - r_i|}{2\sum_{i=1}^{n} l_i(n - l_i)} \tag{2.24}$$

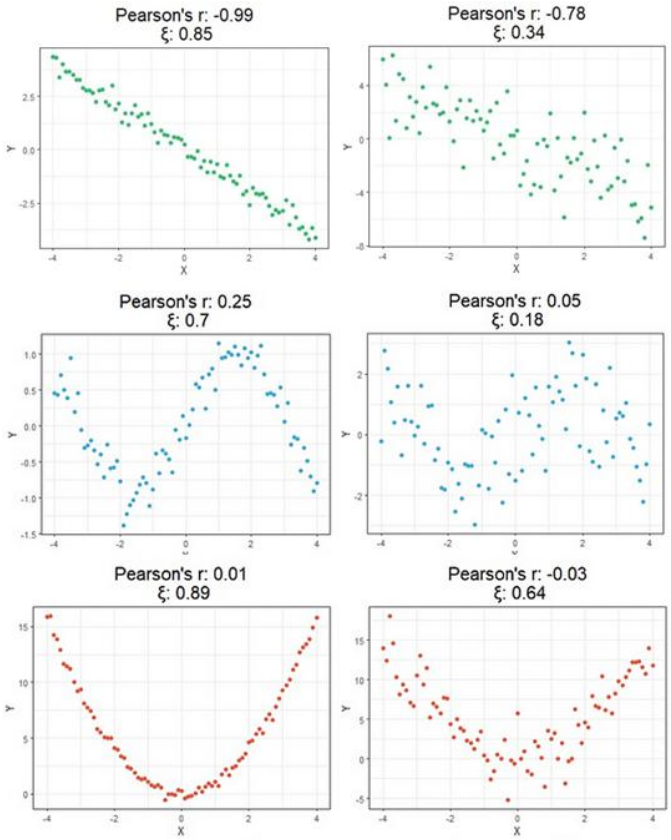

Figure 2.37. Pearson and Chatterjee Correlation comparison (Sumner, 2024)

2.8 Mass Balance Equations of Simulations

2.8.1 Black Oil Simulation Material Balance Equation

In the standard black oil model, reservoir flow consists of three pseudo-components: oil, gas, and water, distributed across three distinct phases. The oil component presents to the oil phase, the gas component can move between the oil and gas phases depending on reservoir conditions, and the water component exists solely within the water phase (Yang, Sun, Li, & Yang, 2019). The model assumes that no mass transfer occurs between the water phase and the oil and gas phases (Chen, Formulations and Numerical Methods of the Black Oil Model in Porous Media, 2001).

The mass conversion equation of these pseudo-components is given below (Chen, Huan, & Ma, 2006a). S_α, T_α, ϕ, Φ_α and B_α are saturation, transmissibility, porosity, potential, and formation volume factor of the α-phase, where α= w (water), o (oil) and g (gas). R_{so} is gas solubility, then $\rho_{\beta s}$ and q_β are density and volumetric rate of the β component, where β = w, o, g (Chen, Huan, & Ma, 2006a).

$$\frac{\partial}{\partial t}\left(\frac{\emptyset S_w}{B_w}\right) = \nabla \cdot (T_w \nabla \Phi_w) + \frac{q_{w_S}}{B_w} \tag{2.25}$$

$$\frac{\partial}{\partial t}\left(\frac{\emptyset S_o}{B_o}\right) = \nabla \cdot (T_o \nabla \Phi_o) + \frac{q_{o_S}}{B_o} \tag{2.26}$$

$$\frac{\partial}{\partial t}\left[\phi\left(\frac{S_g}{B_g} + \frac{(R_{so}S_o)}{B_o}\right)\right] = \nabla \cdot \left(T_g \nabla \Phi_g + R_{so} T_o \nabla \Phi_o\right) + \frac{q_{Gs}}{B_g} + \frac{q_{Os} R_{so}}{B_o} \tag{2.27}$$

2.8.2 Miscible Flood Modeling in Black Oil Simulator

The miscible flood model is based on the empirical approach proposed by Todd and Longstaff (1972). Therefore, Eclipse Black Oil (E100) miscible models are used Todd and Longstaff implementations. It used three component system reservoir oil,

injected gas, and water. Normally, the injected gas and reservoir oil components are assumed to be completely miscible in all proportions, resulting in the presence of only a single hydrocarbon phase within the reservoir. However, PMISC keyword controls miscibility according to reservoir pressure (SLB, 2023). They suggested that an empirical parameter, which is ω and it changes between 0 to 1, to alteration of the viscosity and density calculations in black oil simulations (SLB, 2023).

The effective oil and miscible gas viscosities are calculated by the following formula.

$$\mu_{oeff} = \mu_o^{1-\omega} - \mu_m^{\omega} \tag{2.28}$$

$$\mu_{geff} = \mu_g^{1-\omega} - \mu_m^{\omega} \tag{2.29}$$

$$\mu_m = \frac{(\mu_o \mu_g)}{\left(\frac{S_g'}{S_n'} \cdot \mu_o^{\frac{1}{4}} + \frac{S_o'}{S_n'} \cdot \mu_g^{\frac{1}{4}}\right)} \tag{2.30}$$

where

$$S_o' = S_o - S_{or}, \qquad S_g' = S_g - S_{gc}, \qquad S_n' = S_o' + S_g'$$

The density calculation with mixing parameters is made after the viscosity calculation using the following equations (SLB, 2023).

$$\left(\frac{S_o}{S_n}\right)_{oe} = \frac{\mu_o^{\frac{1}{4}}(\mu_{oeff}^{\frac{1}{4}} - \mu_g^{\frac{1}{4}})}{\mu_{oeff}^{\frac{1}{4}}(\mu_o^{\frac{1}{4}} - \mu_g^{\frac{1}{4}})} \tag{2.31}$$

$$\left(\frac{S_o}{S_n}\right)_{ge} = \frac{\mu_o^{\frac{1}{4}}(\mu_{geff}^{\frac{1}{4}} - \mu_g^{\frac{1}{4}})}{\mu_{geff}^{\frac{1}{4}}(\mu_o^{\frac{1}{4}} - \mu_g^{\frac{1}{4}})} \tag{2.32}$$

Then, the effective oil and gas densities are calculated from findings of Equation 2.31 and 2.32 (SLB, 2023).

$$\rho_{oeff} = \rho_o \left(\frac{S_o}{S_n}\right)_{oe} + \rho_g \left[1 - \left(\frac{S_o}{S_n}\right)_{oe}\right] \tag{2.33}$$

$$\rho_{geff} = \rho_o \left(\frac{S_o}{S_n}\right)_{oe} + \rho_g \left[1 - \left(\frac{S_o}{S_n}\right)_{ge}\right] \quad (2.34)$$

SDENSITY keyword is used to define ρ_g value, which is injected gas density at surface (SLB, 2023).

2.8.3 Compositional Simulation Material Balance Equation

Several assumptions are defined for compositional simulation equations. First, the flow process is considered isothermal. Second, no mass transfer occurs between the water phase and the oil and gas phases. Lastly, diffusive effects are neglected (Chen, Huan, & Ma, 2006b).

S_α, μ_α, ϕ, k, ρ_α, u_α and $k_{r\alpha}$ are saturation, viscosity, porosity, permeability, pressure, volumetric velocity, formation volume factor, and relative permeability of the α-phase, where α= w (water), o (oil) and g (gas). Furthermore, ξ_{io} and ξ_{ig} indicate molar densities of component i in liquid (oil) and vapor (gas) phases, respectively. The molar density of phase α, where N_c is the number of components (Chen, Huan, & Ma, 2006b).

$$\xi_\alpha = \sum_{i=1}^{N_c} \xi_{i\alpha}, \qquad \alpha = o, g. \quad (2.35)$$

$$x_{i\alpha} = \frac{\xi_{i\alpha}}{\xi_\alpha}, \qquad i = 1,2,\ldots.,N_c, \qquad \alpha = o, g. \quad (2.36)$$

$$\frac{\partial}{\partial t}(\phi \xi_w S_w) + \nabla \cdot (\xi_w u_w) = q_w, \quad (2.37)$$

$$\frac{\partial}{\partial t}\left(\phi\left[x_{io}\xi_o S_o + x_{ig}\xi_g S_g\right]\right) + \nabla \cdot \left(x_{io}\xi_o u_o + x_{ig}\xi_g u_g\right) = x_{io}q_o + x_{ig}q_g, \qquad i = 1,2,\ldots.,N_c, \quad (2.38)$$

CHAPTER 3

STATEMENT OF PROBLEM

Enhanced oil recovery (EOR) using CO_2 injection is a widely researched and applied method for improving oil recovery. However, the efficiency of this technique is heavily influenced by various reservoir and fluid properties, including porosity, permeability, API gravity, reservoir pressure, and temperature. A critical factor in miscible CO_2 injection is achieving the minimum miscibility pressure (MMP), which determines whether the process operates under miscible or immiscible conditions.

The main aim of this study is to perform black oil simulations for both miscible and immiscible CO_2 injection using uncertainty runs to investigate the effect of the screening parameters on the recovery factor. While existing studies typically focus on individual reservoirs or fluid types, a more comprehensive approach is required to evaluate a diverse range of fluid samples and their interaction with reservoir parameters is needed to understand their combined impact on recovery factor. For this, five different fluid samples were selected to represent a wide range of API gravities. Reservoir temperature and pressure, oil viscosity and API gravity were altered with every fluid sample. Furthermore, porosity and permeability were chosen as uncertain screening parameters. The combined effects of both on recovery factor were analyzed by uncertainty analyses.

To determine the minimum miscibility pressure (MMP), slim tube simulations and various empirical correlations were employed, with the most suitable results incorporated into the black oil simulations.

Uncertainty runs for porosity and permeability were executed using Petrel's Uncertainty and Optimization (U&O) tool, with parameter limits derived from screening criteria in the literature. Furthermore, sensitivity analyses were conducted for reservoir pressure and temperature with one of the fluid samples to understand

their impact on the recovery factor. Finally, Pearson, Spearman Rank and Chatterjee Rank Correlations were implemented to quantify the relationship between the parameters and recovery factor for both miscible and immiscible runs.

CHAPTER 4

THE FLUID SAMPLES

4.1 The Fluid Samples

In this study, there are five different reservoir fluid samples, which are taken from databases, articles, and books, and are worked. The samples are selected by their API gravity in order to satisfy the screening requirements of miscible and immiscible carbon dioxide injection, which are given at Table 2.4 and 2.5. The names of the fluid samples are F2, F5, D1, H1 and M3. API gravity of F5 and H1 are given in the source materials. However, API gravity of other fluid samples, F2, D1 and M3, are calculated by using density data of each component, but there is no density value for some components in the reference article, in such a case, the density value of that certain component in PVTi component library is utilized for computation. The temperature refers to the reservoir temperature of the fluid which is taken from. Additionally, I assumed that these temperatures were measured at a depth of -2000 meters, which is reservoir entrance depth of this study. In Table 4.1, reservoir temperature and API gravity of the fluids are shown. Furthermore, the compositions of reservoir fluid samples can be seen in Table 4.2 to 4.6.

Table 4.1 Reservoir temperature and API gravity of fluid samples derived from (Jaubert, Avaullee, & Souvay, 2002) (Danesh, 1998) (Krejbjerg & Pedersen, 2006) (Elsharkawy, 2003)

	F2	*F5*	*D1*	*H1*	*M3*
Temperature, ℃	115.0	121.1	110.0	52.0	81.11
API Gravity	37.446	31.914	47.88	10.0	24.058

Table 4.2 F2 Fluid Sample Properties (Jaubert, Avaullee, & Souvay, 2002)

Components	**Mole Percentage (%)**	**Molar Weight (g/mole)**	**Density (kg/m^3)**
H_2S	0.0		
N_2	0.20		
CO_2	1.34		
C1	23.64		
C2	8.56		
C3	6.68		
iC4	1.25		
nC4	4.05		
iC5	1.78		
nC5	2.67		
C6	4.03	86.0	667.5
C7	4.57	96.0	712.0
C8	4.28	108.0	736.4
C9	3.88	122.0	756.6
C10	2.93	136.0	775.3
C11	3.15	145.0	790.9
C12	3.19	157.0	797.6
C13	3.05	175.0	814.0
C14	1.16	198.0	832.6
C15	1.98	213.0	837.6
C16	1.72	225.0	842.4
C17	1.60	237.0	846.4
C18	1.16	248.0	853.6
C19	1.10	280.0	861.1
C20+	12.03	530.0	949.3

Table 4.3 F5 Fluid Sample Properties (Jaubert, Avaullee, & Souvay, 2002)

Components	**Mole Percentage (%)**	**Molar Weight (g/mole)**	**Density (kg/m^3)**
H_2S	0.383		
N_2	0.45		
CO_2	2.07		
C1	26.576		
C2	7.894		
C3	6.73		
iC4	1.485		
nC4	3.899		
iC5	1.937		
nC5	2.505		
C6	3.351	86.2	679.4
C7	4.311	92.6	726.2
C8	4.133	108.9	750.9
C9	3.051	120.1	771.6
C10	2.033	137.9	787.8
C11	2.635	149.0	803.7
C12	2.285	163.0	815.4
C13	2.364	177.0	827.0
C14	2.038	191.0	841.2
C15	1.752	205.0	858.8
C16	1.589	219.0	862.7
C17	1.492	234.0	858.6
C18	1.263	248.0	864.8
C19	0.812	263.0	877.1
C20+	12.962	450.0	956.0

Table 4.4 D1 Fluid Sample Properties (Danesh, 1998)

Components	Mole Percentage (%)	Molar Weight (g/mole)	Density (kg/m^3)
H_2S	0.0		
N_2	0.69		
CO_2	0.12		
C1	47.090		
C2	5.690		
C3	4.390		
iC4	0.950		
nC4	2.420		
iC5	1.110		
nC5	1.460		
C6	2.260		
C7	3.930	91.9	735.0
C8	4.520	105.2	745.0
C9	3.230	121.0	784.0
C10	2.300	133.0	789.0
C11	2.030	148.0	794.0
C12	1.880	163.0	806.0
C13	1.620	177.0	819.0
C14	1.760	190.0	832.0
C15	1.390	204.0	834.0
C16	1.030	217.0	844.0
C17	1.220	235.0	841.0
C18	0.850	248.0	847.0
C19	0.970	260.0	860.0
C20	0.320	269.4	874.0
C21	0.800	282.5	870.0
C22	0.530	297.7	872.0

Table 4.4 (Cont'd)

C23	0.440	310.1	875.0
C24	0.340	321.8	877.0
C25	0.480	332.4	881.0
C26	0.390	351.1	886.0
C27	0.310	370.8	888.0
C28	0.300	381.6	895.0
C29	0.240	393.7	898.0
C30+	2.940	612.0	935.0

Table 4.5 H1 Fluid Sample Properties (Krejbjerg & Pedersen, 2006)

Components	**Mole Percentage (%)**	**Molar Weight (g/mole)**	**Density (kg/m^3)**
H_2S	0		
N_2	0		
CO_2	1.44		
C1	0.14		
C2	0.03		
C3	0.01		
iC4	0.01		
nC4	0.01		
iC5	0.27		
nC5	0.41		
C6	0.13		
C7	0.32	96.0	722.0
C8	0.45	107.0	745.0
C9	0.9	121.0	764.0
C10	1.45	134.0	778.0
C11	1.97	147.0	789.0

Table 4.5 (Cont'd)

C12	2.5	161.0	800.0
C13	2.57	175.0	811.0
C14	2.86	190.0	822.0
C15	2.91	206.0	832.0
C16	2.96	222.0	839.0
C17	2.99	237.0	870.0
C18	3.07	251.0	852.0
C19	2.72	263.0	857.0
C20	2.59	275.0	862.0
C21	2.47	291.0	867.0
C22	2.31	305.0	872.0
C23	2.12	318.0	877.0
C24	1.96	331.0	881.0
C25	0.14	345.0	885.0
C26	1.77	359.0	889.0
C27	1.68	374.0	893.0
C28	1.82	388.0	896.0
C29	1.64	402.0	899.0
C30	1.63	416.0	902.0
C31	1.36	430.0	906.0
C32	1.33	444.0	909.0
C33	1.12	458.0	912.0
C34	1.19	472.0	914.0
C35	1.0	486.0	917.0
C36+	25.17	1038.1	1104.0

Table 4.6 M3 Fluid Sample Properties (Elsharkawy, 2003)

Components	Mole Percentage (%)	Molar Weight (g/mole)	Density (kg/m^3)
H_2S	0.34		
N_2	0.1		
CO_2	1.32		
C1	8.86		
C2	4.13		
C3	5.41		
iC4	1.955		
nC4	1.955		
iC5	1.725		
nC5	1.725		
C6	3.81		
C7+	68.67	243.0	934.0

Subsequently, to shorten the run time of simulations, some components were grouped. PVTi, which is a pre-processor of Eclipse to handle PVT data and simulate the PVT experiments, was utilized for grouping the components and calculated their mole percentages, mol weights and other required data.

The first group is X_{vol}, which consisted of N_2 and CH_4. It characterized the volatile (light) component of the fluid (Alston, Kokolis, & James, 1985) (Emera & Sarma, 2004) (Shokir, 2007).

The second group is C2+ which consisted of C2 to C6 hydrocarbons. The second group depicts intermediate fractions (Glasø, 1985) (Yuan, Johns, Egwuenu, & Dindoruk, 2004).

The next two components are H_2S, and CO_2 that are added as pure component. The initial CO_2 mole fraction had entered separately to simulation because in the

experiment carbon dioxide is used as injection fluid. Furthermore, H_2S had input solitary because of no H_2S in some samples.

The remaining group of compounds is C7+, which holds hydrocarbons where carbon numbers are seven and higher than seven. This group generally considered the heavy components of crude oil (Yellig & Metcalfe, 1980) (Whitson, 1983). Excepting M3 fluid sample, other fluids have many C7+ hydrocarbon compounds. Like hereinbefore, the number of C7+ components should be grouped. For grouping these compounds, a lumping method is needed. In 2013, Moghadamzadeh, et al. (2013) are compared five lumping scheme methods, which are Whitson, Pedersen, Danesh et al., Lee et al. and Behras and Stanndler method, by plotting the phase diagrams of components before and after the lumping. Consequently, they obtained that Lee et al. method can predict almost the exact phase diagram. Nevertheless, it is more complex compared to other methods. Therefore, the second-best method, Whitson's lumping method, was chosen to use in this thesis. The method was created by Whitson (1983) in order to reduce the number of components without losing the composition main characteristics (Whitson, 1983). The method consists of the following two equations. Equation 4.1 is intended to determine how many multi carbon number groups (MCN) are required for correct lumping. Equation 4.2 is utilized to obtain the molecular weight separation value for each MCN group. Like Bender (2016), C7 to Cn+ components lumped into two groups, which means that N_G is equal to 2. The calculation results of Equation 4.2 can be seen in Table 4.7. Afterward, a newly grouped version of the fluids is shown in Table 4.8 to 4.12.

$$N_G = Int[1 + 3.3\log(N - n)] \tag{4.1}$$

where,

N_G = number of MCN groups

N = number of carbon atoms of the last component in the plus fraction

n = number of carbon atoms of the first component in the plus fraction.

$$Mw_I = Mw_n \left(\frac{Mw_N}{Mw_n}\right)^{\frac{1}{N_G}} \quad (4.2)$$

where,

Mw_I = Molecular weight

Mw_n = Molecular weight of first component in the plus fraction

Mw_N = Molecular weight of last component in the plus fraction

The simulator required more information of each grouped component, such as critical temperature and pressure, Z factor at critical points and binary coefficients. These kinds of parameters are calculated by using PVTi for each component for each fluid sample. These data were tabulated in Appendix A: Extended Data of Fluid Samples.

Table 4.7 Parameters and results of Equation 4.2

	F2	*F5*	*D1*	*H1*
Mw_n, g/mole	96.0	92.6	91.9	96.0
Mw_N, g/mole	530.0	450.0	612.0	1038.1
Mw_I, g/mole	225.566	204.132	237.156	315.686

Table 4.8 Grouped components of F2

Components	**Mole Percentage (%)**	**Molar Weight (g/mole)**	**Density (kg/m^3)**
H_2S	0.0	34.076	993.0
CO_2	1.34	44.010	777.0
XVOL	23.84	16.143	428.18
C2+	29.02	52.642	588.80
C7+	28.19	138.90	772.45
C16+	17.61	439.40	918.37

Table 4.9 Grouped components of F5

Components	Mole Percentage (%)	Molar Weight (g/mole)	Density (kg/m^3)
H_2S	2.07	34.076	993.00
CO_2	0.383	44.010	777.00
XVOL	27.026	16.242	431.31
C2+	27.801	52.388	589.01
C7+	22.850	134.30	781.53
C15+	19.870	373.22	924.56

Table 4.10 Grouped components of D1

Components	Mole Percentage (%)	Molar Weight (g/mole)	Density (kg/m^3)
H_2S	0.0	34.076	993.00
CO_2	0.12	44.010	777.00
XVOL	47.78	16.216	430.47
C2+	18.28	51.194	588.28
C7+	24.91	142.72	785.86
C18+	8.91	403.87	892.34

Table 4.11 Grouped components of H1

Components	Mole Percentage (%)	Molar Weight (g/mole)	Density (kg/m^3)
H_2S	0.0	34.076	993.00
CO_2	1.44	44.010	777.00
C1	18.72	16.043	425.00
C2+	0.88	69.702	638.19
C7+	32.86	226.04	839.24
C23+	46.10	743.70	1010.20

Table 4.12 Grouped components of M3

Components	**Mole Percentage (%)**	**Molar Weight (g/mole)**	**Density (kg/m^3)**
H_2S	0.34	34.076	993.00
CO_2	1.32	44.010	777.00
XVOL	8.96	16.177	429.23
C2+	9.54	38.025	567.28
C4+	11.17	71.283	624.90
C7+	68.67	243.00	934.00

CHAPTER 5

RESERVOIR SIMULATION

5.1 Building the Reservoir Simulation Model

The reservoir simulation models of miscible and immiscible cases were created by using Petrel. The model was formed at constant depth, which is 2000 meters. Various reservoir fluids are used in simulation, so that temperature and pressure values were changed with reservoir fluid types. There are two main assumptions made about temperature. First, the reservoir is isothermal. The black oil models cannot solve the energy balance equations. Therefore, the temperature changes inside the reservoir only happen because of the temperature gradient. Second, when the injected carbon dioxide enters the reservoir, the temperature of it is equal to the reservoir temperature of reservoir fluid sample being studied at that time. Additionally, all the injected carbon dioxide is in supercritical phase since all the reservoir pressure and temperature values are higher than critical point value of CO_2, which is 31.1℃ and 73.77 bars (Charles University, 2024). Besides, the models are run in a black oil simulator, which is Eclipse 100, so that carbon dioxide is not soluble in water in this study because of the limitation of black oil models. For this reason, salinity cannot affect CO_2 solubility in water. Metric system units were utilized in these simulations.

5.1.1 Grid of the Reservoir and Wells

The field, which is utilized for simulation, is a cube with 10 x 10 x 10 grids measuring. Thus, the simulated field contains 1000 active grids. The X and Y axes of the field are 300 meters long and the Z axis is 50 meters depth. The dimension of each grid is 30m x 30m x 5m.

Two wells were added to the field. Both wells were placed in the middle of a grid at opposite corners. This design is a quarter five spot well placement pattern (Figure 5.1). The first well is a gas injection well, which is located at (15,15) point on X and Y axes, the depth of the well is -2015 meters. The second well is an oil production well, which is located at (285, 285) point on X and Y-axes. The depth of the production well is -2035 meters. Both wells are completed as open-hole in the reservoir section.

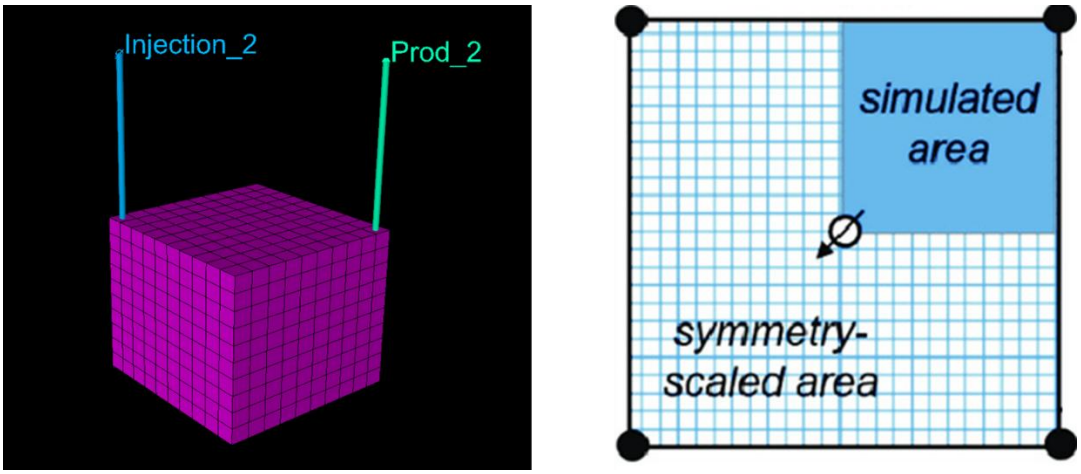

Figure 5.1. Petrel view of the reservoir with wells and 5-spot pattern schematic

5.1.2 Reservoir Fluid and Rock Properties

Three phase fluid model is used in this study. This means that gas, oil, and water are present inside the reservoir. In fluid models, minimum, maximum, reference and contact pressure, reservoir temperature, API gravity of oil, bubble point pressure, gas specific gravity, water salinity and initial conditions with contacts must be defined.

Reservoir temperature and API gravity of oil altered with fluid samples. Gas specific gravity and water salinity values are constant for each fluid sample.

Minimum pressure means that the reservoir pressure could be as low as that value and cannot continue to drop below from this point. Maximum pressure means that

the reservoir pressure could be as high as that value and cannot continue to increase above to this value (SLB, 2010).

Reference pressure is typically the initial pressure of the reservoir (SLB, 2010). In this study, reference pressure and bubble point pressure values are always equal to the minimum pressure values of current fluid sample. Hence, there is no gas production from initial gas in place.

Contact pressure represents pressure value at datum depth, which is always gas-oil contact (GOC) in our cases (SLB, 2010). Additionally, contact pressure should be in between minimum and maximum pressure values.

Furthermore, water oil contact (WOC) and gas oil contact (GOC) have to be described in the simulation to detect simulation may or may not produce water and gas in the initial reservoir system. Hence, the contact depth of initial conditions are always -2000 meters and -2050 meters for gas-oil contact (GOC) and water-oil contact (WOC), respectively. Thanks to these contact values, in simulation runs, there is no water production from the initial water in place since the depth values are top and bottom of the reservoir.

Aforementioned, there are five different reservoir fluids presented. Therefore, the necessary values for fluid model are described for each fluid sample differently. When defining pressure values, I decided to use three fundamental rules, which are seen in the following equations. The calculation results of the MMP values are explained in Chapter 6.1.

$$Minimum\ Pressure = MMP + 10\ bars \tag{5.1}$$

$$Contact\ Pressure = Minimum\ Pressure * 1.1 \tag{5.2}$$

$$Maximum\ Pressure = Minimum\ Pressure * 1.2 \tag{5.3}$$

Equation 5.1 is only valid for miscible cases. Equation 5.2 and Equation 5.3 are valid for both miscible and immiscible cases. The maximum pressure value of the

immiscible cases must not exceed the MMP value, thus; minimum pressure is selected accordingly.

The values of mentioned fluid properties are tabulated for miscible and immiscible cases in Table 5.1 and 5.2, respectively.

Table 5.1 Fluid model properties for each fluid samples for miscible cases

Properties for Miscible Case	**F2**	**F5**	**D1**	**M3**
MMP, bar	286.846	335.249	271.387	428.09
Min Pressure, bar	297.0	345.0	281.0	438.0
Max Pressure, bar	356.4	414.0	337.2	525.6
Ref. Pressure, bar	297.0	345.0	281.0	438.0
Temperature, ℃	115	121.1	110.0	81.11
GOC, m	-2000	-2000	-2000	-2000
WOC, m	-2050	-2050	-2050	-2050
Cont. Pressure, bar	326.7	379.5	309.1	481.8
API	37.446	31.914	47.88	24.058
Bubble P. Pressure, bar	297.0	345.0	281.0	438.0
Gas SG	0.6636	0.6636	0.6636	0.6636
Water Salinity, ppm	30,000	30,000	30,000	30,000

Table 5.2 Fluid model properties for each fluid samples for immiscible cases

Properties for Immiscible Case	**F2**	**F5**	**D1**	**H1**	**M3**
MMP, bar	286.846	335.249	271.387	-	428.09
Min Pressure, bar	200.0	250.0	210.0	250.0	340.0
Max Pressure, bar	240.0	300.0	252.0	300.0	408.0
Ref. Pressure, bar	200.0	250.0	210.0	250.0	340.0
Temperature, ℃	115	121.1	110.0	52.0	81.11
GOC, m	-2000	-2000	-2000	-2000	-2000
WOC, m	-2050	-2050	-2050	-2050	-2050

Table 5.2 (Cont'd)

Cont. Pressure, bar	220.0	275.0	231.0	275.0	374.0
API	37.446	31.914	47.88	10	24.058
Bubble P. Pressure, bar	200.0	250.0	210.0	250.0	340.0
Gas SG	0.6636	0.6636	0.6636	0.6636	0.6636
Water Salinity, ppm	30,000	30,000	30,000	30,000	30,000

The rock properties of the reservoir were created in Petrel. The saturation functions of the reservoir were described by "Sand" preset of Petrel since according to Table 2.4 and Table 2.5, the formation type of the reservoir has no significant effect on the miscible and immiscible CO_2 injection. For the rock compaction data, "consolidated sandstone" preset was used, but the minimum, maximum, reference pressure, and porosity values were entered by author. These values are the same as Table 5.1 and Table 5.2 ones. The saturation functions of the reservoir, which means that relative permeability values, were not changed with fluid samples in order to compare them in the end. However, the rock compaction data were altered with fluid samples because each fluid sample has different reservoir pressure values. Consequently, the simulation has one relative permeability data but various in rock compaction. The saturation values are tabulated at Table 5.3 and the relative permeability curves were plotted, and it can be seen in Figure 5.2.

Table 5.3 Petrel Sand preset saturation table values

Sgcr = 0.05	Sorw = 0.2	Swmin = 0.2
Corey gas = 6	Sorg = 0.2	Swcr = 0.22
Krg@Swmin = 0.9	Corey O/W =3	Corey water =4
Krg@Sorg = 0.8	Corey O/G =3	Kro@Sorw = 0.8
	Kro@Somax = 0.9	Krw@S =1

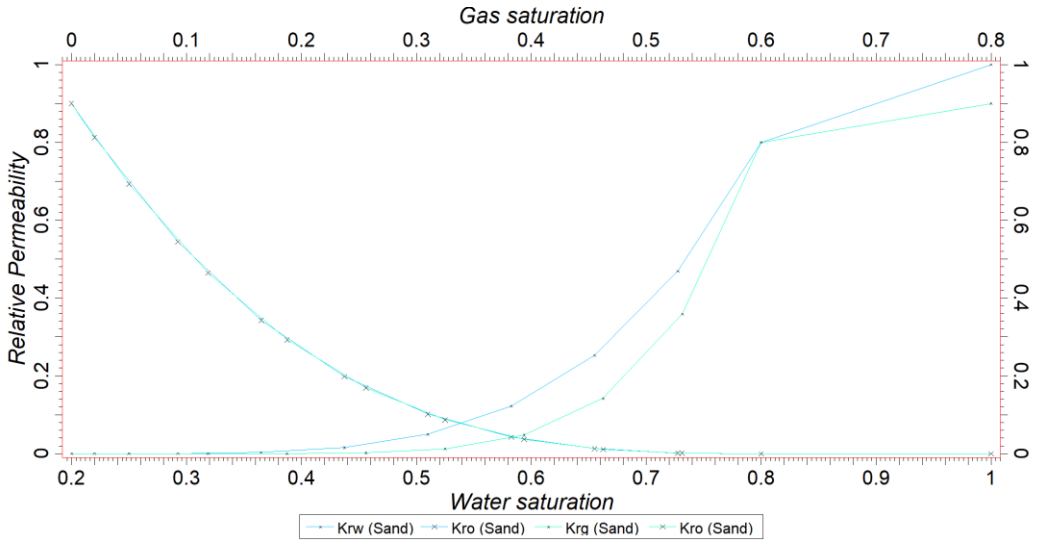

Figure 5.2. Relative permeability curves of simulation

5.1.3 The Development Strategy

Production well and gas injection well were included in the simulation, and they will work for five years. Like production well, the injection well continues to work for five years. Both wells started and stopped together. As mentioned before, the bubble point pressure was assigned as minimum pressure of the reservoir, which is also the minimum bottomhole pressure of the production well. The bottomhole pressure of the production well cannot go below this limitation. Thus, there is no initial gas production. In addition, the maximum pressure of the reservoir was utilized as maximum bottomhole injection pressure to the injection well. Therefore, bottomhole pressure of the injection well cannot go above this value instead of that simulation will change the injection rate, which is normally constant. These bottomhole pressures are altered according to fluid samples, and they can be seen individually for miscible and immiscible cases at Table 5.4 and 5.5.

Table 5.4 Bottomhole pressures of wells at miscible cases

	F2	*F5*	*D1*	*M3*
Injector well maximum BHP, bars	356.4	414.0	337.2	525.6
Production well minimum BHP, bars	297.0	345.0	281.0	438.0

Table 5.5 Bottomhole pressures of wells at immiscible cases

	F2	*F5*	*D1*	*H1*	*M3*
Injector well maximum BHP, bars	240.0	300.0	252.0	300.0	408.0
Production well minimum BHP, bars	200.0	250.0	210.0	250.0	340.0

The injection rate was selected 60,000 m^3 per day since an on-going CO_2 injection project in Türkiye has injected 1 – 2 MMscf per day (28,316.84 – 56,633.69 m^3/day) (Şahin, Kalfa, & Çelebioğlu, 2008).

Furthermore, there was no water production in simulation results but just in case, water cut constrain, which is 0.001, was applied every run. If the water cut exceeds constrain value, the well will be closed immediately. Base cases were created with these logics for each fluid sample.

5.1.4 Miscibility Keywords in Eclipse 100

In Petrel, miscibility cases cannot be formed by simply choosing an injection state option. However, a miscibility case can be created with the pathway of Define Simulation Case → Advanced → Keyword Editor Tool. In Keyword Editor Tool, keyword sections are listed on the left side. When a section is selected, the keywords of the section are listed on the right side. After that, the user can insert the keyword, which is needed to create the case.

In this study, miscibility keywords were added using the aforementioned procedure. Primarily, the “MISCIBLE” keyword was included in the RUNSPEC section, which is the first section of an .DATA file and holds start date, simulation units, phases, dimensions, modelling options data. This keyword defines that the simulation will be run in miscible condition (SLB, 2023).

After that, all other keywords, which were utilized in simulations and added by the user, were inserted into PROPS section. The PROPS section includes pressure and saturation dependent properties, such as relative permeabilities, density of fluids, for black oil simulations (SLB, 2023).

Seven keywords were included in the PROPS section. Four of them were used instead of relative permeability keywords, which were created by Petrel. In Eclipse, there are two relative permeability keyword families, but Petrel can only constitute Family I keywords (SWOF, SGOF, and SLGOF). Nonetheless, the MISCIBLE keyword in RUNSPEC section is only operated with Family II relative permeability keywords (SWFN, SGFN, SOF2, SOF3, and SGWFN). As a result, Family I keywords (SWOF and SGOF), which were created by Petrel, were suppressed, and then replaced with Family II keywords (SGFN, SWFN, SOF3, and SOF2). SWOF and SGOF means that water/oil saturation functions versus water saturation and gas/oil saturation functions versus gas saturation, respectively. SGFN, SWFN, SOF2, and SOF3 represent gas saturation functions, water saturation functions, oil saturation functions (two-phase), and oil saturation functions (three-phase), respectively. SOF2 and SOF3 keywords were used together as PMISC keywords required SOF3 keyword to be activated.

SDENSITY keyword is defined the miscible gas density at surface conditions. In our work, this value is equal to the carbon dioxide gas density at surface conditions.

PMISC shows pressure-dependent miscibility tables, which means that transition between miscibility and immiscibility is controlled by this keyword. It is not obligatory to use within miscible cases, but if not used, Eclipse assumes that miscible

displacement appears at all pressure values. When miscibility is defined as zero at every pressure with using PMISC, the displacement occurs as immiscible.

TLMIXPAR keyword changes Todd-Longstaff mixing parameter (ω) for viscosity and density. It is mandatory keyword for miscible runs. The Todd-Longstaff mixing parameter ranges between 0 to 1. If the ω is equal to 1, fully mixed state formed and a piston like displacement occurs in the reservoir. If the Todd-Longstaff mixing parameter is equal to 0, fully segregated state formed, and displacement works like immiscible cases. Todd-Longstaff have suggested that ω should be equal to 1/3 for field scale simulations (Todd & Longstaff, 1972) (SLB, 2023).

5.1.4.1 Keywords For Miscibility Run

First and foremost, MISCIBLE keyword was included to RUNSPEC section in order to activate miscibility. After, Family II relative permeability keywords were used instead of Family I since Family I keywords do not work with MISCIBLE keyword in RUNSPEC section. To control where miscibility begins, PMISC keyword was inserted according to MMP value of the current case. SDENSITY keyword was added to define surface density of CO_2, which is 1.869 kg/m^3. TLMIXPAR keyword was introduced to describe Todd-Longstaff mixing parameter (ω). The ω was assigned as 0.33 due to suggestion of the authors. In Appendix C, an example of a miscible .DATA file can be seen.

5.1.4.2 Keywords For Immiscibility Run

In immiscibility cases, the aforementioned miscibility keywords were still utilized because the surface density of CO_2 is needed to be defined, so that SDENSITY keyword has to be in .DATA file, but to use SDENSITY keyword, MISCIBLE keyword has to be defined in RUNSPEC section. After doing these, the same relative permeability keywords were utilized instead of Family I. In the end, PMISC and TLMIXPAR keywords were inserted into the .DATA file in order to form an

immiscible situation. Thereby, the miscibility parameter at PMISC was entered as zero for every pressure. Furthermore, Todd-Longstaff mixing parameter in TLMIXPAR keyword was inputted as zero, which means that displacement of injected fluid is immiscible (SLB, 2023) (Todd & Longstaff, 1972). In Appendix E, an example of an immiscible .DATA file can be seen.

5.2 Sampling Creation

For uncertainty runs in U & O tool, Petrel required limit values for each uncertain parameter. These values are defined as min-max and base values. To decide the minimum and maximum number of each parameter, miscible and immiscible carbon dioxide injection screening criteria table (Table 2.4 – 2.5) was utilized. Permeability and porosity were selected as uncertainty variables. After checking Table 2.4 and 2.5, the determined limit values for miscible runs can be seen in Table 5.6 and Table 5.7.

Table 5.6 Limits of uncertainty parameters for miscible runs

Parameter	**Base**	**Min**	**Max**
Permeability at X and Y directions, mD	1000	1	5000
Permeability at Z direction, mD	100	1	500
Porosity, %	10	3	40

Table 5.7 Limits of uncertainty parameters for immiscible runs

Parameter	**Base**	**Min**	**Max**
Permeability at X and Y directions, mD	1000	1	3000
Permeability at Z direction, mD	100	1	300
Porosity, %	10	10	40

Monte Carlo and Central Composite Sampler were used to determine random parameters to simulate uncertainty runs. Monte Carlo Sampler worked with the Latin-hypercube method, which provided more distributed data than the normal Monte Carlo version. Figure 5.4 represents the difference between Latin-hypercube sampling and normal distribution for seven samples. After using both sampling methods, thirty-four different uncertainty parameter groups were created. Central Composite sampling method originated from nine of these groups and rest of them were created via Monte Carlo sampling. Both methods were practiced forming parameters group since the Monte Carlo sampling was taken samples from inside of the boundaries; on the other hand, Central Composite sampling method was selected the samples from corners and central space (SLB, 2010).

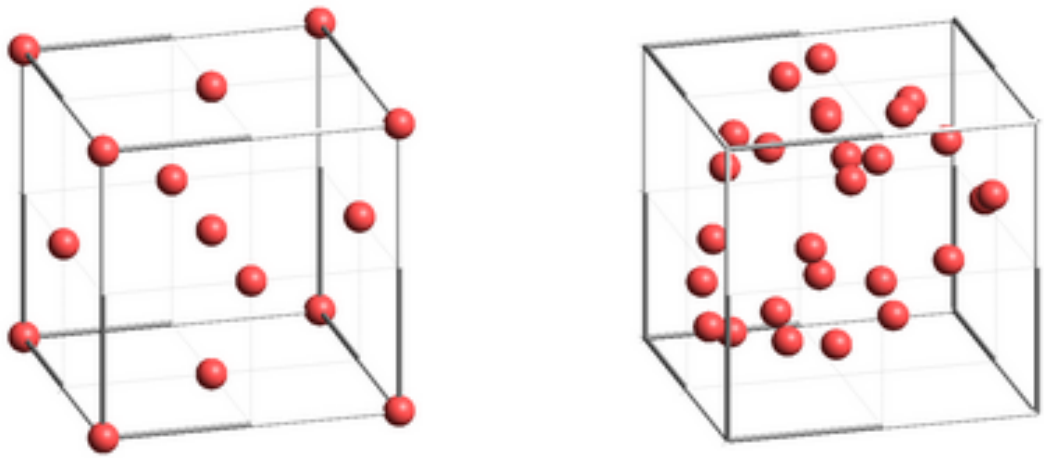

Figure 5.3. Central composite sampling (left) and Monte Carlo sampling (right) (SLB, 2010)

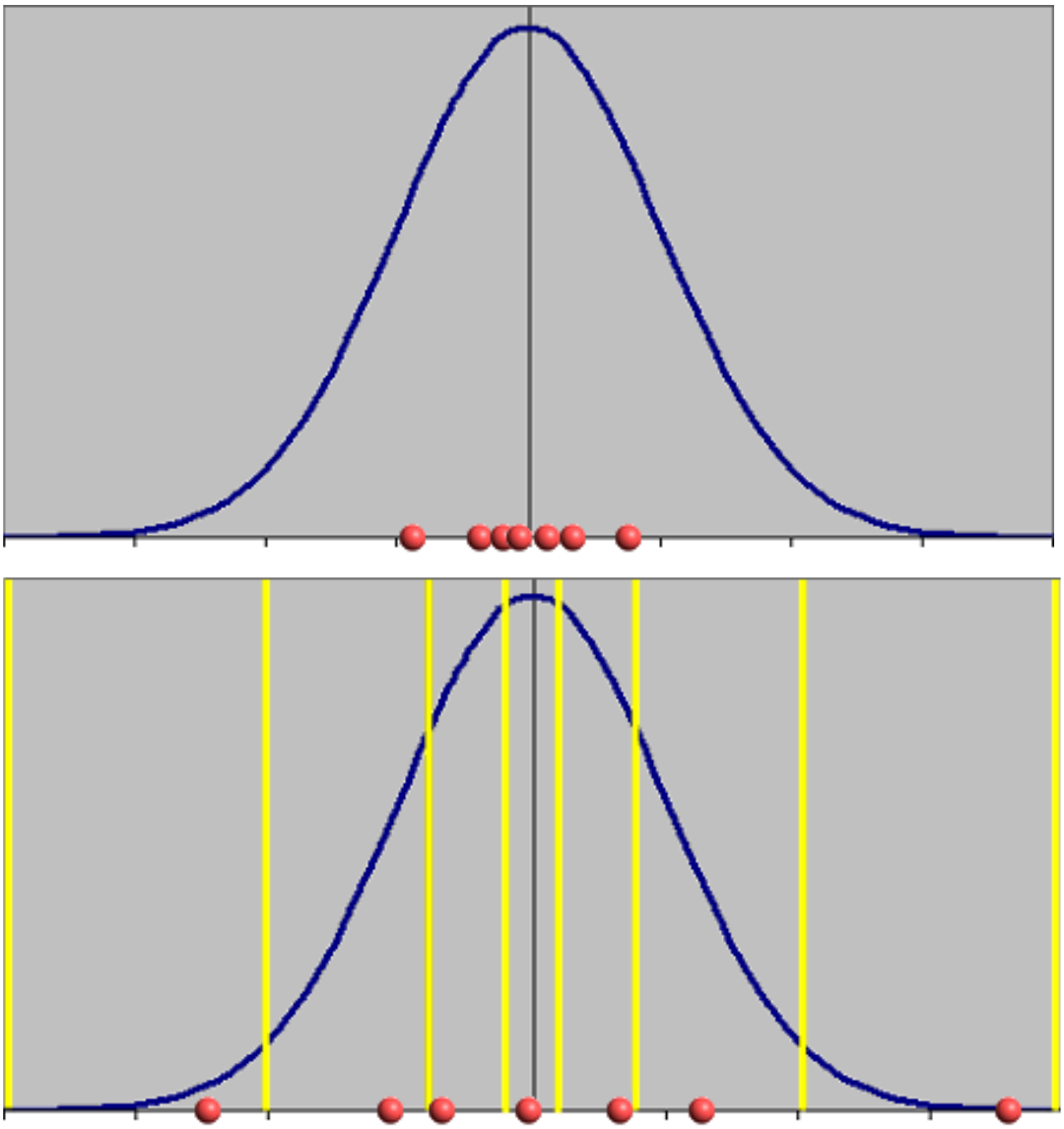

Figure 5.4. Comparison of normal distribution sampling (upper) and Latin-hypercube sampling (lower) (SLB, 2010)

CHAPTER 6

RESULTS AND DISCUSSION

6.1 Minimum Miscibility Pressure Calculations

There are various calculation methods to find the minimum miscibility pressure. Slim tube simulation and ten different empirical correlations were practiced in this thesis to obtain MMP values.

6.1.1 Properties for Empirical Correlations

Empirical correlations are introduced and explained in Chapter 2.6.2. Excluding the graphical correlations, which are Benham, Dowden, & Kunzman (1960), Holm & Josendal (1974) and Mungan (1981) correlations, since graphical reading could be easily misleading, the remaining 10 correlations, Cronquist (1978), Lee (1979), Yellig – Metcalfe (1980), Orr – Jensen (1984), Glasø (1985), Alston, Kokolis, & James (1985), Emera – Sarma (2004), Yuan, Johns, Egwuenu, & Dindoruk (2004), Shokir (2007) and Li, Qin, & Yang (2012), were utilized to compute the minimum miscibility pressure values for each fluid sample. Although, the correlations use functions of reservoir temperature, molecular weight, and mole fraction of reservoir fluids as parameters, each correlation requires different components' molecular weight and mole fraction of reservoir fluids. The necessary parameters for each correlation are also justified in Chapter 2.6.2. Therefore, these values are tabulated according to fluid sample types in Table 6.1.

Table 6.1 Required parameters for empirical correlations

	F2	*F5*	*D1*	*H1*	*M3*
Temperature (°C)	115.0	121.10	110.0	52.00	81.11
X_{vol} (N_2 – CH_4), (mol %)	23.84	27.026	18.28	18.72	8.96
CH_4, (mol %)	23.64	26.576	47.09	18.72	8.86
X_{int} (C_2 – C_6) (mol %)	29.02	27.801	18.28	0.88	20.71
X_{int} (CO_2 – H_2S – C_2 – C_4) (mol %)	21.88	22.461	13.57	1.63	15.11
X_{int} (CO_2 – H_2S – C_2 – C_6) (mol %)	30.36	30.254	18.40	2.32	22.37
C_{5+} (mol %)	54.28	50.513	38.65	79.65	75.93
C_{7+} (mol %)	45.80	42.72	33.82	78.96	68.67
C_{5+} (g/mole)	226.99	219.48	194.80	524.38	227.259
C_{7+} (g/mole)	254.44	245.43	211.52	528.27	243.00

6.1.2 Properties of Slim Tube Simulation

Like every simulation case, the accuracy of the slim tube simulation depends on how close to real world situation. To simulate the slim tube experiment, Eclipse 300 (E300) (compositional reservoir simulation) is used in this study. The properties of the simulated slim tube are 10-meter length, 1 cm height and width, 1000 mD permeability in X and Y direction, 100 mD permeability in Z direction, and 10% porosity. With this data, the pore volume of the slim tube was identified as 100 cm^3. Moreover, Peng-Robinson EoS was utilized in simulation cases.

After describing the slim tube parameters, two wells are inserted into simulation. One of them is the injection well, which is located at the first grid, and the other is the production well, where is located at the last grid of the slim tube. The production well produces oil with constant bottomhole pressure. 1.2-pore volume gas, which is pure CO_2 in this case, is injected to the tube. For simplicity of the reports, the time steps of the simulation divided into 1 hour and every hour 10 cm^3 gas injected (with a constant rate) to test tube, so that total test procedure is finished at 12 hours.

Stalkup Jr. (1984) recommended some procedures to determine minimum miscibility pressure with slim tube simulation. This suggestion was described in detail in Chapter 2.6.1. Briefly, the procedure was stated that the number of the grid block increases, the numerical dispersion will decrease. Hence, this way was utilized for each fluid sample during the calculation.

6.1.3 Minimum Miscibility Pressure (MMP) Results

The calculations were made for each fluid sample since each of them compositions and temperature combination are unique. Empirical correlations and slim tube simulation method were applied for five fluid samples. In the end of the calculations, results are obtained. However, slim tube simulation result has not been reached for H1 fluid sample due to its low API value, which is 10. During the simulation, a variety of pressure values were simulated up to 20,000 atm (293,918.976 psi), which is not a realistic value as a reservoir pressure. Yet, the recovery factor results of the test did not go higher than %83 percentage, which is not enough to obtain the correct MMP value. Therefore, I decided not to include the H1 in miscible simulation cases. Consequently, H1 fluid sample was only simulated in immiscible cases.

Slim tube simulations were run in Eclipse 300 according to aforementioned guidance of Stalkup Jr. (1984). The slim tube simulations result of F5 fluid at different grid sizes (100 grids, 200 grids, 500 grids and infinite grids) and pressures can be seen in Table 6.2. The recovery factor at infinite grid sizes were computed by using linear extrapolations of 100 grids, 200 grids, 500 grids recovery factors at that pressure. After that, the recovery factors at infinite grid sizes vs. pressures used in the simulations were plotted to obtain MMP value for each case. In the plot, there are two lines with different slopes, the line with higher slope represents the immiscible stage of the test and the line with lower slope represents the miscible stage of the test. When the lines are extrapolated forward and backward, the pressure value of the intersection point of the lines is the minimum miscibility pressure value. The example plot for F5 fluid sample is given in Figure 6.1. Consequently, MMP values

of F2, F5, D1 and M3 fluid sample were obtained in the same way, 283.0948 atm (286.846 bars), 330.8649 atm (335.249 bars), 267.8382 atm (271.387 bars) and 422.4918 atm (428.090 bars), respectively. The tables and plots of the remaining fluid samples, F2, D1 and M3, can be seen at Appendix C: Slim Tube Simulation Results' Tables and Graphs chapter.

Additionally, Petrel view of slim tube simulation for F5 fluid sample at 350 bars with 100, 200 and 500 grid blocks can be seen at end of the chapter as an example (Figure 6.2, through 6.5). Figures show 100 grids, 200 grids and 500 grids model from top to bottom in the picture. The colors indicate the gas saturation values of each grid block at that time. The color legend is given in the left part of each figure.

Table 6.2 Slim tube simulation results for F5: Pressures and Recovery Factors

Pressure (atm)	***100 Grids***	***200 Grids***	***500 Grids***	***Infinite Grids***
170.00	74.26%	76.24%	79.09%	82.78%
200.00	79.06%	81.06%	84.25%	88.16%
230.00	83.98%	85.82%	88.66%	92.20%
260.00	88.75%	90.43%	92.32%	95.13%
290.00	92.97%	94.81%	96.43%	99.23%
320.00	95.40%	96.91%	98.04%	100.22%
350.00	96.67%	97.86%	98.70%	100.38%
380.00	97.42%	98.39%	99.06%	100.42%
410.00	97.88%	98.70%	99.26%	100.41%
440.00	98.16%	98.89%	99.38%	100.40%
470.00	98.33%	99.01%	99.45%	100.39%
500.00	98.43%	99.07%	99.49%	100.37%

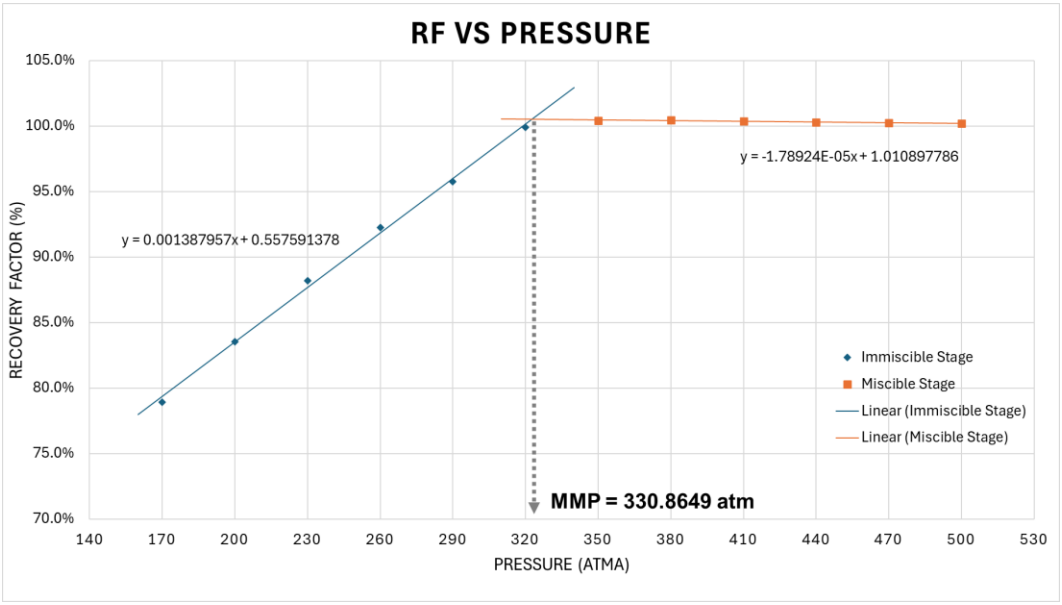

Figure 6.1. Recovery Factor vs Pressure for F5 at Infinite Grids

Afterward, ten empirical correlations, which are not graphical correlations, were executed for each fluid sample. The results of these computations are written in Table 6.3.

Table 6.3 MMP results for F2, F5, D1, H1 and M3

MMP Results, atm	***F2***	***F5***	***D1***	***H1***	***M3***
Cronquist	308.018	315.912	296.548	747.782	202.533
Lee	289.711	313.020	271.406	109.938	179.552
Yellig & Metcalfe	201.856	211.420	194.145	107.069	151.184
Orr & Jensen	304.737	330.225	284.776	111.449	185.458
Glaso	240.770	242.279	197.876	657.289	145.107
Alston et al.	313.443	313.825	235.936	969.108	211.584
Emera & Sarma	301.070	307.127	242.234	534.691	200.451
Yuan et al.	187.978	200.658	530.839	702.359	484.496
Shokir	264.815	276.484	224.808	5.6E+05	191.283
Li et al.	252.638	263.424	231.790	233.115	175.992
Eclipse 300	283.095	330.865	267.838	–	422.492

The black oil simulation required a MMP value for each fluid samples for miscible simulation cases in order to begin miscibility condition of each case. First, the most accurate calculation method has to determine and then, the values of that technique should be used in black oil simulation cases. The results obtained from the correlations are not consistent with each other. There is a significant difference between the minimum and maximum values of the results. The difference of the same correlation according to the outcome of the simulation in different fluid samples also varies. Almost none of the empirical results are more than %1 near by the Eclipse 300 results. The only exception is Orr & Jensen method's calculation result for F5 fluid.

On the other hand, Jaferi, Ashoori, & MK (2019) worked on twelve fluid samples, which all of them have minimum miscibility pressure value from slim tube experiment. They tried to obtain the same values via slim tube simulations on Eclipse 300. As a result, the writer determined MMP values almost the same as the real slim tube experiments. Furthermore, Karamnia & Ashoori (2021) also studied on four samples from the previous twelve ones, but this time, they compared slim tube experiment results with empirical correlations, PVTi calculations and slim tube simulations. Hence, the slim tube simulations are obtained the most accurate results. Moreover, the authors also worked on twenty-four fluid samples, which all of them have slim tube experiments data. They evaluated the accuracy of some well-known empirical correlations. At the end, the writers found that the lowest error of the correlations is 11.93%. Additionally, Adel, Tovar, & Schechter (2016) and Vulin, Gaćina, & Biličić (2018) compared their slim tube experiment and slim tube simulation results, both were found that the simulation outputs are very close to the real slim tube experiment results.

In the light of findings above, slim tube simulations, which were conducted at Eclipse 300, are detected correct results regardless from fluid properties. Thus, 283.0948 atm (286.846 bars), 330.8649 atm (335.249 bars), 267.8382 atm (271.387 bars) and 422.4918 atm (428.090 bars) were accepted as MMP values for F2, F5, D1 and M3 fluids, in that order. Hence, calculated values from slim tube simulations

were utilized in further black oil simulation analysis for miscible CO_2 injection scenarios.

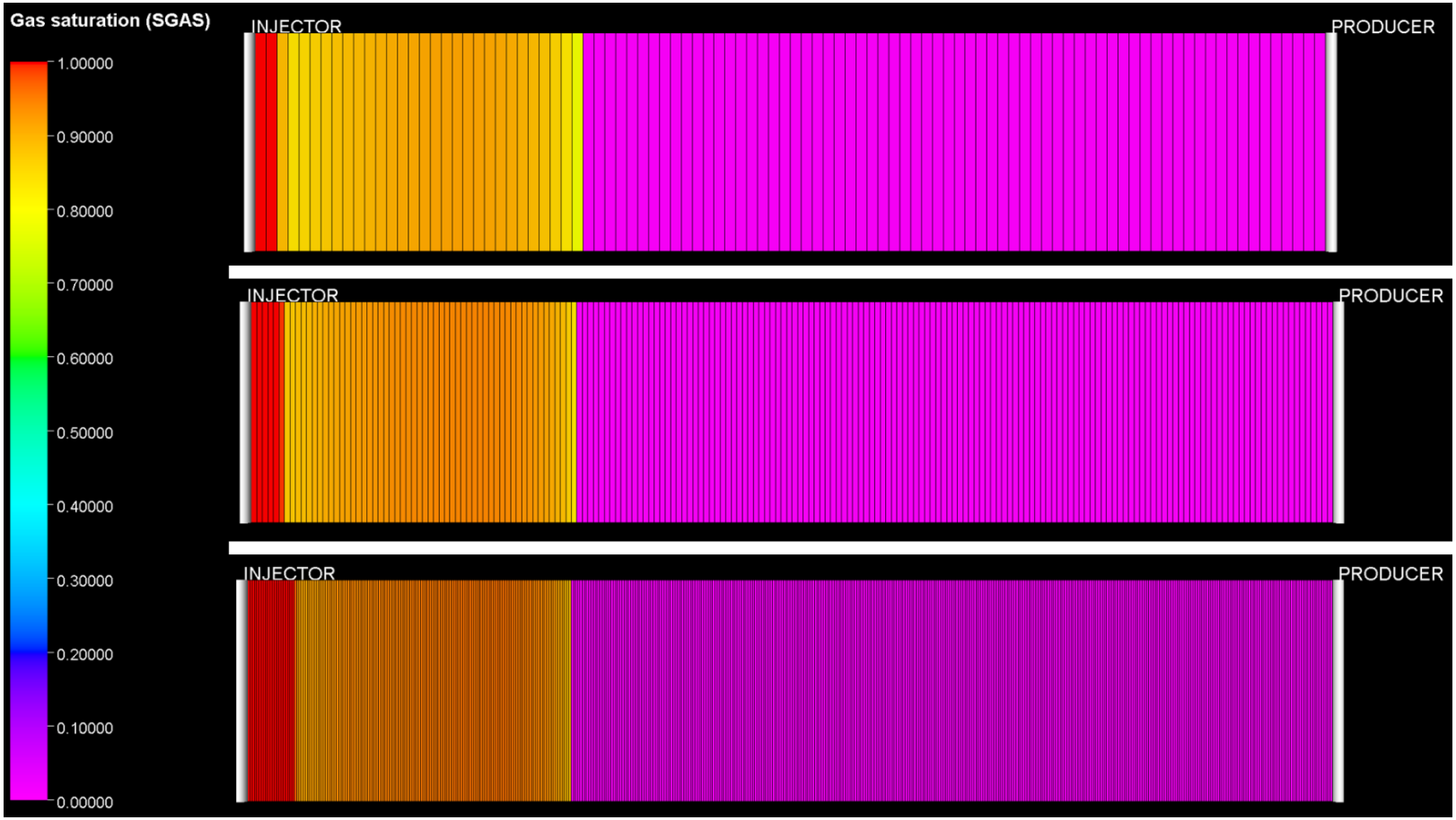

Figure 6.2. Slim tube simulation example views after 3 hours injections (100 grids, 200 grids and 500 grids from top to bottom)

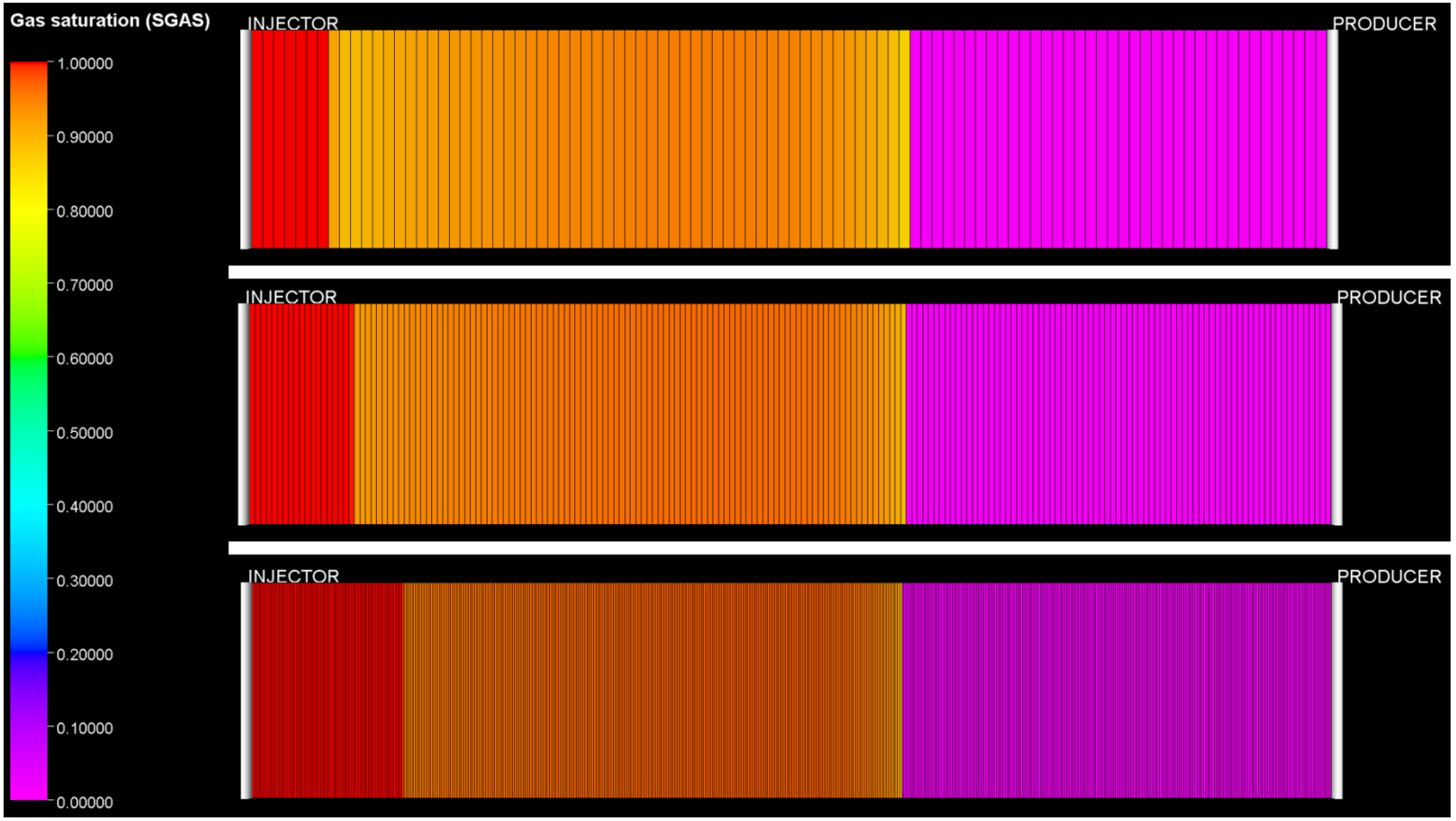

Figure 6.3. Slim tube simulation example views after 6 hours injections (100 grids, 200 grids and 500 grids from top to bottom)

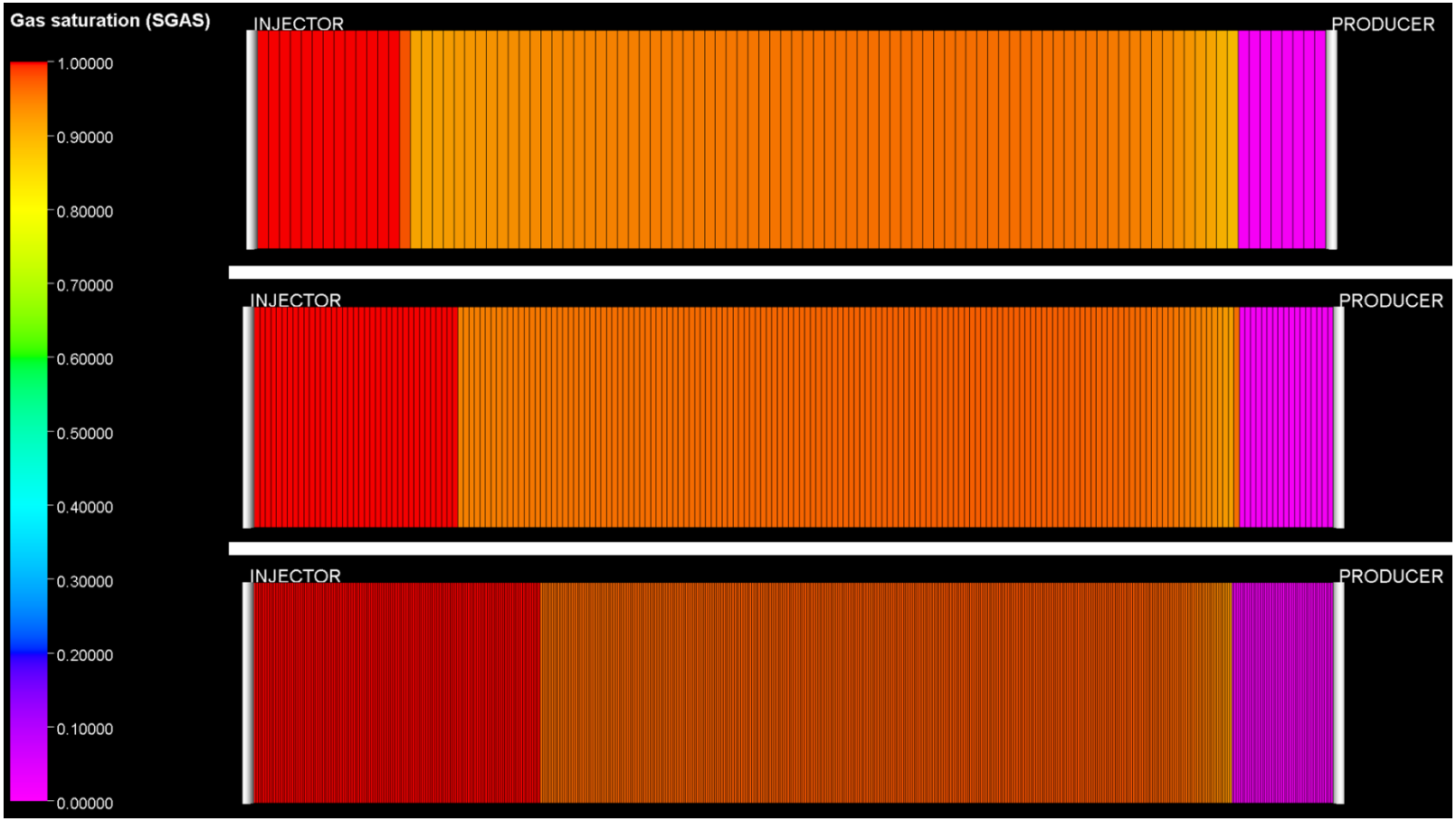

Figure 6.4. Slim tube simulation example views after 9 hours injections (100 grids, 200 grids and 500 grids from top to bottom)

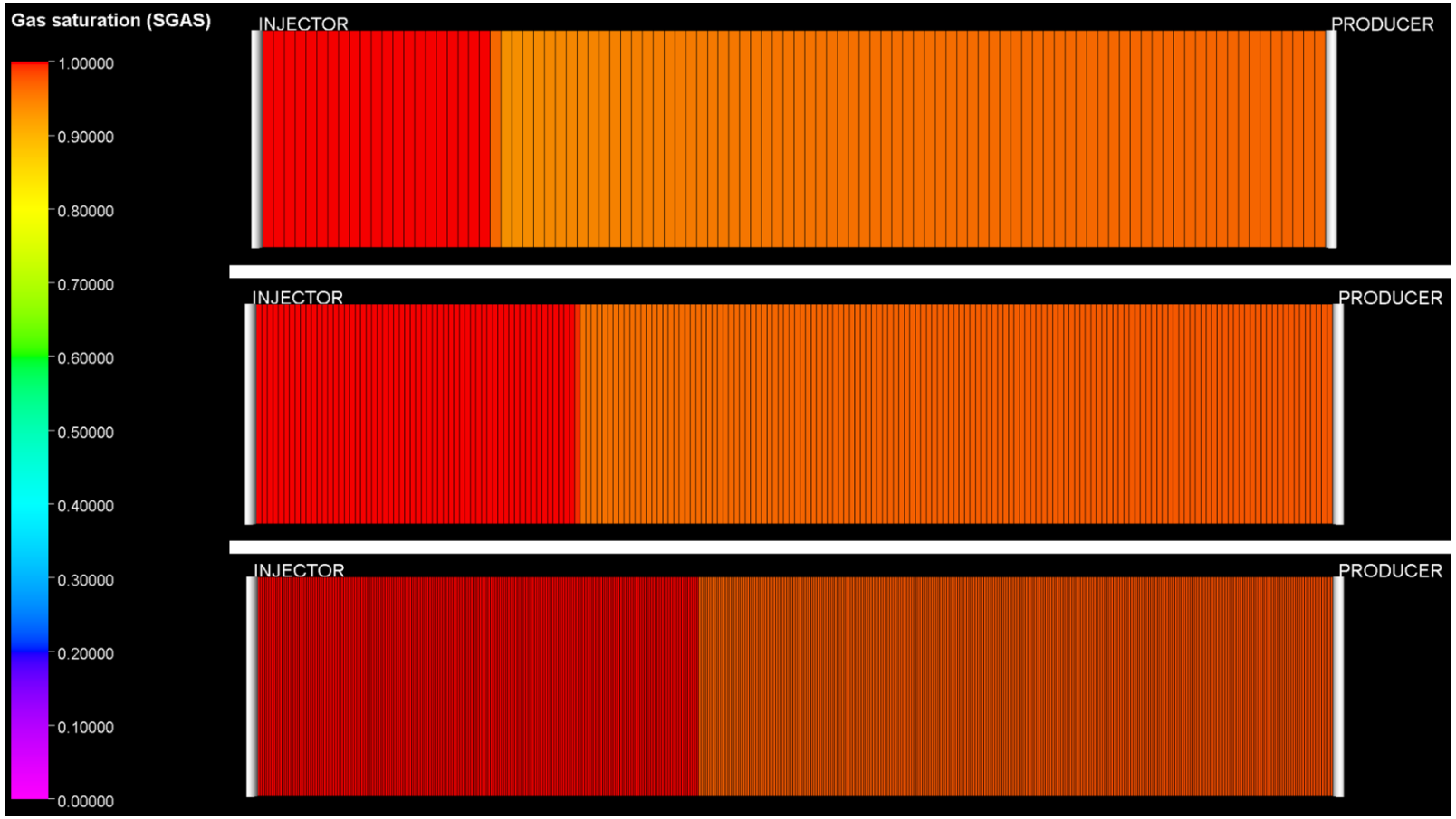

Figure 6.5. Slim tube simulation example views after 12 hours injections (100 grids, 200 grids and 500 grids from top to bottom)

6.2 Porosity & Permeability Effects on Recovery Factor in Miscible Cases

Miscible simulation cases were executed for four of the five fluid samples, which are F2, F5, D1 and M3. It was previously explained why the H1 oil sample was not included in the simulation. The grid model of all the fluid samples is the same, which was introduced in Chapter 5.1. The fluid properties of each fluid type are unique, so that these were created individually in Petrel. The rock compaction data are also distinctive; therefore, they were defined separately to the software. The whole data, which was entered into Petrel, are summaries in Table 5.1. The miscible keywords are also introduced to Eclipse 100 via Keyword Editor Tool inside Petrel in order to make the simulation run in miscible condition.

After that, base cases were formed for each fluid sample with their specific data. The porosity and permeability values of these cases were the same for all fluid samples, which are provided in Table 5.6. Once the base cases were formed, uncertainty cases were generated using the base cases as references. Therefore, thirty-four parameters were generated by using Monte Carlo and Central Composite sampling methods to use for altering the porosity and permeability values during uncertainty runs.

Some of the sampling group (8 data from each fluid sample) and recovery factors of these runs were presented in Table 6.4. The $perm_mult and $poro_mult parameters in Table 6.4 are multipliers of the base case values in Table 5.6. Recovery Factor values are the outcomes of simulations. All sampling data and simulation outputs (recovery factors) are included in Appendix F.

Table 6.4 Example uncertainty parameters and RF of miscible simulations after 5 years

Fluid Types	***Uncertain Parameters***		***Results***
	$perm_mult	*$poro_mult*	*Recovery Factor,%*
F2	2.5005	2.15	20.8888
	0.001	0.3	39.9488
	0.001	4	2.4810
	5	4	13.4388
	0.001	2.15	5.0427
	5	2.15	15.3066
	2.5005	0.3	27.8942
	2.5005	4	16.5527
F5	2.5005	2.15	20.0716
	0.001	0.3	36.3843
	0.001	4	2.1762
	5	4	13.2550
	0.001	2.15	4.4411
	5	2.15	15.3272
	2.5005	0.3	28.7659
	2.5005	4	15.6048
D1	2.5005	2.15	27.8167
	0.001	0.3	54.3540
	0.001	4	3.8742
	5	4	19.6012
	0.001	2.15	7.7461
	5	2.15	23.5841
	2.5005	0.3	46.5695
	2.5005	4	21.9535

Table 6.4 (Cont'd)

M3	2.5005	2.15	21.1588
	0.001	0.3	25.7445
	0.001	4	1.4034
	5	4	15.0639
	0.001	2.15	2.9011
	5	2.15	19.4400
	2.5005	0.3	43.1923
	2.5005	4	16.3043

Primarily, water production did not occur, as the water-oil contact (WOC) is located below the reservoir section. Secondly, each fluid sample was run with the same $perm_mult and $poro_mult parameters (inputs) in order to also detect the impact of the fluid properties on the recovery factor; for instance; in Table 6.4, the inputs are the same, but the outputs (RF) are differed as the fluid properties of samples are different.

When examining the recovery factor values from the simulations, cases with low porosity show earlier onset of injected gas production compared to those with high porosity, provided the permeability values are moderate or high. In this study, porosity value is directly proportional to the reservoir volume since other dimensional parameters remain unchanged. Therefore, these reservoir volume changes cause a negative correlation between porosity and recovery factor. For instance, Misc_F2_60_33 and Misc_F2_60_34 lines in gas production rate graph in Figure 6.7, which clearly presented the impact of early gas production. The permeability multipliers of both cases are 2.5005, porosity multipliers are 0.3 and 4 and recovery factors are 27.8942% and 16.5527%, respectively. These issues were the same for all the fluid samples.

On the other hand, when permeability is low and porosity is moderate or high, gas production does not occur because the gas cannot breakthrough to the production well in such cases because of large pore volume of reservoir. Misc_F2_60_29 and Misc_F2_60_31 cases, where permeability multipliers of both cases are 0.001, porosity multipliers are 4 and 2.15 and recovery factors are 2.4810% and 5.0427 %, respectively, can be given as examples in Figure 6.7. In these situations, gas injections continued but fluid flow inside the reservoir was slow because of the extremely low permeability values, so that the reservoir pressure of the field increases. Furthermore, the sweep efficiency of these cases is more limited compared to scenarios with adequate porosity due to the impact of low permeability. Thus, these situations supported the statement of the high porosities causing negative impact on recovery factors. These issues were the same for all the fluid samples.

Further, if porosity is moderate or high, the recovery factor drops where permeability is high. To illustrate, gas production rate and oil production rate graphs of Misc_F2_60_30 and Misc_F2_60_34 cases, where porosity multipliers of both cases are 4, permeability multipliers are 5 and 2.5005 and recovery factors are 13.4388% and 16.5527%, in Figure 6.7 present gas productions almost started the same date; however, gas production rate of high permeable case was almost always higher than lower one while oil production rate was always lower. Therefore, the recovery factor of high permeability cases was less than moderate permeability cases since high permeabilities give more easily fluid flow chance inside the reservoir.

As a result, it was observed that permeability values had a low effect on the recovery factor except for the extreme cases mentioned above because gas and reservoir oil formed a one-phase fluid in miscible cases.

In addition, oil viscosity values were more dramatically decreasing during the injection where API gravity is low, which causes high oil viscosity. Oil viscosity of D1 oil sample, which has the highest API gravity among four, dropped %7 while %9 decreased for M3 oil sample, which has the lowest API gravity among them.

However, oil densities were not changed significantly regardless of fluid sample. It declines almost %1 for each sample.

In Figure 6.6, the changing of gas saturation in an example case is exhibited during the five years of miscible CO_2 injection. In this example case, the gas breakthrough happened at the beginning of the first year.

The following graphs display the results of given example cases in Table 6.4. When reviewing the simulation plots of four fluid samples with identical input parameters (permeability and porosity), the gas injection rate, gas production rate, oil production rate, and reservoir pressure curves appear to follow a similar pattern, albeit with varying values. These variations are due to differences in fluid properties and pressure values. In some cases, gas injection rate is changed because maximum reservoir pressure identified as constrain for gas injection well's bottom hole pressure. Therefore, the injection rates were arranged in order to not to exceed maximum reservoir pressure.

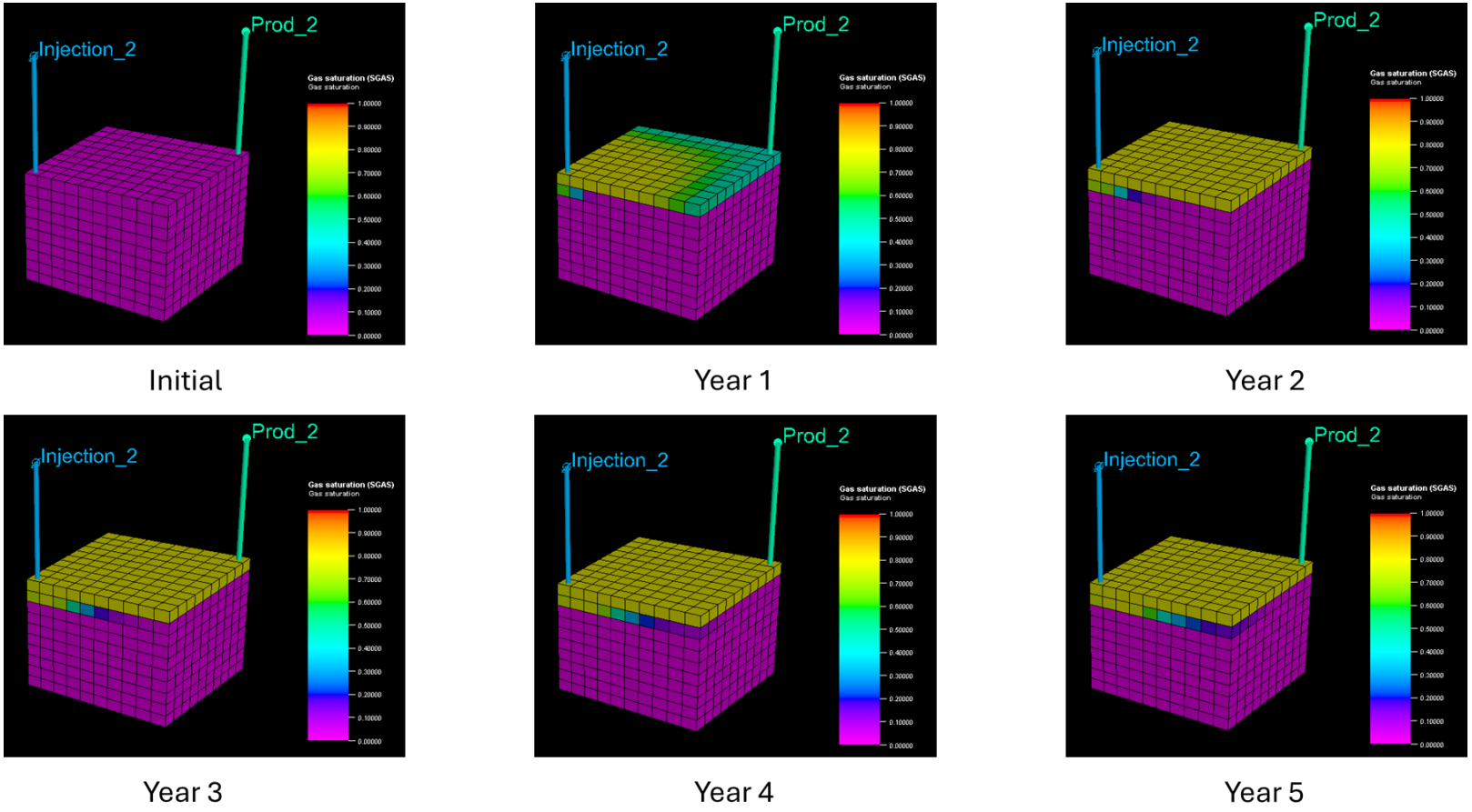

Figure 6.6. Miscible case example

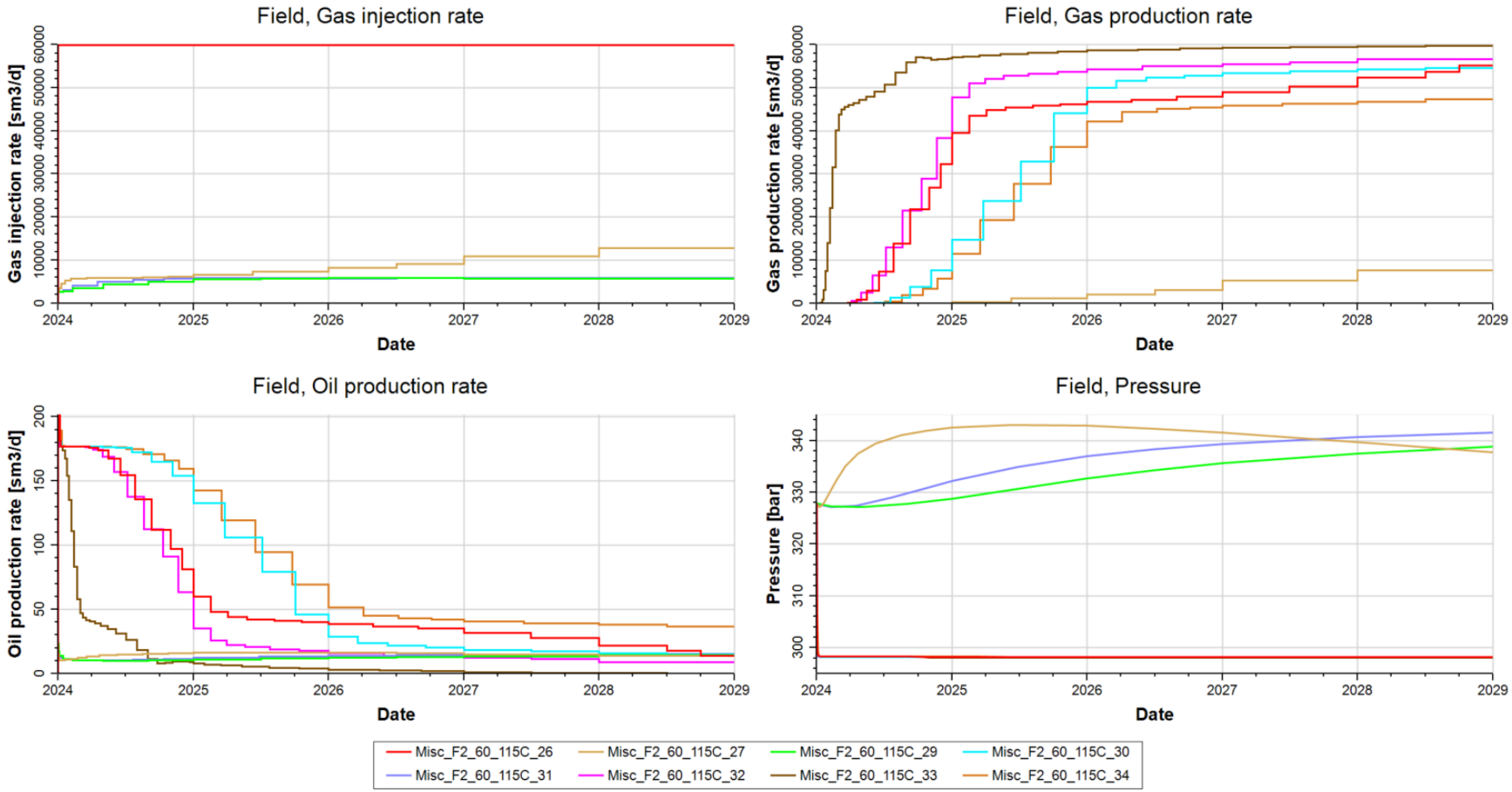

Figure 6.7. Results for F2 fluid of Table 6.4 cases

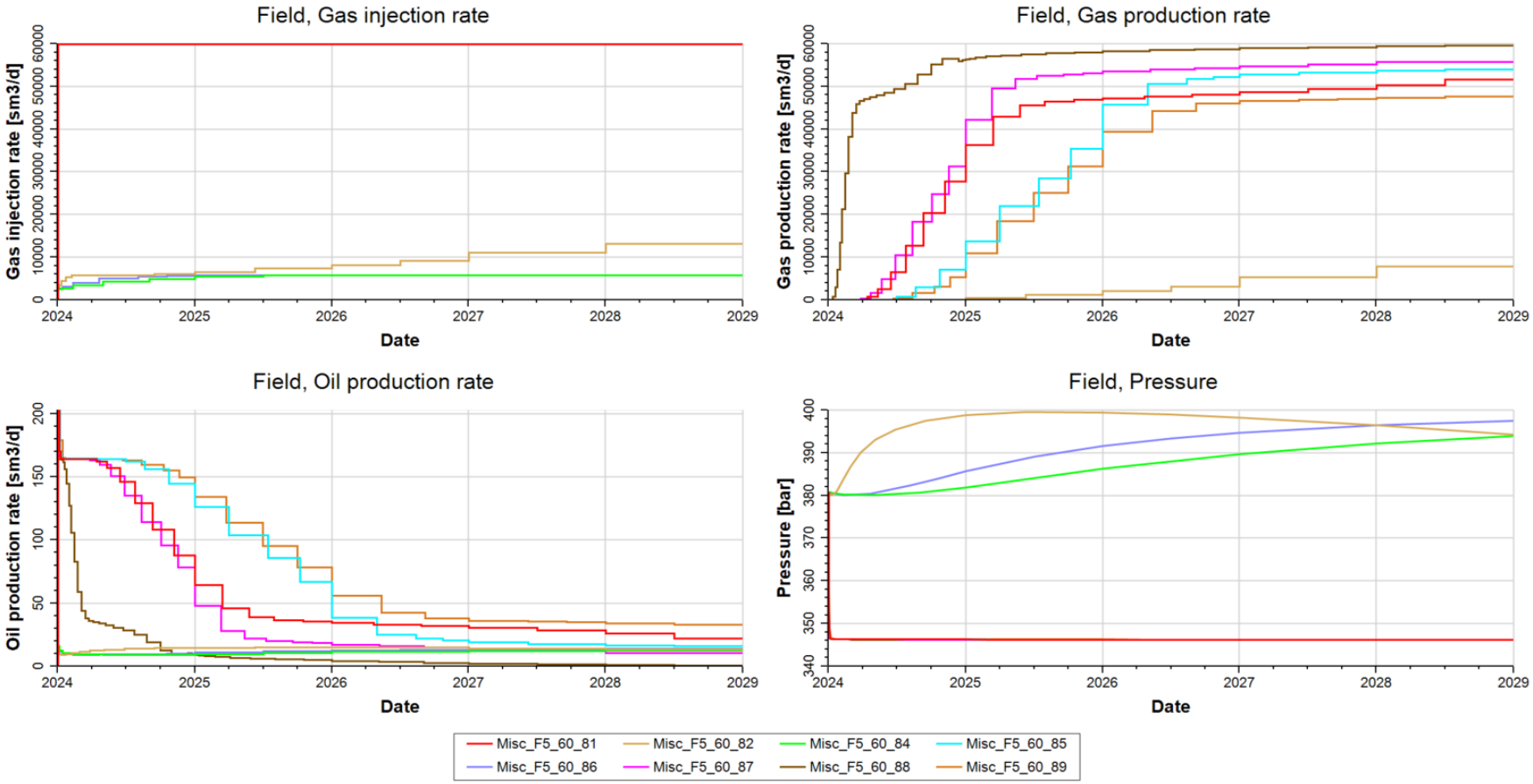

Figure 6.8. Results for F5 fluid of Table 6.4 cases

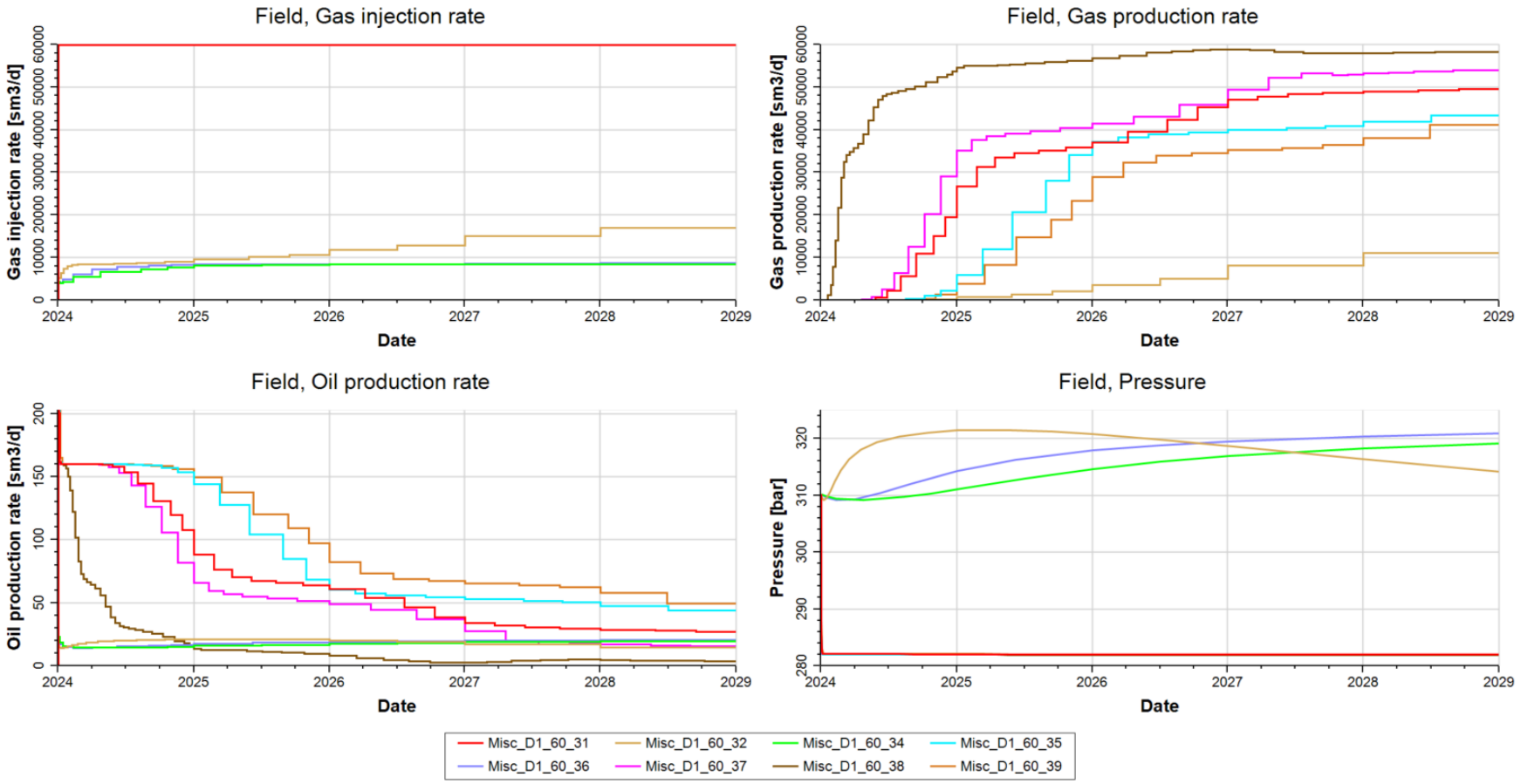

Figure 6.9. Results for D1 fluid Table 6.4 cases

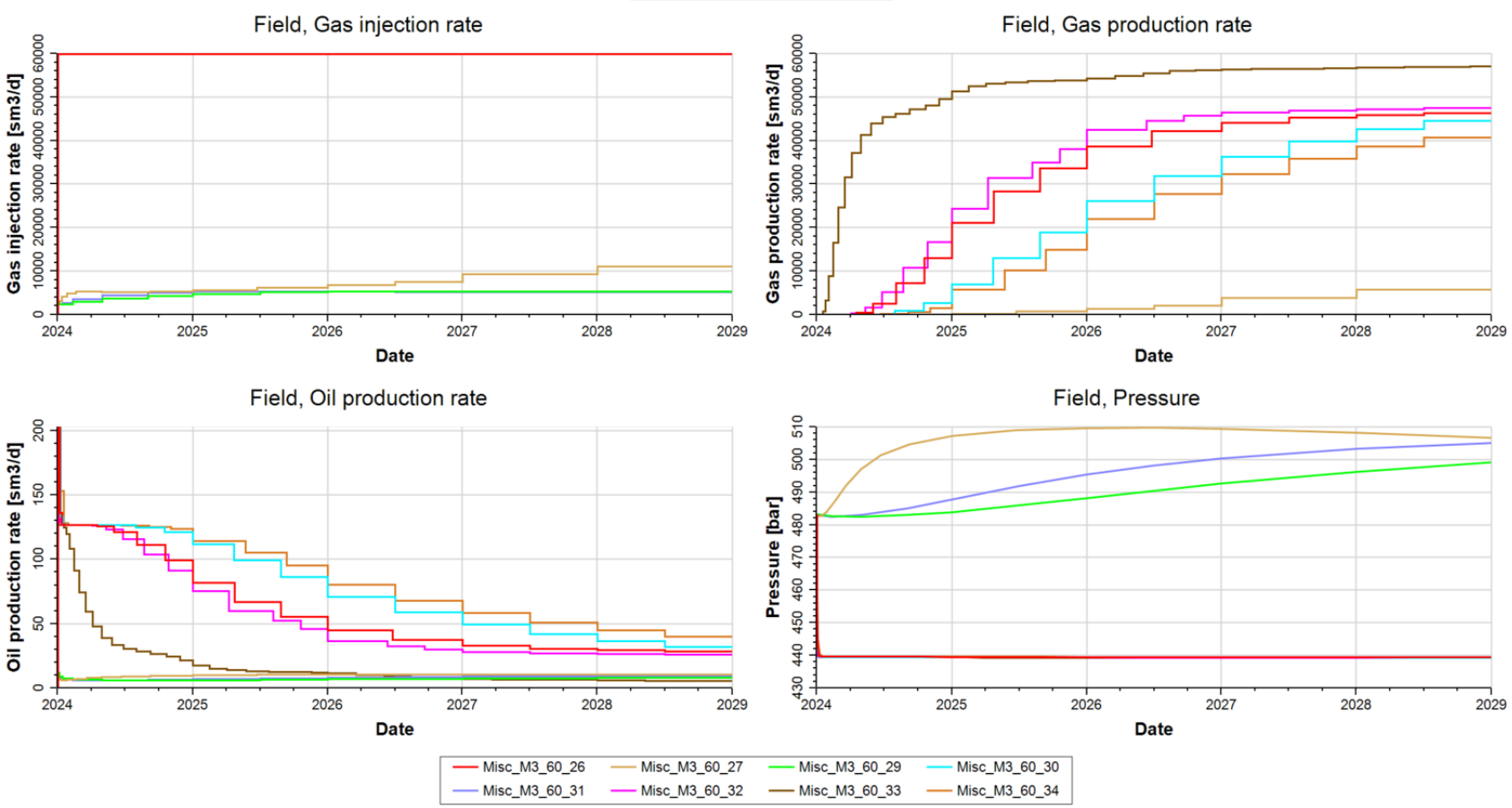

Figure 6.10. Results for M3 fluid of Table 6.4 cases

The reservoir pressure values are various for all fluid samples due to minimum miscibility pressure, so that the recovery factors are also affected by reservoir pressure as well as the fluid properties. To eliminate the pressure effect on the recovery factors, three fluid samples (F2, F5 and D1) were simulated under the same pressure conditions, which is 345 bars for minimum reservoir pressure. It is important to note that MMP values are not changed , the reservoir pressure was the only variable value. Consequently, the recovery factors are only affected by fluid properties. The simulation outputs (RF) are obviously shown that where the API gravity is high the recovery factor is high as well. As a reminder, the API gravity and reservoir temperature values are as follows: F5 has an API of 31.914 and a temperature of 121.1℃, F2 has an API of 37.446 and a temperature of 115.0℃, and D1 has an API of 47.88 and a temperature of 110.0℃. Using the same porosity and permeability parameters as in Table 6.4, the results are presented in Table 6.5 as example cases where reservoir pressures are equal in all fluid samples.

F5 fluid has the lowest API gravity and highest reservoir temperature in this group. As a result, recovery factors of F5 are always the lowest. D1 sample has the peak API gravity and the lowest reservoir temperature among the three, but the recovery factors of D1 are the highest. According to these comparisons, API gravity is seen as more influential than the reservoir temperature on recovery factors. The carbon dioxide solubility causes these situations because solubility of CO_2 is directly proportional with API gravity and inversely proportional with reservoir temperature. Besides, oil viscosity decreases with API increases, which leads to oil flowing more easily inside the reservoir.

The effect of reservoir pressure will be examined in detail for the F5 oil sample in Chapter 6.4.

Table 6.5 Simulation results examples where the pressure is equal in all fluid samples

Uncertain Parameters		***Recovery Factor for three fluids, %***		
$perm_mult	*$poro_mult*	*F5*	*F2*	*D1*
2.5005	2.15	20.0716	20.1918	48.2521
0.001	0.3	36.3843	35.5894	64.5872
0.001	4	2.1762	2.1142	5.1054
5	4	13.2550	13.4213	30.9495
0.001	2.15	4.4411	4.3173	10.1208
5	2.15	15.3272	15.8006	49.3883
2.5005	0.3	28.7659	29.5884	92.7946
2.5005	4	15.6048	15.6090	29.9204

To identify the correlations between recovery factor and uncertain parameters (porosity and permeability), Pearson correlation coefficients were determined by using rank values of Spearman rank correlation coefficients because of presence of ties for both miscible and immiscible cases. The Pearson correlation coefficient method can define the direction of the relationships between two parameters. If the correlation value is negative that means these parameters are inversely proportional; on the other hand, if the correlation value is positive that means these parameters are directly proportional. Chatterjee correlation coefficients can be applied where variables are non-linear and non-monotonic. It only represents strength of the association of the variables because of that the Pearson correlation coefficients were utilized in order to give a thought about the direction of the correlations. Pearson correlation coefficient values were obtained via built-in Excel functions. For calculating Chatterjee correlation coefficients, a MATLAB script, which can be seen at Appendix H, was utilized. The code in the Appendix H is the MATLAB version of a R Language package, which was created by Chatterjee himself to obtain coefficient values, then it is converted to MATLAB by a user named as David

Romero (Romero, 2024). The following table (Table 6.6) represents the correlations of each uncertainty parameter with recovery factor.

Table 6.6 Pearson and Chatterjee correlation coefficients for miscible runs

		Pearson		*Chatterjee*	
Fluid Types	*API*	*Perm_mult*	*Poro_mult*	*Perm_mult*	*Poro_mult*
M3	24.058	-0.0182	-0.8819	0.0026	0.5584
F5	31.914	-0.2262	-0.7715	0.0597	0.3818
F2	37.446	-0.2396	-0.7235	0.0805	0.3143
D1	47.880	-0.1849	-0.8336	0.026	0.4623

According to the Pearson correlation results, permeability and porosity always have negative impact on recovery factors during miscible carbon dioxide injection projects regardless of the API gravity of the crude oil. Moreover, the negative correlation of permeability increases until D1 fluid samples, which has very high API gravity and low oil viscosity. Conversely, the negative correlation of porosity decreases until D1 oil sample. On the other hand, when looking at the Chatterjee correlation, it is said that permeability always has an exceptionally low influence on recovery factor; however, porosity has moderate to high influence on the RF. The impact weight of the porosity decreases with API gravity till the D1 sample while permeabilities influence's increases.

6.3 Porosity & Permeability Effects on Recovery Factor in Immiscible Cases

Immiscible simulation cases were conducted for all fluid samples. Each sample uses the same grid model, as described in Chapter 5.1, but features unique fluid properties, which were individually configured in Petrel. Additionally, distinct rock compaction data were defined separately in the software for each sample. A summary of all data input into Petrel is provided in Table 5.2.Subsequently, base cases were established for each fluid sample using their specific data. Consistent porosity and permeability

values were applied across all fluid samples, as outlined in Table 5.7. Then, these base cases served as reference points for developing uncertainty cases. To introduce variability in porosity and permeability for uncertainty simulations, thirty-four parameters were generated using Monte Carlo and Central Composite sampling methods. A selection of sampling groups (8 data points from each fluid sample) and their corresponding recovery factors are displayed in Table 6.7. In this table, the $perm_mult and $poro_mult parameters represent multipliers applied to the base case values listed in Table 5.7, with recovery factors reflecting the simulation results. The complete set of sampling data and simulation outcomes (recovery factors) can be found in Appendix G.

Table 6.7 Example uncertainty parameters and RF of immiscible simulations

Fluid Types	***Uncertain Parameters***		***Results***
	$perm_mult	*$poro_mult*	*Recovery Factor, %*
F2	1.9225	1.9870	17.0392
	1.5005	2.5	19.7695
	0.001	1	3.1687
	0.001	4	0.7698
	3	4	13.9028
	0.001	2.5	1.1439
	1.5005	1	20.5262
	1.5005	4	18.7075
F5	1.9225	1.9870	17.8732
	1.5005	2.5	20.3834
	0.001	1	3.0924
	0.001	4	0.7626
	3	4	14.4339
	0.001	2.5	1.1364
	1.5005	1	21.4889
	1.5005	4	19.0976

Table 6.7 (Cont'd)

D1	1.9225	1.9870	21.6029
	1.5005	2.5	22.9352
	0.001	1	5.9799
	0.001	4	1.2959
	3	4	15.5926
	0.001	2.5	2.0370
	1.5005	1	23.3976
	1.5005	4	22.0135
M3	1.9225	1.9870	22.3180
	1.5005	2.5	23.7386
	0.001	1	2.1608
	0.001	4	0.5938
	3	4	16.9672
	0.001	2.5	0.8744
	1.5005	1	26.9680
	1.5005	4	21.5398
H1	1.9225	1.9870	19.9578
	1.5005	2.5	21.4054
	0.001	1	0.1145
	0.001	4	0.0341
	3	4	15.8092
	0.001	2.5	0.0513
	1.5005	1	22.9608
	1.5005	4	19.9887

Firstly, it is important to note that no water production occurred, as the water-oil contact (WOC) is located below the reservoir section. Additionally, each fluid

sample was simulated with identical $perm_mult and $poro_mult parameters to assess the impact of fluid properties on the recovery factor. For instance, in Table 6.7, while the input parameters remain consistent, the recovery factor (RF) outcomes differ due to variations in the fluid properties of each sample.

In examining the recovery factor values from the simulations, cases with low porosity start earlier injected gas production compared to those with higher porosity, where moderate or high permeability. In this study, porosity directly influences reservoir volume since other dimensional parameters stay constant. Therefore, these reservoir volume changes cause a negative correlation between porosity and recovery factor. For example, in Table G.3, the 28th and 33rd rows represent cases where the porosity multipliers are 1.0 for both, but the permeability multipliers are 3.0 and 1.5005, with recovery factors of 15.8537% and 23.3976%, respectively. Early gas breakthrough in cases with higher permeability can explain these results, as injected gas production tends to reduce oil production. These trends were consistent across all fluid samples.

Conversely, in cases where permeability is low and porosity is moderate or high, gas production does not occur because the gas cannot break through to the production well due to the reservoir's large pore volume. For instance, in Figure 6.14, the cases Immisc_D1_KY_29 and Immisc_D1_KY_31 demonstrate this scenario, where the permeability multipliers are 0.001, the porosity multipliers are 4.0 and 2.5, and the recovery factors are 1.2959% and 2.0370%, respectively. In such cases, continuous gas injection encounters significant challenges due to the extremely low permeability, which severely restricts fluid flow within the reservoir and leads to an increase in reservoir pressure. Additionally, the sweep efficiency in these scenarios is significantly lower than in cases with sufficient permeability, further contributing to the increase in reservoir pressure. This supports the observation that high porosity negatively impacts recovery factors. These effects were consistent across all fluid samples.

Furthermore, when porosity is moderate or high, the recovery factor decreases in cases with high permeability. For instance, in Figure 6.14, the gas production and oil production rate graphs for the Immisc_D1_KY_30 and Immisc_D1_KY_34 cases illustrate this trend. Both cases have porosity multipliers of 4.0, permeability multipliers of 3.0 and 1.5005, and recovery factors of 15.5927% and 22.0135%, respectively. Gas production in the high permeability case began approximately five months earlier due to the ease of fluid flow created by high permeability within the reservoir. At the end of the five-year simulation period, the gas production rate in the high-permeability case approached the injection rate, suppressing oil production. In contrast, the gas production rate in the low-permeability case did not reach the levels observed in the high-permeability case. Consequently, recovery factors were lower in high-permeability cases compared to those with moderate permeability.

In H1 fluid cases, reservoir pressure does not immediately drop to a minimum after production begins. Unlike other samples where pressures quickly fall, H1 maintains pressure at a plateau for an extended period before eventually declining to the minimum level. This behavior is attributed to H1's classification as ultra-heavy oil, characterized by low API gravity and high viscosity, which makes it highly resistant to flow within the reservoir (SLB, 2024). As a result, reservoir pressure is sustained for a longer duration. However, recovery factors for the H1 fluid sample were consistently the lowest among all samples.

Additionally, the H1 fluid has the lowest reservoir temperature among the five samples. Since reservoir temperature is inversely proportional to oil viscosity, lower temperatures result in more viscous crude oil compared to other samples (SPE, 2024). This high viscosity limits the ability of injected gas to effectively sweep the crude oil due to an undesirable mobility ratio. However, the impact of gas injection on oil viscosity is noticeable in the H1 base case scenario. In immiscible cases, viscosity reduction was smaller compared to miscible cases but still significant. The viscosity of H1 decreased from 16.76 cP to 16.23 cP, reflecting a reduction of approximately 3.15%. This demonstrates that immiscible CO_2 injection can reduce oil viscosity and improve its flow within the reservoir. For all samples, viscosity

decreased by roughly 3% in base case scenarios, while oil density showed minimal change, dropping by approximately 0.5% regardless of the fluid sample.

Figure 6.11 illustrates the change in gas saturation during five years of miscible CO_2 injection for an example case. In this scenario, the injected gas does not reach breakthrough within the five-year simulation period.

The following graphs display the results of given example cases in Table 6.7. Reviewing the simulation plots of five fluid samples with identical input parameters (permeability and porosity) reveals that the gas injection rate, gas production rate, oil production rate, and reservoir pressure curves exhibit almost similar patterns, though with differing values. These variations result from the distinct fluid properties and pressure levels in each case. In some cases, gas injection rate is changed because maximum reservoir pressure identified as constrain for gas injection well's bottom hole pressure. Therefore, the injection rates were arranged in order to not to exceed maximum bottomhole pressure of injection well, which is also the maximum reservoir pressure.

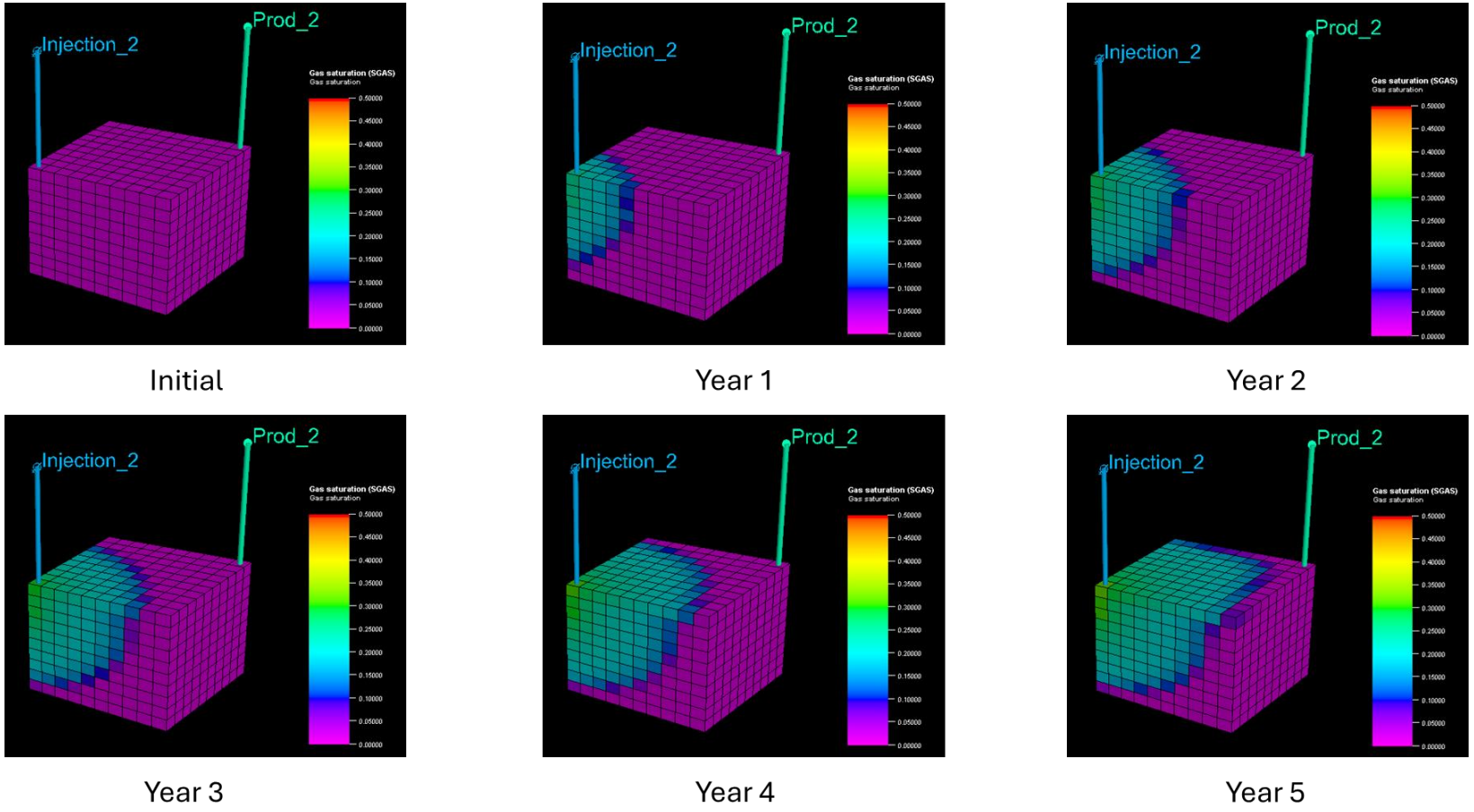

Figure 6.11. Immiscible case example

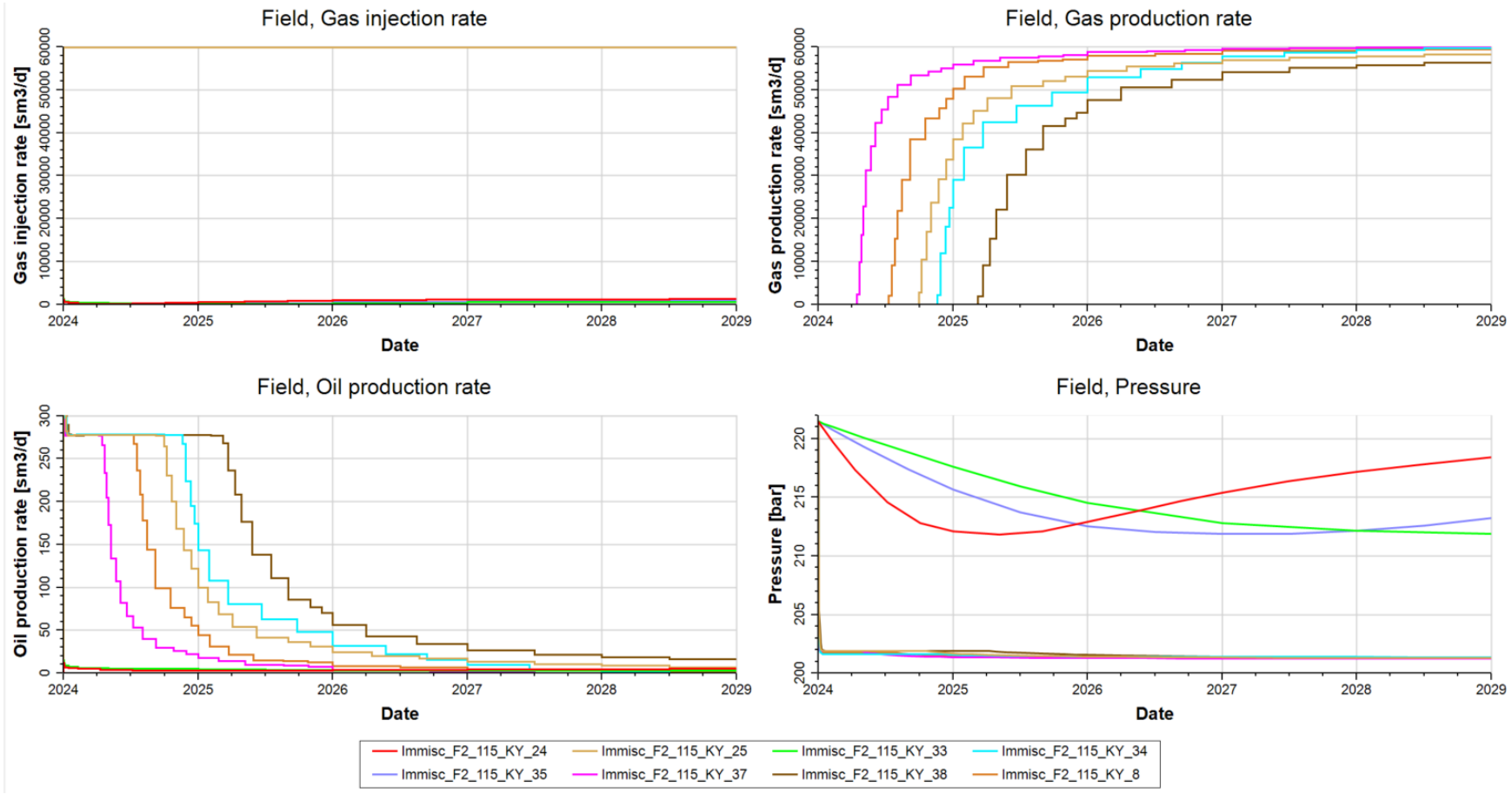

Figure 6.12. Results for F2 fluid of Table 6.7 cases

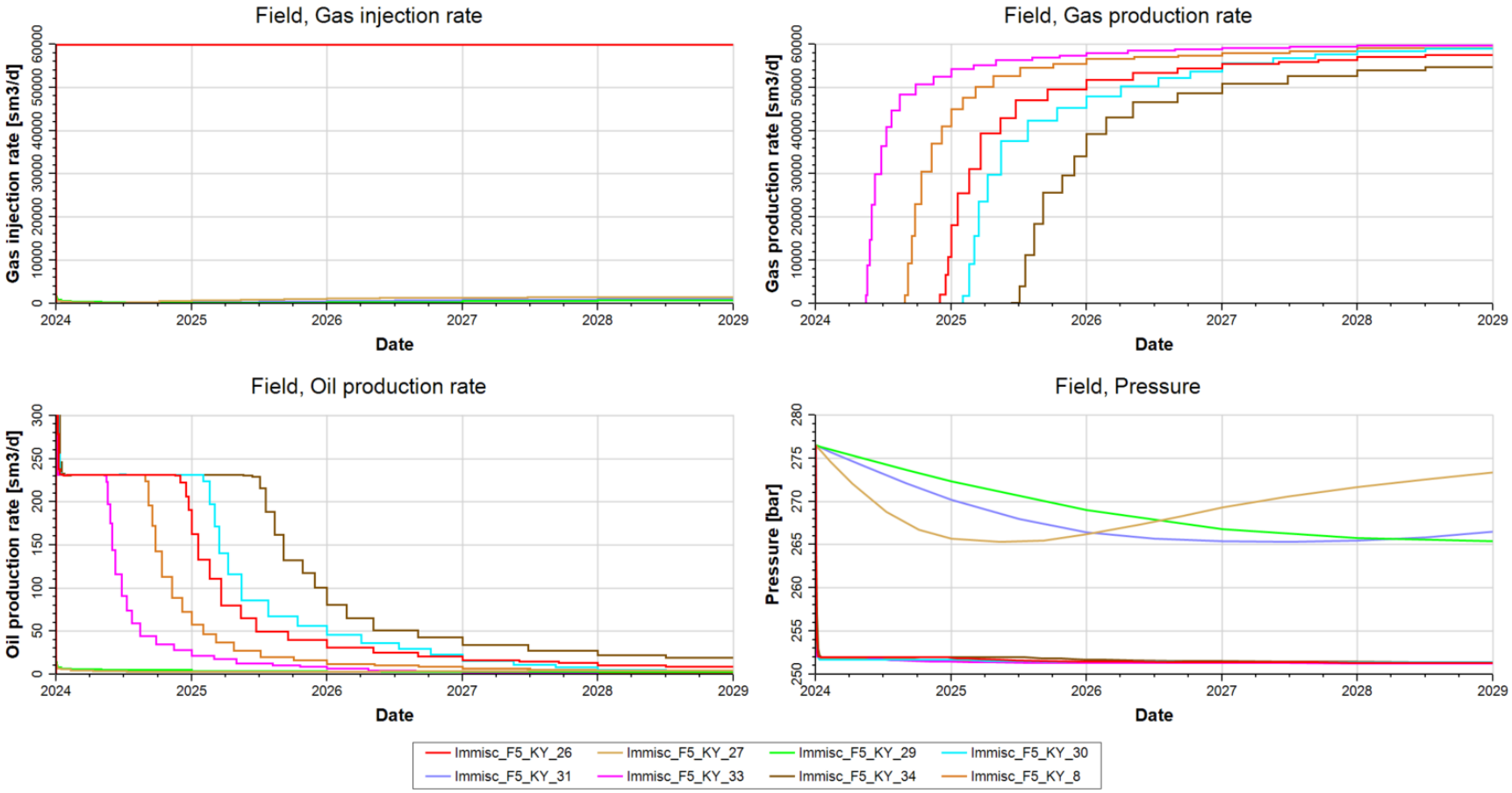

Figure 6.13. Results for F5 fluid of Table 6.6 cases

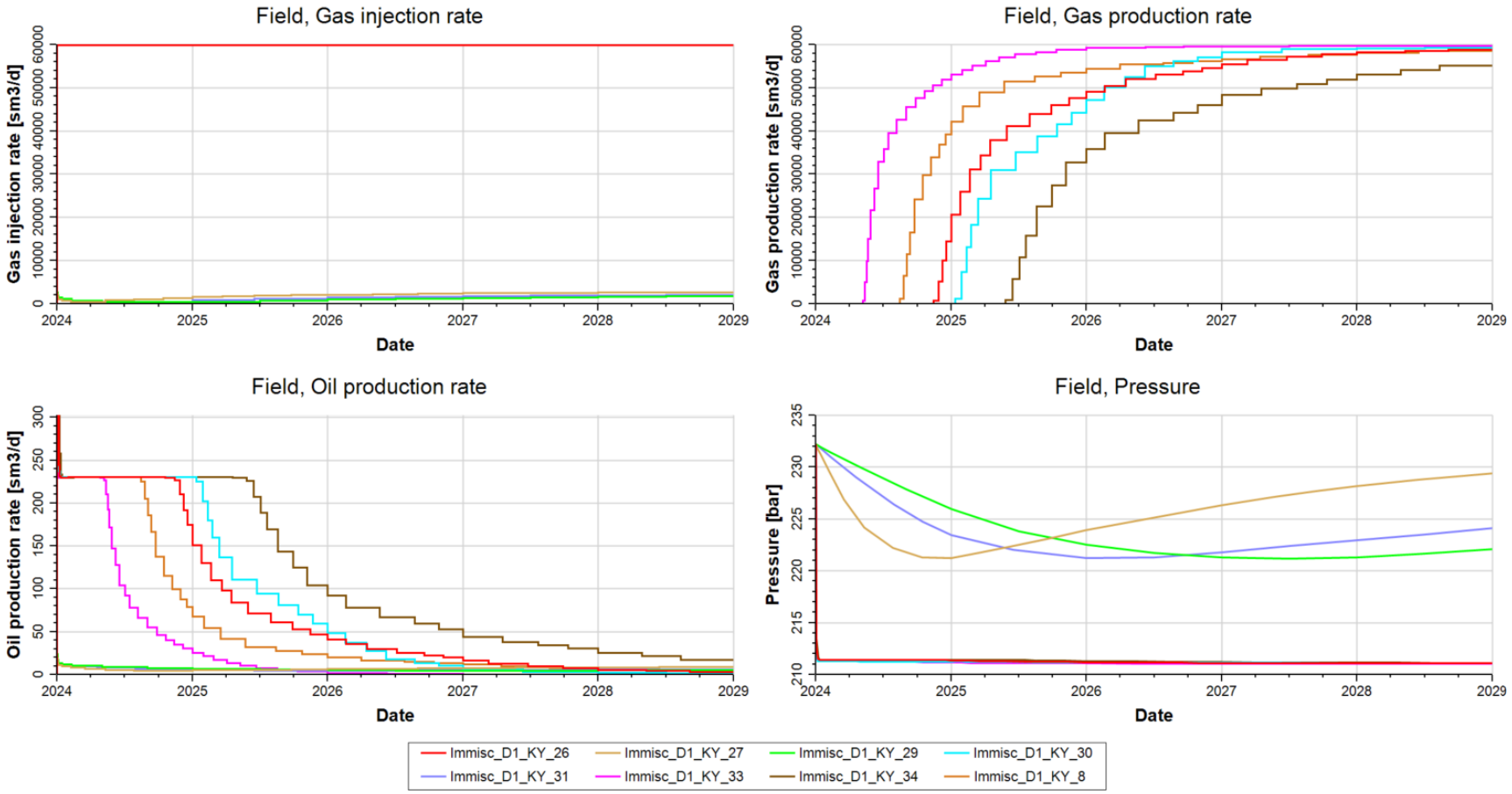

Figure 6.14. Results for D1 fluid of Table 6.7 cases

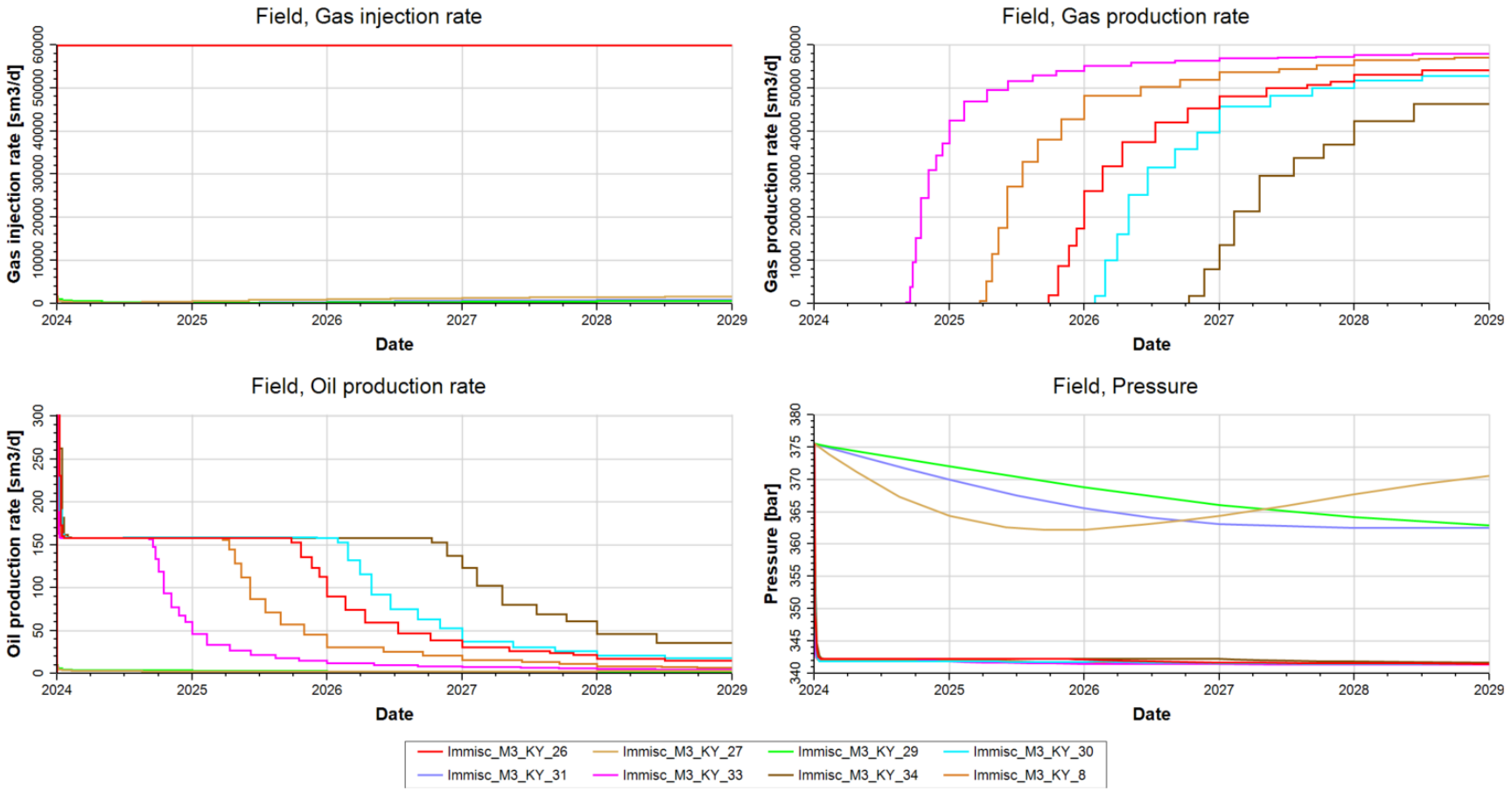

Figure 6.15. Results for M3 fluid of Table 6.7 cases

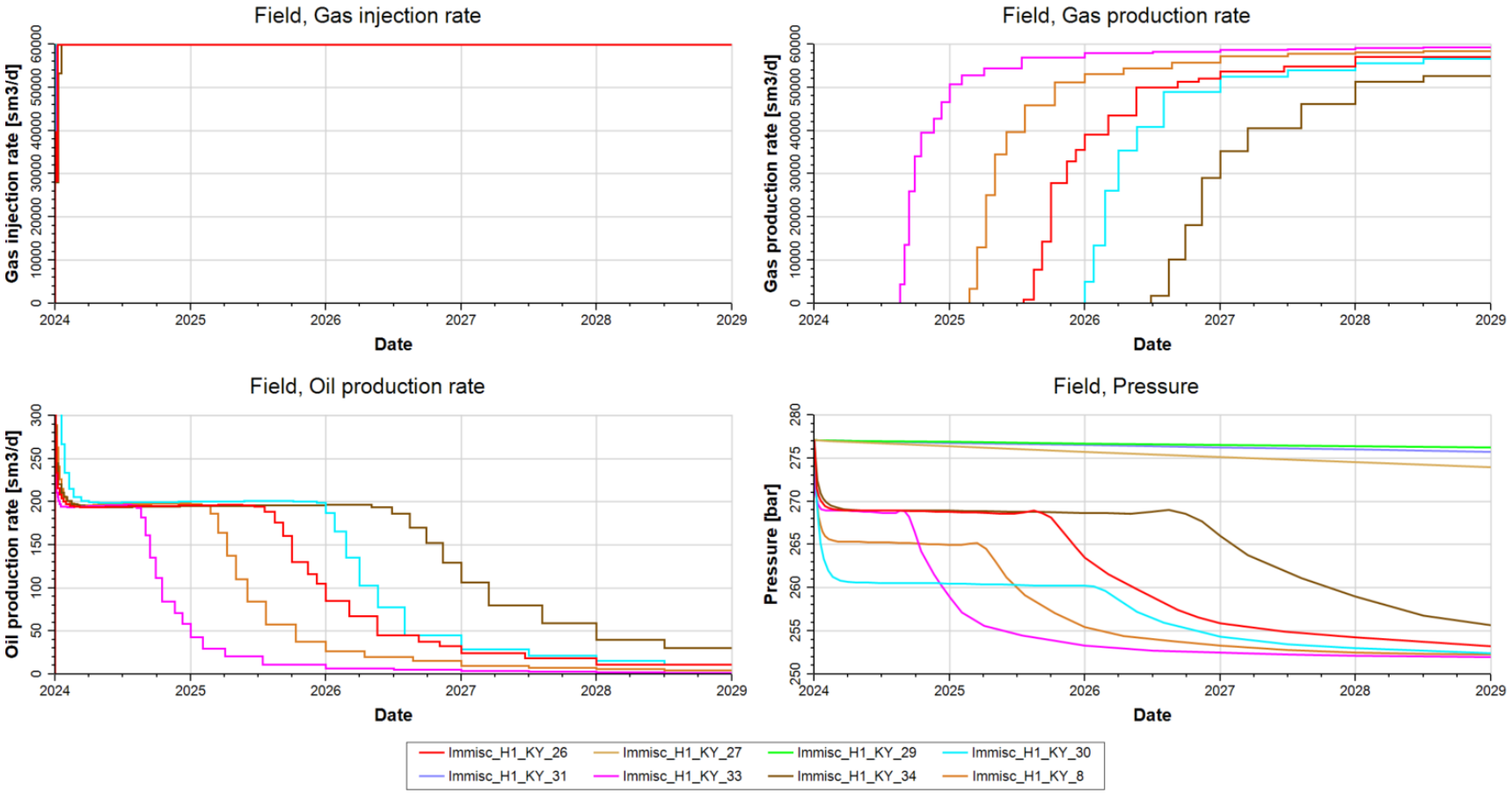

Figure 6.16. Results for H1 fluid of Table 6.7 cases

The reservoir pressure varies among the fluid samples due to differences in their minimum miscibility pressure (MMP), which in turn impacts the recovery factors. To isolate the effect of pressure on recovery factors, all fluid samples were simulated under identical pressure conditions, with a minimum reservoir pressure set to 200 bars. It is important to note that the MMP values remained unchanged, and reservoir pressure was the only variable parameter. Consequently, the recovery factors were influenced solely by fluid properties.

The simulation results clearly demonstrate that higher API gravity correlates with higher recovery factors. For reference, the API gravity and reservoir temperature values for each sample are as follows: H1 (API 10.0, 52°C), M3 (API 10.0, 81.11°C), F5 (API 31.914, 121.1°C), F2 (API 37.446, 115.0°C), and D1 (API 47.88, 110.0°C). Using the same porosity and permeability parameters outlined in Table 6.7, the results for scenarios where reservoir pressures were equal across all fluid samples are presented in Table 6.8 as example cases.

Examining the simulation results of equal pressure runs reveals that pressure does not affect the recovery factor significantly in immiscible cases. The pressure values, which were used in normal immiscible cases, may cause these consequences because the reservoir pressure of four of the five them are close to the 200 bars. Only the reservoir pressure of M3 fluid sample is changed notably, which is 340 bars in the normal runs. As a result, the recovery factor changes in M3 fluid are more dramatical than the others.

The effect of reservoir pressure will be examined in detail for the F5 oil sample in Chapter 6.4.

Similar to the miscible cases, Pearson product moment and Chatterjee's rank correlations were used to obtain relation between uncertain input parameters and recovery factors in immiscible cases. The Pearson method utilized the rank values of Spearman rank correlation because of repeated data in the dataset. Both were calculated using MS Excel and Chatterjee correlation values were computed via a MATLAB script. The results of these calculations are presented in Table 6.9.

Table 6.8 Simulation results examples where the pressure is equal in all fluid samples

Uncertain Parameters		***Recovery Factors for five fluids, %***				
$perm_mult	*$poro_mult*	*H1*	*M3*	*F5*	*F2*	*D1*
1.9225	1.9870	19.9578	22.3180	17.8732	17.0392	21.6029
1.5005	2.5	21.2800	18.0595	18.8665	19.7695	22.4969
0.001	1	0.0679	0.7865	2.1148	3.1687	5.5837
0.001	4	0.0204	0.2509	0.5614	0.7698	1.2171
3	4	15.8267	12.9854	13.3482	13.9028	15.3283
0.001	2.5	0.0305	0.3620	0.8253	1.1439	1.8961
1.5005	1	22.6874	18.6081	23.5102	20.5262	23.0628
1.5005	4	20.0711	17.3064	18.0590	18.7075	21.5062

Table 6.9 Pearson and Chatterjee correlation coefficients for immiscible runs

		Pearson		*Chatterjee*	
Fluid Types	*API*	*Perm_mult*	*Poro_mult*	*Perm_mult*	*Poro_mult*
H1	10.000	-0.0870	-0.2051	0.6831	0.1532
M3	24.058	-0.4715	-0.1687	0.6156	0.1299
F5	31.914	-0.3418	-0.1733	0.5065	0.0494
F2	37.446	-0.4730	-0.1518	0.5065	0.0545
D1	47.880	-0.5082	-0.0182	0.7558	0.1610

According to the Pearson correlation results, permeability and porosity always have negative impact on recovery factors during immiscible carbon dioxide injection projects regardless of the API gravity of the crude oil. The negative correlation of permeability increases from lower API to higher API fluid except F5 in the between. Permeability has both a negative and more dominant effect on the recovery factor. This is because, in high-permeability scenarios, the injected gas, being less dense than the oil in the reservoir, can easily flow through the reservoir from the injection

well to the production well. After a certain period of producing both oil and gas from the production well, gas production begins to dominate, suppressing oil production.

The negative correlation of porosity in Pearson technique declines through higher API gravity oil. According to Chatterjee method, permeability has a high to very high influence on recovery factor in immiscible runs while porosity has low or very low influence.

6.4 Reservoir Pressure Effects on Recovery Factor for Miscible and Immiscible Cases

In the earlier simulation results chapters, the miscible and immiscible cases with four and five different fluid samples were introduced. In those cases, fluid properties, reservoir temperature and pressures varied due to sample type. Therefore, the effect of the reservoir pressure cannot be clearly seen on the recovery factors. To see the effect of reservoir pressure, F5 fluid sample is selected as base fluid for further analyses. There are five different pressures defined in Petrel as minimum, maximum, reference, bubble point pressure and contact pressure. This concept and some fundamental rules, which are accepted for this study, were explained in Chapter 5.1.2 and 5.1.3 in detail. The same rules for determining pressure values are utilized here as well. Therefore, MMP is obtained for miscible cases, then, the other pressure value is obtained by following the rules for miscible cases. In immiscible cases, maximum pressures must not exceed the MMP value, so that the minimum pressures are chosen accordingly. Moreover, maximum bottomhole pressure for the injection well and minimum bottomhole pressure for the production well are also described with this procedure.

Afterward, investigations of the miscible and immiscible cases are performed separately, once again. This time, porosity and permeability values are constant in order to solely detect the impact of reservoir pressure. These constant values are selected as 1000 mD, 100 mD and %10 for permeability at X and Y direction,

permeability at Z direction and porosity, respectively. In Table 5.1 and Table 5.2, the base case properties of F5 fluid sample are introduced and they are utilized for this study, except pressure values. The pressure values in these tables will change in order to acquire the effect of it. The used pressure values are given distinctly in Table 6.10 and Table 6.11 for miscible and immiscible cases.

Table 6.10 Properties for miscible constant temperature cases

	F5	**F5**	**F5**	**F5**	**F5**
MMP, bar	335.249	335.249	335.249	335.249	335.249
Min Pressure, bar	345.0	375.0	400.0	425.0	450.0
Max Pressure, bar	414.0	450.0	480.0	510.0	540.0
Ref. Pressure, bar	345.0	375.0	400.0	425.0	450.0
Temperature, °C	121.1	121.1	121.1	121.1	121.1
GOC, m	-2000	-2000	-2000	-2000	-2000
WOC, m	-2050	-2050	-2050	-2050	-2050
Cont. Pressure, bar	379.5	412.5	440.0	467.5	495.0
API	31.914	31.914	31.914	31.914	32.914
Permeability X and Y, mD	1000	1000	1000	1000	1000
Permeability Z, mD	100	100	100	100	100
Porosity, %	10	10	10	10	10
Bubble Point Pressure, bar	345.0	375.0	400.0	425.0	450.0
Gas SG	0.6636	0.6636	0.6636	0.6636	0.6636
Water Salinity, ppm	30,000	30,000	30,000	30,000	30,000
BHP_{max} for Injector well, bar	414	450	480	510	540
BHP_{min} for Prod. well, bar	345	375	400	425	450

Table 6.11 Properties for immiscible constant temperature cases

	F5	**F5**	**F5**	**F5**	**F5**	**F5**
MMP, bar	335.249	335.249	335.249	335.249	335.249	335.249
Min Pressure, bar	240.0	220.0	200.0	180.0	150.0	100.0
Max Pressure, bar	288.0	264.0	240.0	216.0	180.0	120.0
Ref. Pressure, bar	240.0	220.0	200.0	180.0	150.0	100.0
Temperature, ℃	121.1	121.1	121.1	121.1	121.1	121.1
GOC, m	-2000	-2000	-2000	-2000	-2000	-2000
WOC, m	-2050	-2050	-2050	-2050	-2050	-2050
Cont. Pressure, bar	264.0	242.0	220.0	198.0	165.0	110.0
API	33.914	31.914	31.914	32.914	32.914	33.914
Permeability X & Y, mD	1000	1000	1000	1000	1000	1000
Permeability Z, mD	100	100	100	100	100	100
Porosity, %	10	10	10	10	10	10
Bubble Point Pres, bar	240.0	220.0	200.0	180.0	150.0	100.0
Gas SG	0.6636	0.6636	0.6636	0.6636	0.6636	0.6636
Water Salinity, ppm	30,000	30,000	30,000	30,000	30,000	30,000
BHPmax for Inj. well, bar	288	264	240	216	180	120
BHPmin for Prd. well, bar	240	220	200	180	150	100
WOC, m	-2050	-2050	-2050	-2050	-2050	-2050
Cont. Pressure, bar	264.0	242.0	220.0	198.0	165.0	110.0
API	33.914	31.914	31.914	32.914	32.914	33.914
Permeability X & Y, mD	1000	1000	1000	1000	1000	1000

The simulations were practiced for the immiscible cases where the minimum reservoir pressures are 100, 150, 180, 200, 220 and 240 bars and 345, 375, 400, 425 and 450 bars for the miscible cases. The outcomes of these simulations are presented

in Table 6.12. Notably, the immiscible results show a decreasing trend with increasing pressure, while the miscible results exhibit an increasing trend.

The decrease in recovery factor of immiscible cases can be attributed to the compressibility of the injected gas, which is carbon dioxide. The gas compressibility formula is given at Equation 6.1 to 6.3. According to Guo, Sun, & Ghalambor (2008), the second term on the right-hand side is typically small, thus; gas compressibility is fundamentally equal to the reciprocal of pressure value. Hence, when the pressure increases, the gas compressibility declines. Consequently, in these immiscible simulation cases gas compressibility can play a significant role in determining recovery factors.

$$c_g = -\frac{1}{V}\left(\frac{\partial V}{\partial P}\right)_T \tag{6.1}$$

$$\frac{\partial V}{\partial P} = nRT\left(\frac{1}{P}\frac{\partial y}{\partial x} - \frac{Z}{P^2}\right) \tag{6.2}$$

$$c_g = \frac{1}{P} - \frac{1}{Z}\frac{\partial Z}{\partial P} \tag{6.3}$$

Carbon dioxide injected as miscible for the five remaining cases. The outputs of these simulations show that when the pressure increases, the recovery factor also increases in miscible situations. Abdullah & Hasan (2021) worked on miscible CO_2 injection scenarios for a field, and then they also obtained that the same results with this study. These results can be explained by carbon dioxide injection enhances oil recovery by causing the oil to swell, decreasing its viscosity, and mobilizing lighter oil components, which together improve sweep efficiency (Abdullah & Hasan, 2021).

Table 6.12 Simulation results for constant temperature cases

Miscibility Condition	*Pressure, bar*	*Recovery Factor, %*
Immiscible Cases	100	22.36712
	150	20.76563
	180	19.76778
	200	19.37719
	220	19.18600
	240	19.17010
Miscible Cases	345	30.57244
	375	32.99066
	400	35.94322
	425	42.65297
	450	50.68224

6.5 Reservoir Temperature Effects on Recovery Factor for Miscible and Immiscible Cases

In Chapters 6.2 and 6.3, the miscible and immiscible cases with four and five different fluid samples were introduced. In those cases, fluid properties, reservoir temperature and pressures varied due to sample type. The effect of the reservoir temperature cannot be clearly observed on the recovery factors due to these alterations, which is similar to constant reservoir pressure analysis in the previous chapter. To see the effect of reservoir temperature, F5 fluid sample is selected as base fluid for further analyses. In these analyses, minimum miscibility pressure (MMP) must be recalculated according to the new reservoir temperature value since the MMP value is a function of the reservoir temperature.

In this study, the temperature values of 70°C, 95°C, 121.1°C, 150°C, and 170°C were utilized. Therefore, new MMP values were calculated with new reservoir

temperature using slim tube simulations. The pressures and recovery factors tables and pressures vs recovery factors at infinite grid sizes plot, which are the results of these simulations, are presented in Appendix C: Slim Tube Simulation Results' Tables and Graphs. The results are shown in Table 6.10. Moreover, it was observed that MMP values increased with rising temperature, as suggested by Yellig & Metcalfe (1980).

Table 6.13 MMP results of F5 fluid with various temperature (℃)

	F5	*F5*	*F5*	*F5*	*F5*
Temperature, ℃	70.0	95.0	121.1	150.0	170.0
MMP, bar	275.177	300.209	335.249	343.929	352.499

Afterward, investigations of the miscible and immiscible cases are performed separately, once again. This time, porosity and permeability values are constant to solely detect the impact of reservoir pressure. These constant values are selected as 1000 mD, 100 mD and %10 for permeability at X and Y direction, permeability at Z direction and porosity, respectively. To calculate the recovery factors, seven different minimum pressure values are selected. These pressure values are given in Table 6.11. Five distinct pressures—minimum, maximum, reference, bubble point, and contact pressure—are defined in Petrel. The concept and fundamental guidelines applied to this study are completely explained in Chapters 5.1.2 and 5.1.3. These same guidelines for determining pressure values are also applied in this section. The remaining reservoir properties are the same as the previous chapter ones.

Table 6.14 Pressure values which are used in simulations

	F5	*F5*	*F5*	*F5*	*F5*	*F5*
Min Pressure, bar	370.0	345.0	310.0	250.0	225.0	200.0
Max Pressure, bar	444.0	414.0	372.0	300.0	270.0	240.0
Ref. Pressure, bar	370.0	345.0	310.0	250.0	225.0	200.0
Contact Pressure, bar	407.0	379.5	341.0	275.0	247.5	220.0
Bubble Point Pres, bar	370.0	345.0	310.0	250.0	225.0	200.0
BHP_{min} for Prod. well, bar	370.0	345.0	310.0	250.0	225.0	200.0
BHP_{max} for Inj. well, bar	444.0	414.0	372.0	300.0	270.0	240.0

Finally, the miscibility condition of simulation with the pressure values in Table 6.13 are determined and presented in Table 6.15. New reservoir temperature and MMP values, which are calculated by using new temperatures, are listed on the left-hand side of the table. In the right-hand side, seven minimum reservoir pressure values are entered, then utilizing the checkbox method indicated which minimum reservoir pressure valued simulation is miscible or immiscible at the temperature in the same row. The symbol of "✓" means that the pressure value at that column is miscible at the temperature in that row. The symbol of "☒" means that the pressure value at that column is immiscible at the temperature in that row. The symbol of "☐" means that the minimum pressure value at that column is immiscible at the temperature in that row but the maximum pressure of it is miscible; thus, these cell values were not simulated.

Afterwards, the simulations were executed, and their results can be seen in Table 6.13. The table should first be read by selecting a temperature value from the left-hand side, then checking the desired pressure column in the same row. The miscible or immiscible conditions of the pressures are written in the row above.

Table 6.15 Miscibility condition of F5 fluid for new temperatures according to Table 6.14 pressure values

Fluid Properties		*Miscibility Condition at Various Pressure, bar*					
Temp, ℃	MMP, bar	200	225	250	310	345	370
70.0	275.177	☒	☒	☐	✓	✓	✓
95.0	300.209	☒	☒	☒	✓	✓	✓
121.1	335.249	☒	☒	☒	☐	✓	✓
150.0	343.929	☒	☒	☒	☐	✓	✓
170.0	352.499	☒	☒	☒	☐	☐	✓

Table 6.16 Simulation results for constant temperature cases for various pressure

Fluid Properties		*Immiscible Cases Pres., bar & Recovery Factors, %*			*Miscible Cases Pres., bar & Recovery Factors, %*		
Temp, ℃	MMP, bar	200	225	250	310	345	370
70.0	275.177	17.563	17.743	–	28.405	34.127	46.780
95.0	300.209	18.493	18.444	18.596	28.003	31.161	34.561
121.1	335.249	19.642	19.462	19.449	–	30.572	32.562
150.0	343.929	19.891	19.516	19.296	–	28.674	30.234
170.0	352.499	20.557	20.235	20.011	–	–	30.117

The analysis results indicate that in immiscible cases, as temperature increases, the recovery factor also rises, whereas in miscible cases, the recovery factor decreases. Reservoir temperature is inversely related to oil viscosity, meaning that as temperature increases, oil viscosity decreases (SPE, 2024). Consequently, the low reservoir temperature in this case results in more viscous crude oil compared to other samples, which impacts recovery factors in both miscible and immiscible scenarios. To illustrate the effect of reservoir temperature on oil viscosity and density, one immiscible and one miscible simulation group were selected. The pressures for these

control groups were set at 200 bars and 370 bars, as both were simulated for all temperature values. At 370 bars, oil viscosities were 0.448 cP at 70°C and 0.287 cP at 170°C. Similarly, at 200 bars, oil viscosities were 0.700 cP at 70°C and 0.378 cP at 170°C. These results indicate a viscosity reduction of 36% for miscible cases and 46% for immiscible cases due to increasing reservoir temperature. Thus, an increase in reservoir temperature positively impacts recovery factors, with the effect being more pronounced in immiscible cases.

On the other hand, carbon dioxide solubility is one of the primary factors contributing to the reduction in recovery factors in miscible cases, as CO_2 solubility typically decreases with increasing temperature under high-pressure conditions (Behnoudfar, Rostami, & Hemmati-Sarapardeh, 2018) (Perera, et al., 2016). This reduction in solubility limits CO_2's ability to swell the oil and reduce its viscosity effectively. Oil density data at 200 bars and 370 bars were selected as control groups. At 370 bars, oil densities were 557.126 kg/m^3 at 70°C and 574.387 kg/m^3 at 170°C. In contrast, at 200 bars, oil densities were 672.522 kg/m^3 at 70°C and 668.328 kg/m^3 at 170°C. These results demonstrate that oil density increases with temperature in miscible cases, whereas it decreases in immiscible cases. As a consequence, these outcomes prove that CO_2 solubility is inversely proportional with increasing reservoir temperatures at high-pressure reservoirs.

Additionally, minimum miscibility pressure increases with temperature, so that pressure differences between MMP and reservoir pressure are decreasing.

Abdullah & Hasan (2021) and Perera, et al. (2016) applied sensitivity analyses on reservoir temperature for CO_2 injection. Both articles were obtained that oil production increased with temperature rises. However, they did not mention the recovery factor of the production. Furthermore, both papers did not consider the effect of temperature changes on minimum miscibility pressure and did not recalculate the MMP for new temperature values. Nevertheless, MMP is a function of the reservoir temperature, so that in this thesis, MMP values were recomputed at altered reservoir temperature values.

CHAPTER 7

CONCLUSION

This thesis provides a fast check of the effect of screening parameters on miscible and immiscible CO_2 EOR applications on five crude oil samples which have different API gravity. Various software, including PVTi, Petrel, Eclipse 100 and 300, and MATLAB, were used at distinct stages of the research. The minimum miscibility pressures of the fluids were found through slim tube simulations using 1-D Eclipse compositional simulations (E300) and empirical MMP correlations. According to the literature, compositional simulations are considered more accurate than empirical correlations. This observation aligned with our findings, as the correlation results displayed a wide range of pressures. However, slim tube simulation cannot obtain MMP value for H1 fluid because of its API gravity, which is 10.0. Conversely, empirical correlations provided MMP values for H1, but these values were highly scattered and inconsistent.

In a small, homogeneous hypothetical field with one injection well and one production well, miscible, and immiscible CO_2 injection simulations were conducted using Petrel's Uncertainty and Optimization tool within a black oil simulation framework. Porosity and permeability were selected as uncertain screening parameters to evaluate their combined impact on recovery factors within the defined screening criteria range. The results revealed that for both injection types, gas breakthrough does not occur when permeability is low, except in reservoirs with low porosity. In such cases, reservoir pressure increases due to the continued injection of CO_2, while flow within the reservoir remains restricted because of extremely low permeability. These issues were consistent across all fluid samples. Additionally, the results demonstrated that gas injection, gas production, oil production, and reservoir pressure trends generally follow similar patterns, regardless of fluid properties, in both injection scenarios.

In immiscible flooding, the H1 oil sample behaved differently from the other fluid samples. Instead of an immediate decrease in reservoir pressure to the minimum, H1 maintained the pressure at a plateau for some time before gas breakthrough occurred. This behavior was triggered by the high viscosity of H1 oil, which resisted the sweeping effects of carbon dioxide.

In miscible cases, the reduction in oil viscosity was nearly double that observed in immiscible cases, proving that miscible carbon dioxide injection is more effective at reducing oil viscosities. Additionally, the drop in oil density was higher in miscible cases; however, it was only about 1%, which had a negligible impact on recovery factors.

All cases were initially simulated under different reservoir pressures. When all samples were simulated under the same pressure, aligned with their miscibility conditions, the results for miscible cases indicated that higher API gravity led to higher recovery factors. Immiscible cases generally followed a similar trend.

Based on these results, Pearson, Spearman Rank, and Chatterjee Rank Correlations were applied to analyze the relationships between porosity, permeability, and recovery factors. The findings revealed that both porosity and permeability negatively impacted recovery factors. In miscible runs, porosity had a stronger influence, whereas permeability played a more significant role in immiscible runs. Recovery factors were consistently higher in cases with higher API gravity for both injection types.

For immiscible flooding under the same pressure, the correlations showed that the influence of both permeability and porosity increased as API gravity rose. In the same pressure miscible cases, the impact of porosity increased with API gravity, while the influence of permeability decreased.

To investigate the reservoir pressure and temperature effect on recovery factors, sensitivity analyses were conducted using one of the fluid samples. In these analyses, either reservoir pressure or temperature was varied depending on the case, while all

other fluid and rock properties were held constant. The results showed that, in immiscible runs, recovery factors decreased as reservoir pressure increased, whereas in miscible conditions, both reservoir pressure and recovery factors increased together. This behavior is explained by the inverse relationship between gas compressibility and reservoir pressure, which contributes to the decline in recovery factors in immiscible cases.

Sensitivity analyses on reservoir temperature first required calculating new MMP values for the adjusted temperatures. After determining the new MMP values for each temperature, various pressure values were tested for both immiscible and miscible cases. In immiscible scenarios, recovery factors increased with rising temperature, whereas in miscible cases, recovery factors decreased. This trend is attributed to the inverse relationship between carbon dioxide solubility and reservoir temperature. Reduced CO_2 solubility limits the effects of oil swelling and viscosity reduction, both of which depend on gas solubility.

For future work, machine-learning algorithms, like random forest, could be applied to conduct extensive uncertainty runs on the dataset to establish the relationship between screening parameters and recovery factor. Additionally, this approach could be extended to other Enhanced Oil Recovery (EOR) methods, such as nitrogen injection.

REFERENCES

Abdullah, N., & Hasan, N. (2021). Effects of miscible CO2 injection on production recovery. *Journal of Petroleum Exploration and Production Technology*.

Adel, I. A., Tovar, F. D., & Schechter, D. S. (2016). Fast-Slim Tube: A Reliable and Rapid Technique for the Laboratory Determination of MMP in CO2 - Light Crude Oil Systems. *SPE Improved Oil Recovery Conference.* Tulsa: Society of Petroleum Engineers.

Al Adasani, A., & Bai, B. (2011). Analysis of EOR projects and updated screening criteria. *Journal of Petroleum Science and Engineering*, 10-24.

Aleidan, A., & Mamora, D. (2011). Comparative Study of Oil Recovery during Miscible CO2 Injection in Carbonate Cores and Slimtube. *SPE Saudi Arabia section Young Professionals Technical Symposium.* Dhahran,: Society of Petroleum Engineers.

Al-Mjeni, R., Arora, S., Edwards, J., Felber, B. J., Gurpinar, O., Hirasaki, G. J., . . . Ramamoorthy, R. (2010). Has the Time Come for EOR? *Oilfield Review*.

Alston, R. B., Kokolis, G. P., & James, C. F. (1985). CO2 Minimum Miscibility Pressure A Correlation for Impure CO2 Streams and Live Oil Systems. *Society of Petroleum Engineers Journal*, 268-274.

Alvarado, V., Ranson, A., Hernández, K., Manrique, E., Matheus, J., Liscano, T., & Prosperi, N. (2002). Selection of EOR/IOR Opportunities Based on Machine Learning. *SPE 13th European Petroleum Conference.* Aberdeen: Society of Petroleum Engineers.

Amao, A. M., Siddiqui, S., Menouar, H., & L., B. (2012). A New Look at the Minimum Miscibility Pressure (MMP) Determination from Slimtube Measurements. *Eighteenth SPE Improved Oil Recovery Symposium.* Tulsa.

Behnoudfar, P., Rostami, A., & Hemmati-Sarapardeh, A. (2018). Chapter Four - Miscible Gas Injection Processes. In A. Bahadori, *Fundamentals of*

Enhanced Oil and Gas Recovery from Conventional and Unconventional Reservoirs (pp. 102 - 138). Gulf Professional Publishing .

Bender, S. (2016, December 8). Optimization of CO2 EOR and Storage Design Under Uncertainity. *Optimization of CO2 EOR and Storage Design Under Uncertainity*. Ankara, Türkiye: METU. Retrieved from https://open.metu.edu.tr/handle/11511/26197

Benham, A. L., Dowden, W. E., & Kunzman, W. J. (1960). Miscible Fluid Displacement--Prediction of Miscibility. *AIChE-SPE Joint Symposium.* San Francisco: Society of Petroleum Engineers.

Bourdarot, G., & Ghedan, S. (2011). Modified EOR Screening Criteria as Applied to a Group of Offshore Carbonate Oil Reservoirs. *SPE Reservoir Characterisation and Simulation Conference and Exhibition.* Abu Dhabi: Society of Petroleum Engineers.

BP. (2024). *BP Energy Outlook 2024.* BP.

Brashear, J. P., & Kuuskra, V. A. (1978). The Potential and Economics of Enhanced Oil Recovery. *Journal of Petroleum Technology*, 1231 - 1239.

Carcoana, A. N. (1982). Enhanced Oil Recovery in Rumania. *hird JOint Symposium on Enhanced Oil Recovery of the Society of Petroleum Engineers* (pp. 367 - 379). Tulsa, OK: Society of Petroleum Engineers.

Charles University. (2024, November 6). *Critical State of Carbon Dioxide.* Retrieved from Collection of Physics Experiments: https://physicsexperiments.eu/1771/critical-state-of-carbon-dioxide

Chatterjee, S. (2020). A New Coefficient of Correlation. *Journal of the American Statistical Association*.

Chen, Z. (2001). Formulations and Numerical Methods of the Black Oil Model in Porous Media. *SIAM Journal on Numerical Analysis*, 489-514.

Chen, Z., Huan, G., & Ma, Y. (2006a). The Black Oil Model. In Z. Chen, G. Huan, & Y. Ma, *Computational Methods for Multiphase Flows in Porous Media* (pp. 283-346). Philadelphia: Society for Industrial and Applied Mathematics.

Chen, Z., Huan, G., & Ma, Y. (2006b). The Compositional Model. In Z. Chen, G. Huan, & Y. Ma, *Computational Methods for Multiphase Flows in Porous Media* (pp. 347-380). Philadelphia: Society for Industrial and Applied Mathematics.

Cohen, J. (1988). *Statistical Power Analysis for the Behavioral Sciences.* Lawrence Erlbaum Associates.

Comberiati, J. R., & Zammerilli, A. M. (1982). *Effects of Petroleum Reservoir Conditions on Oil Recovery by Carbon Dioxide Injection.* Morgantown: United States Department of Energy Morgantown Energy Technology Center.

Cronquist, C. (1978). Carbon dioxide dynamic miscibility with light reservoir oils. *4th Annual U.S. DOE Symposium.* Tulsa.

Dai, C., You, Q., Zhao, M., Zhao, G., & Zhao, F. (2023). 10. Thermal Oil Recovery. In C. Dai, Q. You, M. Zhao, G. Zhao, & F. Zhao, *Principles of Enhanced Oil Recovery* (pp. 319-356). China University of Petroleum Press.

Dai, C., You, Q., Zhao, M., Zhao, G., & Zhao, F. (2023). 9. Gas Miscible Flooding. In C. Dai, Q. You, M. Zhao, G. Zhao, & F. Zhao, *Principles of Enhanced Oil Recovery* (pp. 270-318). China University of Petroleum Press.

Danesh, A. (1998). *PVT and Phase Behaviour of Petroleum Reservoir Fluids.* Elsevier Science & Technology Books.

Delforouz, F. B., Movaghar, M. R., & Shariaty, S. (2019). New empirical correlations for predicting Minimum Miscibility Pressure (MMP) during CO2 injection; implementing the Group Method of Data Handling (GMDH) algorithm and Pitzer's acentric factor. *Oil & Gas Science and Technology*.

Dindoruk, B., Johns, R., & Orr Jr., F. O. (2020). Measurement and Modeling of Minimum Miscibility Pressure: A State-of-the-Art Review. *SPE Improved Oil Recovery Conference,*. Society of Petroleum Engineers.

Elsharkawy, A. M. (2003). An empirical model for estimating the saturation pressures of crude oils. *Journal of Petroleum Science and Engineering*, 57-77.

Emera, M. K., & Sarma, H. K. (2004). Use of genetic algorithm to estimate CO2–oil minimum miscibility pressure—a key parameter in design of CO2 miscible flood. *Journal of Petroleum Science and Engineering*, 37 - 52.

Energy Institute. (2024). *Statistical Review of World Energy*. Energy Institute.

Fujita, A., Sato, J. R., Demasi, M. A., Sogayar, M. C., Ferreira, C. E., & Miyano, S. (2009). Comparing Pearson, Spearman and Hoeffding's D Measure for Gene Expression Association Analysis. *Journal of Bioinformatics and Computational Biology*, 663 - 684.

Gao, P., Towler, B., & Pan, G. (2010). Strategies for Evaluation of the CO2 Miscible Flooding Process. *Abu Dhabi International Petroleum Exhibition & Conference.* Abu Dhabi,: Society of Petroleum Engineers.

Geffen, T. (1977). Improved Oil Recovery Could Ease Energy Shortage. *World Oil*, 84-88.

Gharbi, R. B. (2000). An expert system for selecting and designing EOR processes. *Journal of Petroleum Science and Engineering*, 33-47.

Ghedan, S. (2009). Global laboratory experience of CO2-EOR flooding. *SPE/EAGE Reservoir Characterization and Simulation Conference.* Abu Dhabi: Society of Petroleum Engineers.

Glasø, Ø. (1985). Generalized Minimum Miscibility Pressure Correlation . *Society of Petroleum Engineers Journal*, 927-934.

Göktaş, A., & İşçi, Ö. (2011). A Comparison of the Most Commonly Used Measures of Association for Doubly Ordered Square Contingency Tables via Simulation. *Metodološki zvezki*, 17 - 37.

Green, D. W., & Willhite, G. P. (2018). Introduction to EOR Processes. In D. W. Green, & G. P. Willhite, *Enhanced Oil Recovery* (pp. 1 - 15). Richardson,TX: Society of Petroleum Engineers.

Guerillot, D. R. (1988). EOR Screening With an Expert System. *Petroleum Industry Applications of Microcomputers.* San Jose, CA: Society of Petroleum Engineers.

Guo, B., Sun, K., & Ghalambor, A. (2008). Properties of Petroleum Fluids. In B. Guo, K. Sun, & A. Ghalambor, *Well Productivity Handbook* (pp. 15 - 41). Gulf Publishing Company.

Guo, H., Dong, J., Wang, Z., Liu, H., Ma, R., Kong, D., . . . She, H. (2018). 2018 EOR Survey in China-Part 1. *SPE Improved Oil Recovery Conference.* Tulsa: Society of Petroleum Engineers.

Hamdi, Z., & Awang, M. (2014). CO2 Minimum Miscibility Pressure Determination of Pure Hydrocarbons in Different Temperatures Using Slimtube Simulations. *Research Journal of Applied Sciences, Engineering and Technology*, 3159-3163.

Hassan, A., Azad, M. S., & Mahmoud, M. (2023). An analysis of nitrogen EOR screening criteria parameters based on the up-to-date review. *Journal of Petroleum Science and Engineering*.

Høier, L., & Whitson, C. H. (1998). Miscibility Variation in Compositionally Grading Reservoirs. *1998 SPE Annual Technical Conference and Exhibition.* New Orleans: Society of Petroleum Engineers.

Holm, L. W., & Josendal, V. A. (1974). Mechanisms of Oil Displacement By Carbon Dioxide. *Journal of Petroleum Technology*, 1427–1438.

Iyoho, A. (1978). Selecting Enhanced Recovery Processes. *World Oil*, 61-64.

Jaferi, S., Ashoori, S., & MK, G. A. (2019). Determination of the minimum miscibility pressure using the eclipse 300 simulator and compare it with the laboratory results. *International Journal of Petrochemical Science & Engineering*, 97 - 107.

Jaubert, J.-N., Avaullee, L., & Souvay, J.-F. (2002). A crude oil data bank containing more than 5000 PVT and gas injection data. *Journal of Petroleum Science and Engineering*, 65 - 107.

Jaubert, J.-N., Wolff, L., Neau, E., & Avaullee, L. (1998). A Very Simple Multiple Mixing Cell Calculation to Compute the Minimum Miscibility Pressure Whatever the Displacement Mechanism. *Industrial & Engineering Chemistry Research*, 4854-4859.

Johns, R. T., & Dindoruk, B. (2013). Chapter 1 - Gas Flooding. In J. J. Sheng, *Enhanced Oil Recovery Field Case Studies* (pp. 1-22). Gulf Professional Publishing.

Kanakaki, E. M., Samnioti, A., Koffa, E., Dimitrellou, I., Obetzanov, I., Tsiantis, Y., . . . Stamataki, S. (2023). Prospects of an Acid Gas Re-Injection Process into a Mature Reservoir. *Energies*.

Karamnia, V., & Ashoori, S. (2021). Determination of Minimum Miscibility Pressure Using PVTi Software, Eclipse 300, and Empirical Correlations. *Iranian Journal of Oil & Gas Science and Technology*, 107 - 126.

Koottungal, L. (2014). *2014 Worldwide EOR Survey.* Oil and Gas Journal.

Krejbjerg, K., & Pedersen, K. S. (2006). Controlling VLLE Equilibrium with a Cubic EoS in Heavy Oil Modeling. *Petroleum Society's 7th Canadian International Petroleum Conference.* Calgary: Petroleum Society Journals.

Lee, J. I. (1979). *Effectiveness of carbon dioxide displacement under miscible and immiscible conditions.* Calgary: Petroleum Recovery Institute.

Li, H., Qin, J., & Yang, D. (2012). An Improved CO2−Oil Minimum Miscibility Pressure Correlation for Live and Dead Crude Oils. *Industrial & Engineering Chemistry Research*, 3516 - 3523 .

Liu, Z.-x., Liang, Y., Wang, Q., Guo, Y.-j., Gao, M., Wang, Z.-b., & Liu, W.-l. (2020). Status and progress of worldwide EOR field applications. *Journal of Petroleum Science and Engineering*.

Moghadamzadeh, H., Maghsoodloorad, H., Zarabpour, A., Hemmati, A., Shahsavar, S., & Shahsavari, S. (2013). Impact of Lumping Techniques for Fluid Characterization in Gas Condensate Reservoir. *Australian Journal of Basic and Applied Sciences*, 320-333.

Moreno, J., Gürpinar, Ö., Liu, Y., Al-Kinani, A., & Çakır, N. (2014). EOR Advisor System: A Comprehensive Approach to EOR Selection. *International Petroleum Technology Conference.* Kuala Lumpur: Society of Petroleum Engineers.

Mungan, N. (1981). Carbon Dioxide Flooding-fundamentals . *Journal of Canadian Petroleum Technology*.

National Petroleum Council (NPC). (1976). *Enhanced Oil Recovery-An Analysis of the Potential for Enhanced Oil Recovery from Known Fields in the United States.* Washington, DC.

National Petroleum Council (NPC). (2021). *Chapter Eight – CO2 Enhanced Oil Recovery.*

Neau, E., Avaullée, L., & Jaubert, J. (1996). A New Algorithm for Enhanced Oil Recovery Calculations. *Fluid Phase Equilibria*, 265-272.

Orr Jr., F. M., & Jensen, C. M. (1984). Interpretation of Pressure-Composition Phase Diagrams for CO2/Crude-Oil Systems. *Society of Petroleum Engineers Journal*, 485-497.

Orr Jr., F. M., & Jessen, K. (2007). Compositional Simulation. In J. Franklin M. Orr, *Theory of Gas Injection Processes* (pp. 213-240). Tie Line Publications.

OTA, O. o. (1978). *Enhanced Oil Recovery Potential in the United States.* Washington, DC: Government Printing Office,.

Parada, C. H., & Ertekin, T. (2012). A New Screening Tool for Improved Oil Recovery Methods Using Artificial Neural Networks. *SPE Western Regional Meeting.* Bakersfield, CA: Society of Petroleum Engineers.

Perera, M. S., Gamage, R. P., Rathnaweera, T. D., Ranathunga, A. S., Koay, A., & Choi, X. (2016). A Review of CO2-Enhanced Oil Recovery with a Simulated Sensitivity Analysis. *Energies*.

Romero, D. (2024, October 26). *Chaterjee's Xi Correlation.* Retrieved from MATLAB Central File Exchange: https://www.mathworks.com/matlabcentral/fileexchange/112530-chaterjee-s-xi-correlation

Saini, D. (2019). *CO2-Reservoir Oil Miscibility Experimental and Non-experimental Characterization and Determination Approaches.* Springer.

Sehbi, B. S., Frailey, S. M., & Lawal, A. S. (2001). Analysis of Factors Affecting Microscopic Displacement Efficiency in CO2 Floods. *SPE Permian Basin Oil and Gas Recovery Conference.* Midland, Texas: Society of Petroleum Engineers.

Sheng, J. J. (2013a). Chapter 11 - Foams and Their Applications in Enhancing Oil Recovery. In J. J. Sheng, *Enhanced Oil Recovery Field Case Studies* (pp. 251-280). Gulf Professional Publishing.

Sheng, J. J. (2013b). Chapter - 19 Introduction to MEOR and Its Field Applications in China. In J. J. Sheng, *Enhanced Oil Recovery Field Case Studies* (pp. 543-559). Gulf Professional Publishing.

Shokir, E. M.-M. (2007). CO2–oil minimum miscibility pressure model for impure and pure CO2 streams. *Journal of Petroleum Science and Engineering*, 173-185.

SLB. (2010). *Petrel Help Manual.* Schlumberger.

SLB. (2023). *Eclipse Industry-reference reservoir simulator Reference manual.* Schlumberger.

SLB. (2024, November 12). *Energy Glossary*. Retrieved from ultraheavy oil: https://glossary.slb.com/en/terms/u/ultra_heavy_oil

SPE. (2024, 11 16). *Oil viscosity*. Retrieved from PetroWiki: https://petrowiki.spe.org/Oil_viscosity

Stalkup Jr, F. I. (1983). Status of Miscible Displacement. *Journal of Petroleum Technology*, 815-826.

Stalkup Jr., F. I. (1984). Miscible Displacement. *Monograph Series.* Richardson, TX: Society of Petroleum Engineers.

Stalkup Jr., F. I. (1990). Effect of Gas Enrichment and Numerical Dispersion on Enriched·Gas·Drive Predictions. *SPE Reservoir Engineering*, 647–655.

Sumner, T. (2024, August 21). *A New Coefficient of Correlation*. Retrieved from Towards Data Science: https://towardsdatascience.com/a-new-coefficient-of-correlation-64ae4f260310

Sun, Q., & Ertekin, T. (2020). Screening and optimization of polymer flooding projects using artificial-neural-network (ANN) based proxies. *Journal of Petroleum Science and Engineering*.

Surguchev, L., & Li, L. (2000). IOR Evaluation and Applicability Screening Using Artificial Neural Networks. *Improved Oil Recovery Symposium.* Tulsa, OK: Society of Petroleum Engineers.

Şahin, S., Kalfa, Ü., & Çelebioğlu, D. (2008). Bati Raman Field Immiscible CO2 Application—Status Quo and Future Plans. *SPE Latin American & Caribbean Petroleum Engineering Conference.* Buenos Aires: Society of Petroleum Engineers.

Taber, J. J., & Martin, F. D. (1983). Technical Screening Guides for the Enhanced Recovery of Oil. *58th Annual Technical Conference and Exhibition.* San Francisco, CA: Society of Petroleum Engineers.

Taber, J. J., Martin, F. D., & Seright, R. S. (1997a). EOR Screening Criteria Revisited - Part 1: Introduction to Screening Criteria and Enhanced Recovery Field Projects. *Improved Oil Recovery Sympostum.* Tulsa, OK: Society of Petroleum Engineers.

Taber, J. J., Martin, F. D., & Seright, R. S. (1997b). EOR Screening Criteria Revisited Part 2: Applications and Impact of Oil Prices. *Improved Oil Recovery Symposium.* Tulsa, OK: Society of Petroleum Engineers.

Thomas, A. (2019). *Essentials of Polymer Flooding Technique.* John Wiley & Sons.

Todd, M. R., & Longstaff, W. J. (1972). The Development, Testing, and Application Of a Numerical Simulator for Predicting Miscible Flood Performance. *Journal of Petroleum Technology*, 874-882.

Turta, A. (2013). Chapter 18 - In Situ Combustion. In J. J. Sheng, *Enhanced OilRecoveryFieldCaseStudies* (pp. 447-536). Gulf ProfessionalPublishing.

Vulin, D., Gaćina, M., & Biličić, V. (2018). Slim-tube simulation model for carbon dioxide enhanced oil recovery. *The Mining-Geology-Petroleum Engineering Bulletin.*

Whitson, C. H. (1983). Characterizing Hydrocarbon Plus Fractions. *SPE Journal*, 683-694.

Yan, W., Michlesen, M. L., & Stenby, E. H. (2012). Calculation of Minimum Miscibility Pressure Using Fast Slimtube Simulation. *Eighteenth SPE Improved Oil Recovery Symposium.* Tulsa: Society of Petroleum Engineers.

Yang, H., Sun, S., Li, Y., & Yang, C. (2019). A fully implicit constraint-preserving simulator for the black oil model of petroleum reservoirs. *Journal of Computational Physics*, 347-363.

Yellig, W. F., & Metcalfe, R. S. (1980). Determination and prediction of CO2 minimum miscibility pressures. *Journal of Petroleum Technology*.

Yuan, H., Johns, R. T., Egwuenu, A. M., & Dindoruk, B. (2004). Improved MMP Correlations for CO2 Floods Using Analytical Gas Flooding Theory. *SPE/DOE Fourteenth Symposium on Improved Oil Recovery.* Tulsa: Society of Petroleum Engineers.

Zhang, N., Wei, M., & Bai, B. (2017). Applicability of Worldwide CO2 Worldwide Immiscible Flooding and Prediction. *Carbon Management Technology Conference.* Houston.

Zhang, N., Wei, M., & Bai, B. (2018a). Statistical and analytical review of worldwide CO2 immiscible field applications. *Fuel*, 89-100.

Zhang, N., Wei, M., & Bai, B. (2018b). Comprehensive Review of Worldwide CO2 Immiscible Flooding. *SPE Improved Oil Recovery Conference.* Tulsa: Society of Petroleum Engineers.

Zhang, N., Wei, M., Fan, J., Aldhaheri, M., Zhang, Y., & Bai, B. (2019b). Development of a hybrid scoring system for EOR screening by combining conventional screening guidelines and random forest algorithm. *Fuel*.

Zhang, N., Yin, M., Wei, M., & Bai, B. (2019a). Identification of CO2 sequestration opportunities: CO2 miscible flooding guidelines. *Fuel*, 459 - 467.

APPENDICES

A. Extended Data of Fluid Samples

The data in the following tables are required during executing slim tube simulation in Eclipse 300.

Table A.1 Extended Data of F2 Part-1

Components	*Mol Percentage (%)*	*Pcrit (atm)*	*Tcrit (Kelvin)*	*Omega A*	*Omega B*
H_2S	0.0	88.2	373.6	0.45724	0.077796
CO_2	1.34	72.9	304.7	0.45724	0.077796
XVOL	23.84	45.34	190.06	0.45724	0.077796
C2+	29.02	40.066	392.78	0.45724	0.077796
C7+	28.19	24.807	618.59	0.45724	0.077796
C16+	17.61	8.3394	929.91	0.45724	0.077796

Table A.2 Extended Data of F2 Part-2

Components	*Mol Weight (g/mole)*	*Acentric Factor*	*Parachors*	*Z Crit*	*Z Crit (viscosity)*
H_2S	44.01	0.10	80.0	0.28195	0.28195
CO_2	16.143	0.225	780	0.27408	0.27408
XVOL	52.642	0.01323	76.698	0.28471	0.28471
C2+	138.9	0.17419	173.48	0.29045	0.29045
C7+	439.4	0.44779	395.15	0.2685	0.2685
C16+	44.01	1.27	1110.5	0.18939	0.18939

Table A.3 Extended Data of F5 Part-1

Components	*Mol Percentage (%)*	*Pcrit (atm)*	*Tcrit (Kelvin)*	*Omega A*	*Omega B*
H_2S	2.07	88.2	373.6	0.45724	0.077796
CO_2	0.383	72.9	304.7	0.45724	0.077796
XVOL	27.026	45.241	189.53	0.45724	0.077796
C2+	27.801	40.162	392.77	0.45724	0.077796
C7+	22.85	26.128	617.35	0.45724	0.077796
C15+	19.87	10.562	896.94	0.45724	0.077796

Table A.4 Extended Data of F5 Part-2

Components	*Mol Weight (g/mole)*	*Acentric Factor*	*Parachors*	*Z Crit*	*Z Crit (viscosity)*
H_2S	34.076	0.10	80.0	0.28195	0.28195
CO_2	44.01	0.225	78.0	0.27408	0.27408
XVOL	16.242	0.01345	76.401	0.2847	0.2847
C2+	52.388	0.17387	172.62	0.28959	0.28959
C7+	134.30	0.43093	384.08	0.27142	0.27142
C15+	373.22	1.1139	947.29	0.20761	0.20761

Table A.5 Extended Data of D1 Part-1

Components	*Mol Percentage (%)*	*Pcrit (atm)*	*Tcrit (Kelvin)*	*Omega A*	*Omega B*
H_2S	0.0	88.2	373.6	0.45724	0.077796
CO_2	0.0595	72.9	304.7	0.45724	0.077796
XVOL	8.7354	45.268	189.67	0.45724	0.077796
C2+	10.551	40.258	389.58	0.45724	0.077796
C7+	40.083	25.295	627.88	0.45724	0.077796
C18+	40.571	9.1053	890.49	0.45724	0.077796

Table A.6 Extended Data of D1 Part-2

Components	*Mol Weight (g/mole)*	*Acentric Factor*	*Parachors*	*Z Crit*	*Z Crit (viscosity)*
H_2S	34.076	0.10	80.0	0.28195	0.28195
CO_2	44.01	0.225	78.0	0.27408	0.27408
XVOL	16.216	0.01339	76.48	0.2847	0.2847
C2+	51.194	0.1743	169.94	0.28771	0.28771
C7+	142.72	0.45937	402.65	0.27512	0.27512
C18+	403.87	1.1935	1022.9	0.2009	0.2009

Table A.7 Extended Data of H1 Part-1

Components	*Mol Percentage (%)*	*Pcrit (atm)*	*Tcrit (Kelvin)*	*Omega A*	*Omega B*
H_2S	0.0	88.2	373.6	0.45724	0.077796
CO_2	0.1504	72.9	304.7	0.45724	0.077796
CH_4	0.71273	45.44	190.6	0.45724	0.077796
C2+	0.14557	34.359	456.43	0.45724	0.077796
C7+	12.275	17.917	719.9	0.45724	0.077796
C23+	86.716	5.734	1087.3	0.45724	0.077796

Table A.8 Extended Data of H1 Part-2

Components	*Mol Weight (g/mole)*	*Acentric Factor*	*Parachors*	*Z Crit*	*Z Crit (viscosity)*
H_2S	34.076	0.10	80.0	0.28195	0.28195
CO_2	44.01	0.225	78	0.27408	0.27408
CH_4	16.043	0.013	77	0.28473	0.28473
C2+	69.702	0.24416	226.37	0.27403	0.27403
C7+	206.24	0.66833	540.84	0.24582	0.24582
C23+	678.17	1.5864	1699.5	0.16855	0.16855

Table A.9 Extended Data of M3 Part-1

Components	*Mol Percentage (%)*	*Pcrit (atm)*	*Tcrit (Kelvin)*	*Omega A*	*Omega B*
H_2S	0.34	88.2	373.6	0.45724	0.077796
CO_2	1.32	72.9	304.7	0.45724	0.077796
XVOL	8.96	45.307	189.88	0.45724	0.077796
C2+	9.54	44.627	341.93	0.45724	0.077796
C7+	11.17	33.295	462.57	0.45724	0.077796
C15+	68.67	17.416	814.56	0.45724	0.077796

Table A.10 Extended Data of M3 Part-2

Components	*Mol Weight (g/mole)*	*Acentric Factor*	*Parachors*	*Z Crit*	*Z Crit (viscosity)*
H_2S	34.076	0.1	80	0.28195	0.28195
CO_2	44.01	0.225	78	0.27408	0.27408
XVOL	16.177	0.013301	76.598	0.28471	0.28471
C2+	38.025	0.12911	131.99	0.28231	0.28231
C4+	71.283	0.24333	227.94	0.2684	0.2684
C7+	243	0.74736	626.07	0.23612	0.23612

B. Example Eclipse .DATA File for Slim Tube Simulation

```
RUNSPEC
=========================================================
OIL
GAS

FULLIMP

DIMENS
200   1   1  /

-- Cartesian co-ord system

CART

-- Units: Lab

LAB
-- cm for length

-- Number of components: implies compositional run
COMPS
6 /

MISCIBLE
/

GRID
=========================================================
DX
200*5 /

--Cross section is 1 square cm

DY
200*1.0 /

DZ
200*1.0 /

-- Porosity and permeability

PORO
-- 200*0.38 /
200*0.1 /
```

```
PERMX
200*1000.0 /

PERMY
200*1000.0 /

PERMZ
200*100.0 /

--Depth of cell centres

MIDS
200*100.0 /

INIT

PROPS
============================================================
-- Properties section: PVT data from INCLUDE file

EOS
PR    /

CNAMES
H2S  CO2  'XVOL'  'C2+'  'C7+'  'C15+' /

MISCEXP
--  miscibility  exponent  allows  the  exponent  of  the
surface tension ratio to be changed
0.2 /

BIC
-- H2S  CO2  'XVOL'  'C2+'  'C7+'  'C15+'
0.096
0.0521   0.09814
0.05     0.1     0.00489
0.05     0.1     0.04239     0.00526
0.05     0.1     0.06208     0.00526    0 /

PCRIT
-- atm
-- H2S  CO2  'XVOL'  'C2+'  'C7+'  'C15+'
88.2  72.9  45.241  40.162  26.128  10.562 /
--73.76 46.00 48.8 31.6 16.3 /

TCRIT
-- Kelvin
```

```
-- H2S CO2 'XVOL' 'C2+' 'C7+' 'C15+'
373.6 304.7 189.53 392.77 617.35 896.94 /

MW
34.076 44.01 16.242 52.388 134.3 373.22 /

ACF
-- Acentric factor
0.1 0.225 0.01345 0.17387 0.43093 1.1139 /

ZCRIT
0.28195 0.27408 0.2847 0.28959 0.27142 0.20761 /

ZCRITVIS
0.28195 0.27408 0.2847 0.28959 0.27142 0.20761 /

OMEGAA
0.45724 0.45724 0.45724 0.45724 0.45724 0.45724 /

OMEGAB
0.077796 0.077796 0.077796 0.077796 0.077796 0.077796 /

PARACHOR
80 78 76.401 172.62 384.08 947.29 /

STCOND
-- Standart condition
-- Temp Pres 15.56 C 1 atma
15.0 1.0 /

DENSITY
-- OIL WATER GAS KG/M3
865.20      1020.34       0.81172 /


RTEMP
-- Reservoir temperature: Deg C
121.1 /

-- Rock and properties

ROCK
-- REF_pressure rock_comp
-- atm 1/atm
235    0.00012227 /
```

SGFN

```
-- GAS_SAT        KRG           PCOG
         0                  0       0
      0.05                  0       0
   0.11875     3.051757813E-06       0
    0.1875       0.0001953125       0
   0.25625      0.002224731445       0
     0.325              0.0125       0
   0.39375       0.04768371582       0
    0.4625       0.1423828125       0
   0.53125       0.3590362549       0
       0.6                0.8       0
       0.8                0.9       0       /
```

SOF2

```
-- SAT_OIL KROG
0.0000          0
0.2000          0
0.2725          0.001587826
0.3450          0.012702604
0.4175          0.042871289
0.4900          0.101620833
0.5625          0.19847819
0.6350          0.342970313
0.7075          0.544624154
0.7800          0.812966667
0.8000          0.9             /
```

SOLUTION

```
============================================================
-- Solution section: define explicitly
```

PRESSURE

```
-- Initial pressure, atm
200*350.0 /
```

SGAS

```
-- Initial gas saturation
200*0.0 /
```

XMF

```
-- Specifies cell initial oil composition
-- H2S   CO2    'XVOL'   'C2+'   'C7+' 'C15+'
200*0.0207 200*0.00383 200*0.27026 200*0.27801 200*0.2285 200*0.1987 /
```

YMF

```
-- Specifies cell initial oil composition
-- H2S    CO2     'XVOL'    'C2+'    'C7+' 'C16+'
200*0.0207  200*0.00383  200*0.27026  200*0.27801  200*0.2285  200*0.1987 /

--  Calculate initial oil and gas in place at surface
conditions

FIELDSEP
-- Introduces a field separator
-- Stage_index Temp, Cel Pressure, atm
1  15.0  1.0 /
/

RPTSOL
-- Controls on output from SOLUTION section
PRES  SOIL  SGAS  /

RPTRST
-- Controls on output to the RESTART file
PRES  SOIL  SGAS /

SUMMARY
============================================================
=

WOPR
 -- well oil production rate
PRODUCER  /

FOPR
-- Field oil production rate

WOPT
-- Well oil production total
PRODUCER  /

WGOR
-- Well gas oil ratio
PRODUCER  /

RUNSUM
--  data  in  the  SUMMARY  files  should  be  output  in  a
tabulated format in addition

ALL

MSUMLINS
```

```
-- Returns the total number of linear iterations since
the start of the run

MSUMNEWT
-- Returns the total number of Newton iterations since
the start of the run

SCHEDULE
============================================================
CVCRIT
-- Convergence criteria
-- Max Pres change over an iteration
-0.001 /

SEPCOND
-- Introduces a new separator condition stage
-- Name group index Temp Pres
SEPP  G2  1  15.0  1.0 /
/

WELSPECS
-- General specification data for wells
-- Name group I J BHP PHASE
INJECTOR G1   1 1 1* GAS  /
PRODUCER G2 200 1 1* OIL  /
/

WSEPCOND
-- Specify the separator conditions for wells
-- WellName AssociatedSeperatorName
PRODUCER SEPP /
/

COMPDAT
-- Well completion specification data
--   Name   I   J   K_UP   K_LOW   open/shut   Sat_table_num
Transmissibility
INJECTOR   1 1   1   1   OPEN 1 5000 /
PRODUCER 200 1   1   1   OPEN 1 5000 /
/

WELLSTRE
-- Set composition of injection stream
--     NameofWellStream     MoleFractionofFirstComponent
MoleFractionofSecondComponent etc.
LEANGAS 0 1 /
```

```
/

--Total pore volume is 100ccs, inject 1/10 PV per hour

WCONINJE
-- Control data for injection wells
--     name     type     open/shut     control     mode
SurfaceFlowRateTargetorUpperLimit
ReservoirFluidVolumeRateTargetorUpperLimit
INJECTOR   GAS OPEN RESV  1*  10.0 /
/

WINJGAS
-- Specify the nature of injection gas
-- WellName Character
INJECTOR STREAM LEANGAS /
/

WCONPROD
-- Control data for production wells
-- Name open/shut control mode BHP target or lower limit
PRODUCER   OPEN BHP   5*   350.0   /
/

RPTPRINT
-- Control printed simulation reports
1 1 1 1 1    1 1 1 0 0 /

RPTSCHED
-- Controls on output from SCHEDULE section
PRESSURE   SOIL   SGAS /

--Limit max step to get at least 500 timesteps per 10
hours = 1 PV injected

TSCRIT
-- Timestepping criteria
-- LengthofInitialStep MinStep MaxStep hr
0.001  0.0001  0.02 /

--Run for 12 hours - ie 1.2 pore volumes injected

TIME
-- Advances simulator to new report time
1 2 3 4 5 6 7 8 9 10 11 12 /

END
```

C. Slim Tube Simulation Results' Tables and Graphs

Table C.1 Slim tube simulation results for F2: Pressures and Recovery Factors

Pressure (atm)	100 Grids	200 Grids	500 Grids	Infinite Grids
120.0	67.17%	68.34%	69.56%	71.46%
150.0	70.70%	72.33%	74.50%	77.43%
180.0	75.02%	76.88%	79.86%	83.51%
210.0	79.96%	81.79%	84.91%	88.60%
240.0	85.19%	86.87%	89.36%	92.54%
270.0	89.90%	91.69%	93.35%	96.12%
300.0	93.21%	95.02%	96.55%	99.27%
350.0	95.71%	97.09%	98.12%	100.11%
400.0	96.80%	97.91%	98.72%	100.31%
450.0	97.26%	98.25%	98.94%	100.35%
500.0	97.38%	98.33%	99.00%	100.35%

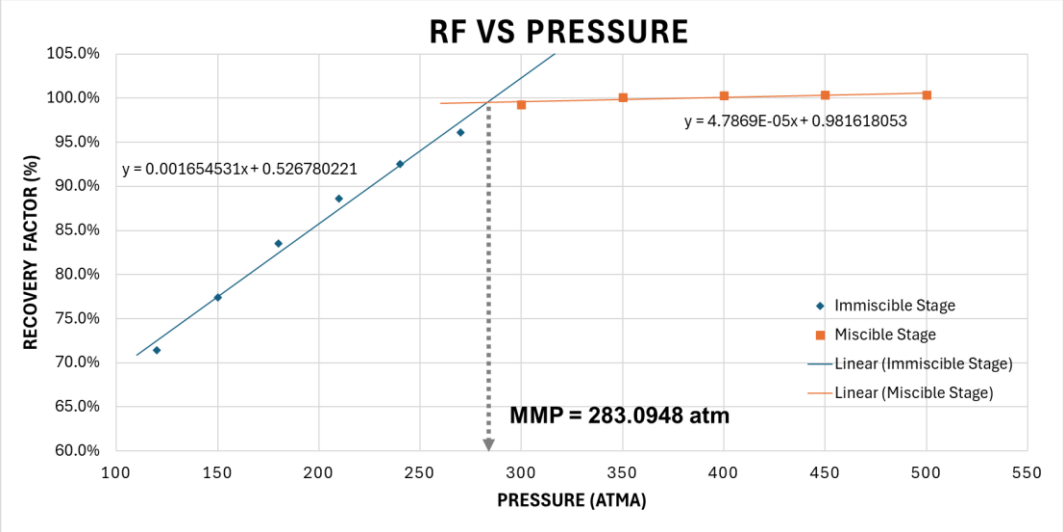

Figure C.1. Recovery Factor vs Pressure for F2 at Infinite Grids

Table C.2 Slim tube simulation results for D1: Pressures and Recovery Factors

Pressure (atm)	100 Grids	200 Grids	500 Grids	Infinite Grids
230.0	88.68%	90.66%	93.14%	96.60%
260.0	95.00%	96.30%	97.48%	99.48%
290.0	97.81%	98.57%	99.13%	100.21%
320.0	99.37%	99.64%	99.82%	100.19%
350.0	99.74%	99.87%	99.94%	100.12%
380.0	99.88%	99.95%	99.99%	100.08%
410.0	99.95%	99.99%	100.00%	100.05%
440.0	99.98%	100.00%	100.00%	100.02%
470.0	99.99%	100.00%	100.00%	100.01%

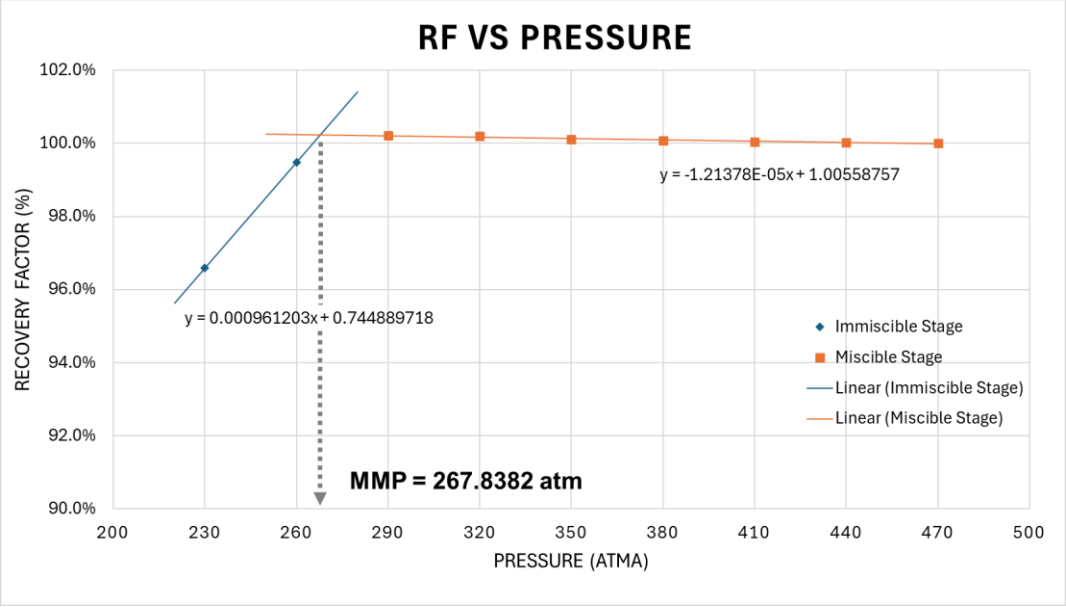

Figure C.2. Recovery Factor vs Pressure for D1 at Infinite Grids

Table C.3 Slim tube simulation results for M3: Pressures and Recovery Factors

Pressure (atm)	100 Grids	200 Grids	500 Grids	Infinite Grids
200.0	65.67%	66.49%	67.70%	69.25%
250.0	71.24%	72.36%	73.76%	75.72%
300.0	76.87%	78.35%	80.13%	82.67%
350.0	81.91%	83.84%	86.22%	89.57%
400.0	86.17%	88.44%	91.05%	94.87%
450.0	89.50%	91.90%	94.19%	97.95%
500.0	91.91%	94.27%	96.28%	99.83%
550.0	93.53%	95.25%	97.37%	100.36%
600.0	93.59%	96.12%	97.98%	101.61%
650.0	94.21%	96.60%	98.32%	101.73%
700.0	94.52%	96.86%	98.27%	101.43%

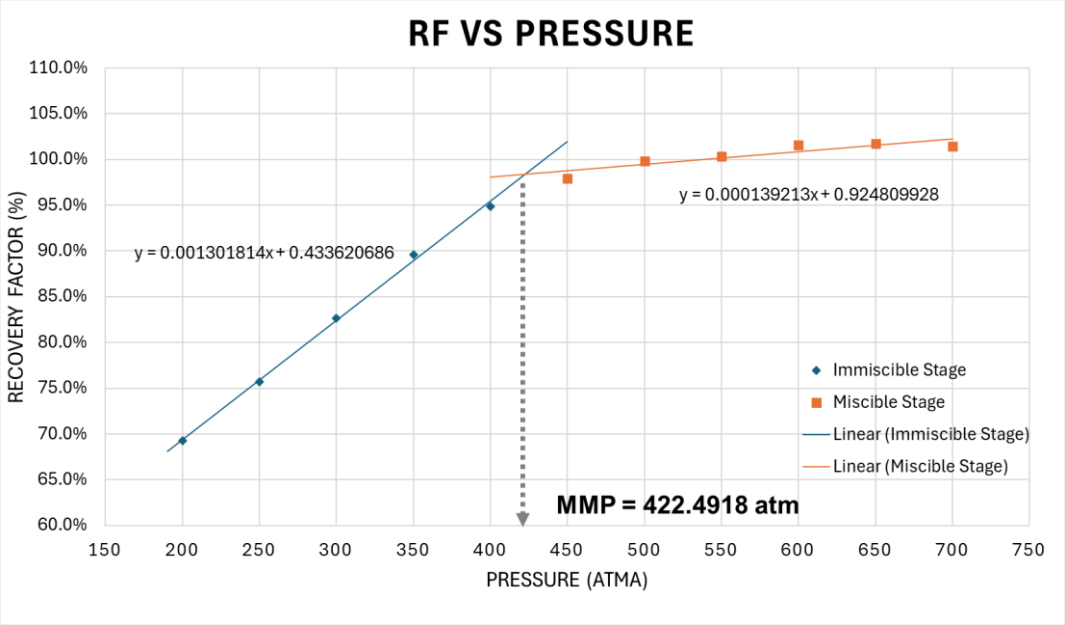

Figure C.3. Recovery Factor vs Pressure for M3 at Infinite Grids

Table C.4 Slim tube simulation results for F5 when Temp = 70°C: Pressures and Recovery Factors

Pressure (atm)	100 Grids	200 Grids	500 Grids	Infinite Grids
170.00	80.18%	82.27%	85.55%	89.60%
200.00	84.80%	86.64%	89.47%	93.01%
230.00	88.84%	90.53%	92.41%	95.21%
260.00	92.14%	94.10%	95.86%	98.87%
290.00	93.91%	95.67%	97.08%	99.67%
320.00	94.80%	96.39%	97.61%	99.91%
350.00	95.29%	96.76%	97.88%	100.02%
380.00	95.55%	96.95%	98.02%	100.05%
410.00	95.66%	97.03%	98.07%	100.06%
440.00	95.69%	97.04%	98.07%	100.04%
470.00	95.64%	97.00%	98.04%	100.01%
500.00	95.56%	96.93%	97.98%	99.97%

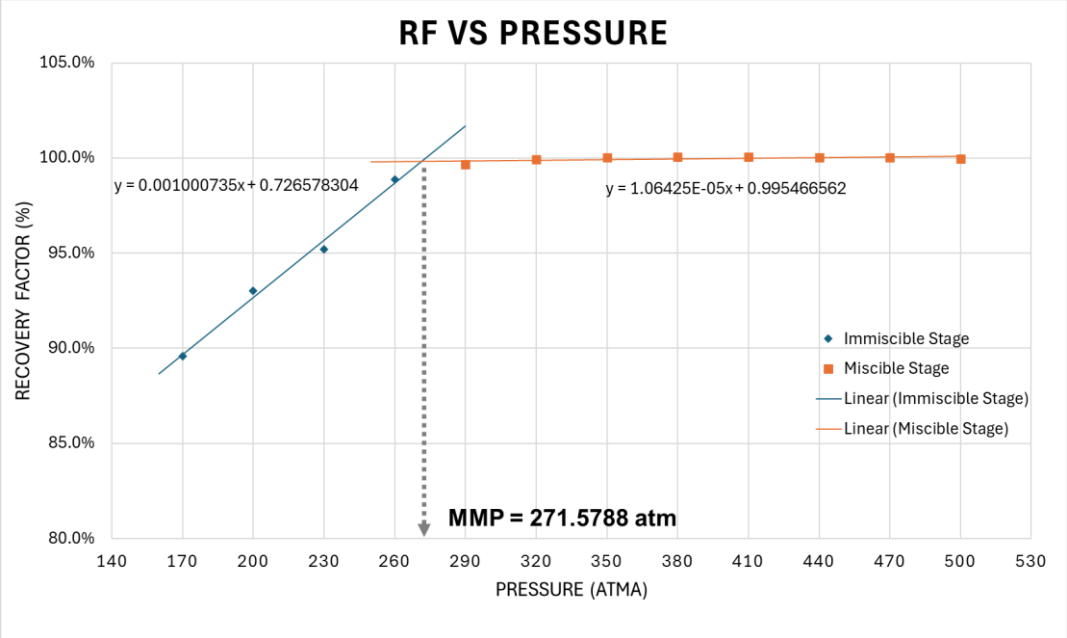

Figure C.4. Recovery Factor vs Pressure for F5 when Temp = 70°C at Infinite Grids

Table C.5 Slim tube simulation results for F5 when Temp = 95℃: Pressures and Recovery Factors

Pressure (atm)	100 Grids	200 Grids	500 Grids	Infinite Grids
170.00	74.26%	76.24%	79.09%	82.78%
200.00	79.06%	81.06%	84.25%	88.16%
230.00	83.98%	85.82%	88.66%	92.20%
260.00	88.75%	90.43%	92.32%	95.13%
290.00	92.97%	94.81%	96.43%	99.23%
320.00	95.40%	96.91%	98.04%	100.22%
350.00	96.67%	97.86%	98.70%	100.38%
380.00	97.42%	98.39%	99.06%	100.42%
410.00	97.88%	98.70%	99.26%	100.41%
440.00	98.16%	98.89%	99.38%	100.40%
470.00	98.33%	99.01%	99.45%	100.39%
500.00	98.43%	99.07%	99.49%	100.37%

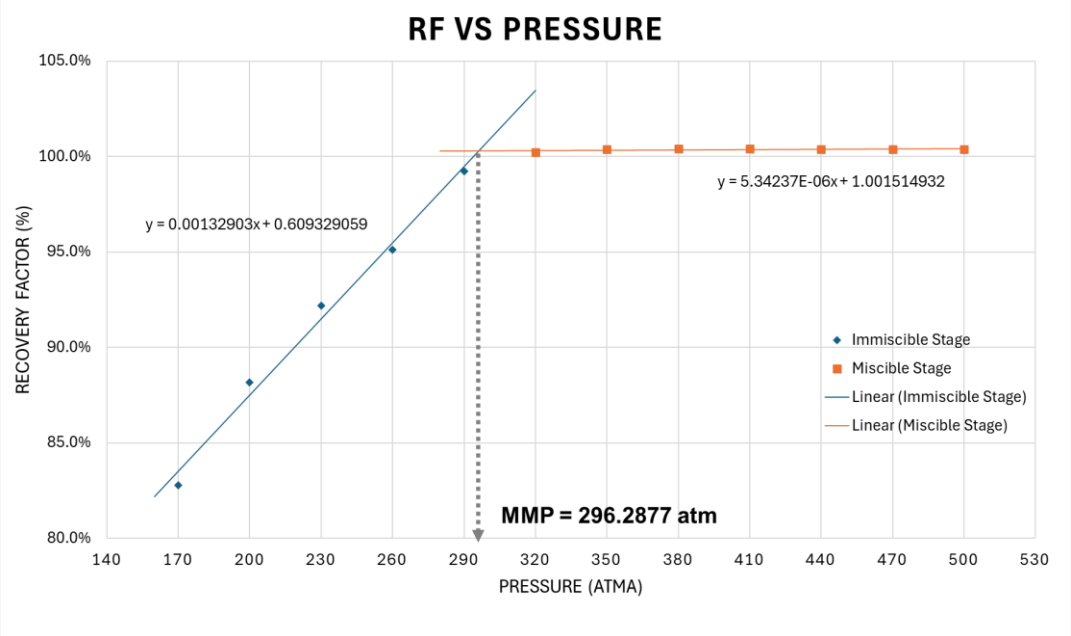

Figure C.5. Recovery Factor vs Pressure for F5 when Temp = 95℃ at Infinite Grids

Table C.6 Slim tube simulation results for F5 when Temp = 150℃: Pressures and Recovery Factors

Pressure (atm)	100 Grids	200 Grids	500 Grids	Infinite Grids
170.00	70.49%	71.92%	73.83%	76.40%
200.00	73.79%	75.39%	77.80%	80.84%
230.00	77.56%	79.25%	81.94%	85.24%
260.00	81.88%	83.56%	86.24%	89.53%
290.00	86.77%	88.41%	90.45%	93.31%
320.00	91.88%	93.60%	95.11%	97.72%
350.00	95.76%	97.24%	98.30%	100.41%
380.00	97.85%	98.71%	99.28%	100.46%
410.00	98.93%	99.40%	99.70%	100.35%
440.00	99.50%	99.76%	99.90%	100.24%
470.00	99.81%	99.93%	100.00%	100.16%
500.00	99.97%	100.00%	100.00%	100.03%

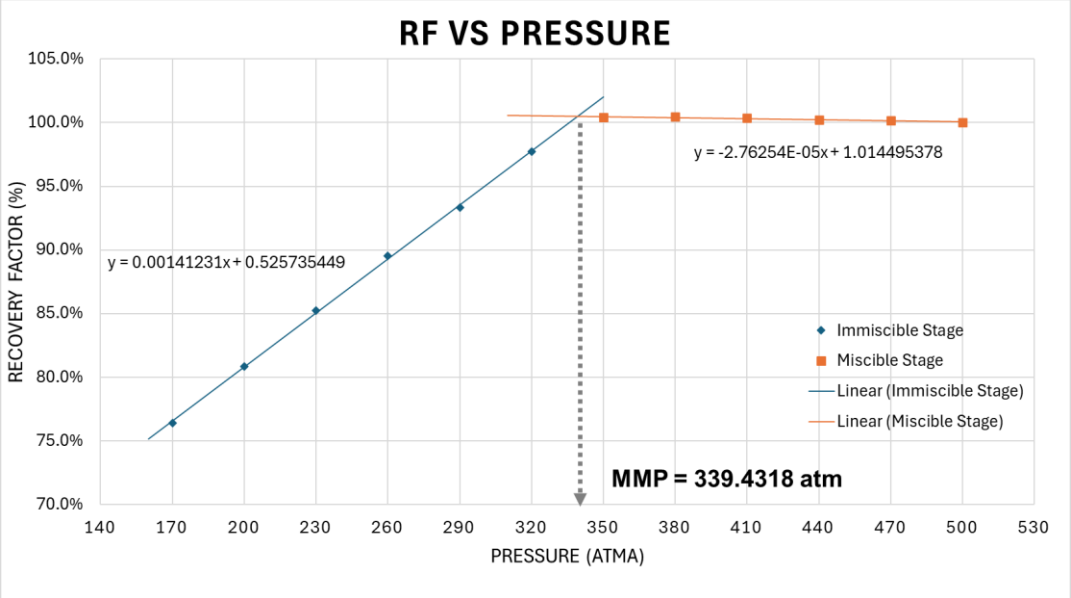

Figure C.6. Recovery Factor vs Pressure for F5 when Temp = 150℃ at Infinite Grids

Table C.7 Slim tube simulation results for F5 when Temp = 170°C: Pressures and Recovery Factors

Pressure (atm)	100 Grids	200 Grids	500 Grids	Infinite Grids
170.00	70.46%	71.77%	73.50%	75.85%
200.00	73.57%	75.04%	77.27%	80.07%
230.00	77.10%	78.67%	81.18%	84.26%
260.00	81.16%	82.77%	85.30%	88.43%
290.00	85.84%	87.44%	89.48%	92.30%
320.00	90.93%	92.58%	94.11%	96.67%
350.00	95.23%	96.82%	98.03%	100.34%
380.00	97.71%	98.62%	99.22%	100.48%
410.00	98.96%	99.43%	99.71%	100.35%
440.00	99.60%	99.81%	99.93%	100.22%
470.00	99.91%	99.99%	100.00%	100.09%
500.00	100.00%	100.00%	100.00%	100.00%

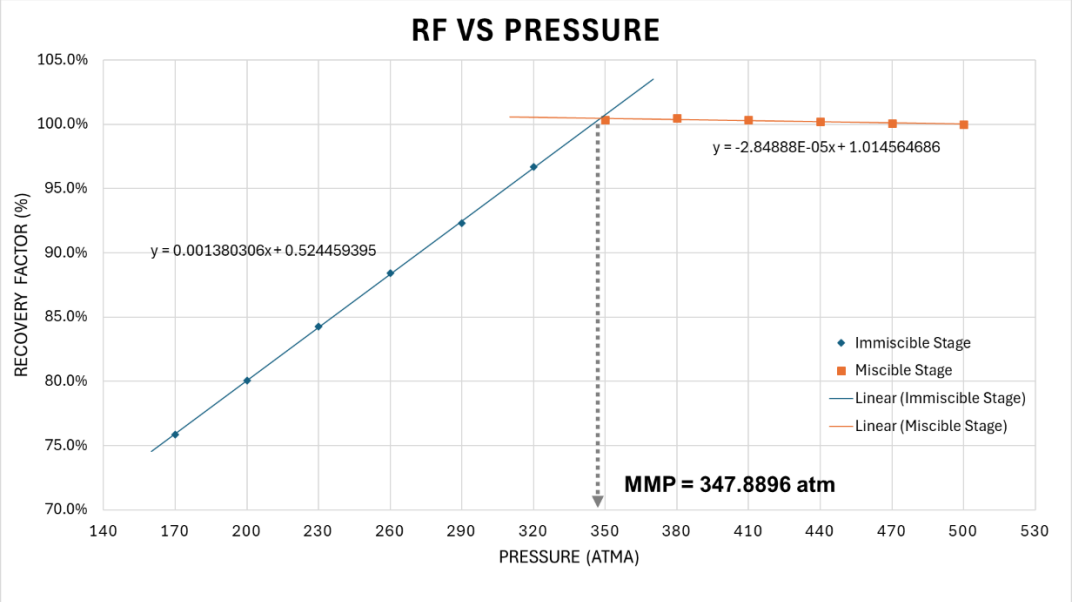

Figure C.7. Recovery Factor vs Pressure for F5 when Temp = 170°C at Infinite Grids

D. Example Eclipse .DATA File for Miscible Run

```
RUNSPEC
TITLE
'MISC_F5_60'
WELLDIMS
   2  7  3  2  /
START
   1  JAN  2024  /
WATER
OIL
GAS
PETOPTS
INITNNC  /
MONITOR

CPR
   /
MULTOUT
METRIC
DIMENS
   10  10  10  /
TABDIMS
   12*  1  /
MISCIBLE
 1  20  'NONE'  /
GRID
INCLUDE
INIT
GRIDFILE
   0  0  /
GRIDUNIT
   METRES  /
MAPUNITS
   METRES  /
MAPAXES
   0  -700  0  300  1000  300  /
PINCH
   4*  ALL  /
PROPS
ROCKOPTS
   2*  ROCKNUM  /
ROCK
                  345       0.000122267  /
```

PVTW

345	1.0382	4.4308E-05	0.25515	0 /

PVDO

345	1.501344326	0.342437756
348.6315789	1.500226654	0.3439219343
352.2631579	1.499132834	0.3454197781
355.8947368	1.49806211	0.3469310667
359.5263158	1.497013758	0.348455582
363.1578947	1.495987085	0.3499931082
366.7894737	1.494981426	0.3515434322
370.4210526	1.493996142	0.3531063428
374.0526316	1.49303062	0.3546816311
377.6842105	1.492084271	0.3562690902
381.3157895	1.491156532	0.3578685151
384.9473684	1.490246857	0.3594797027
388.5789474	1.489354726	0.3611024517
392.2105263	1.488479634	0.3627365622
395.8421053	1.4876211	0.3643818361
399.4736842	1.486778657	0.366038077
403.1052632	1.485951857	0.3677050895
406.7368421	1.485140269	0.3693826799
410.3684211	1.484343477	0.3710706557
414	1.48356108	0.3727688257

/

PVDG

345	0.004124698708	0.02533146411
348.6315789	0.004094324853	0.02547634683
352.2631579	0.004064689702	0.02562095729
355.8947368	0.004035767367	0.02576528731
359.5263158	0.004007533088	0.02590932928
363.1578947	0.00397996318	0.02605307606
366.7894737	0.003953034974	0.02619652103
370.4210526	0.003926726769	0.02633965802
374.0526316	0.003901017781	0.0264824813
377.6842105	0.0038758881	0.0266249856
381.3157895	0.003851318645	0.02676716601
384.9473684	0.003827291127	0.02690901804
388.5789474	0.003803788003	0.02705053754
392.2105263	0.003780792449	0.02719172073
395.8421053	0.00375828832	0.02733256417
399.4736842	0.003736260119	0.02747306471
403.1052632	0.003714692968	0.02761321953
406.7368421	0.003693572575	0.02775302607
410.3684211	0.00367288521	0.02789248206
414	0.00365261768	0.02803158549

/
DENSITY
865.05 1020.3 0.81172 /
FILLEPS
SDENSITY
1.869 /
SOF3
-- So Kro(o-w) Kro (o-g-wi)
0.0000 0 0
0.2000 0 0
0.2725 0.001587826 0.001353963
0.3450 0.012702604 0.010831706
0.4175 0.042871289 0.036557007
0.4900 0.101620833 0.086653646
0.5625 0.19847819 0.169245402
0.6350 0.342970313 0.292456055
0.7075 0.544624154 0.464409383
0.7800 0.812966667 0.693229167
0.8000 0.9 0.9 /
SOF2
-- SAT_OIL KROG
0.0000 0
0.2000 0
0.2725 0.001587826
0.3450 0.012702604
0.4175 0.042871289
0.4900 0.101620833
0.5625 0.19847819
0.6350 0.342970313
0.7075 0.544624154
0.7800 0.812966667
0.8000 0.9 /
SWFN
--Sw Krw Pcw
0.2 0 0
0.22 0 0
0.2925 0.0001953125 0
0.365 0.003125 0
0.4375 0.0158203125 0
0.51 0.05 0
0.5825 0.1220703125 0
0.655 0.253125 0
0.7275 0.4689453125 0
0.8 0.8 0
1 1 0 /

```
SGFN
-- GAS_SAT        KRG           PCOG
          0                 0       0
       0.05                 0       0
    0.11875  3.051757813E-06        0
     0.1875     0.0001953125        0
    0.25625    0.002224731445        0
      0.325            0.0125        0
    0.39375     0.04768371582        0
     0.4625     0.1423828125        0
    0.53125     0.3590362549        0
        0.6              0.8        0
        0.8              0.9        0        /
PMISC
1.0     0.0
100.0  0.0
150.0  0.0
200.0  0.0
335.0  0.0
335.249  1.0
450.0     1.0   /
TLMIXPAR
0.33 /
REGIONS

SOLUTION
EQUIL
      2000   379.5   2050   0   2000   0 0 0 0 /
RPTRST
   BASIC=3 FLOWS /
RPTSOL
   SGAS RESTART=2 FIP SSOL /
SUMMARY
FOE
GMCTP
 /
GMCTG
 /
WGIGR
 /
WAPI
 /
WSTAT
 /
FWGR
```

WWGR
/
GWGR
/
FWCT
WWCT
/
GWCT
/
FRV
WTHP
/
TIMESTEP
FRS
FVPR
WVPR
/
GVPR
/
FVPT
WVPT
/
GVPT
/
FVIR
WVIR
/
GVIR
/
FVIT
WVIT
/
GVIT
/
WPI
/
FWPR
WWPR
/
GWPR
/
FOPR
WOPR
/
GOPR

/
FGPR
WGPR
/
GGPR
/
WEPR
/
FWPT
WWPT
/
GWPT
/
FOPT
WOPT
/
GOPT
/
FGPT
WGPT
/
GGPT
/
FPR
FWIP
FOIPG
FGIPL
FOIP
FOIPL
FGIP
FGIPG
FWIR
WWIR
/
GWIR
/
FOIR
WOIR
/
GOIR
/
FGIR
WGIR
/
GGIR

```
 /
FWIT
WWIT
 /
GWIT
 /
FOIT
WOIT
 /
GOIT
 /
FGIT
WGIT
 /
GGIT
 /
FGOR
WGOR
 /
GGOR
 /
WBHP
 /
SCHEDULE
RPTSCHED
  SGAS FIP WELLS SSOL /
RPTRST
  BASIC=3 FLOWS FREQ /
WELSPECS
--'PROD_2' is the simulation well name used to describe
flow from 'Prod_2'
--'ECTION_2' is the simulation well name used to describe
flow from 'Injection_2'
  PROD_2 PRODG 10 1 1* OIL /
  ECTION_2 INJG 1 10 1* GAS /
  /
COMPDAT
  PROD_2 10 1 1 1 OPEN 1* 64.8173 0.1905 5000 0 1* Z 5.9397 /
  PROD_2 10 1 2 2 OPEN 1* 64.8173 0.1905 5000 0 1* Z 5.9397 /
  PROD_2 10 1 3 3 OPEN 1* 64.8173 0.1905 5000 0 1* Z 5.9397 /
  PROD_2 10 1 4 4 OPEN 1* 64.8173 0.1905 5000 0 1* Z 5.9397 /
  PROD_2 10 1 5 5 OPEN 1* 64.8173 0.1905 5000 0 1* Z 5.9397 /
  PROD_2 10 1 6 6 OPEN 1* 64.8173 0.1905 5000 0 1* Z 5.9397 /
  PROD_2 10 1 7 7 OPEN 1* 64.8173 0.1905 5000 0 1* Z 5.9397 /
  ECTION_2 1 10 1 1 OPEN 1* 64.8173 0.1905 5000 0 1* Z 5.9397 /
```

```
  ECTION_2  1  10  2  2  OPEN  1*  64.8173  0.1905  5000  0  1*  Z  5.9397  /
  ECTION_2  1  10  3  3  OPEN  1*  64.8173  0.1905  5000  0  1*  Z  5.9397  /
  /
GRUPTREE
  PRODG  FIELD  /
  INJG  FIELD  /
  /
WCONPROD
  PROD_2  OPEN  BHP  5*  345  /
  /
WCONINJE
  ECTION_2  GAS  OPEN  RATE  60000  1*  414  /
  /
WECON
  PROD_2  2*  0.001  2*  NONE  /
  /
GCONPROD
  PRODG  NONE  5*  YES  1*  INJV  /
  /
DATES
  1  JAN  2025  /
  /
DATES
  1  JAN  2026  /
  /
DATES
  1  JAN  2027  /
  /
DATES
  1  JAN  2028  /
  /
DATES
  1  JAN  2029  /
  /
```

E. Example Eclipse .DATA File for Immiscible Run

```
RUNSPEC
TITLE
'IMMISC_F5_KY'
WELLDIMS
   2  7  3  2  /
START
   1  JAN  2024  /
WATER
OIL
GAS
PETOPTS
INITNNC  /
MONITOR
CPR
   /
MULTOUT
METRIC
DIMENS
   10  10  10  /
TABDIMS
   12*  1  /
MISCIBLE
 1  20  'NONE'  /
GRID
INIT
GRIDFILE
   0  0  /
GRIDUNIT
   METRES  /
MAPUNITS
   METRES  /
MAPAXES
   0  -700  0  300  1000  300  /
PINCH
   4*  ALL  /
EDIT

PROPS
ROCKOPTS
   2*  ROCKNUM  /
```

ROCK

250 0.000122267 /

PVTW

250 1.0401 4.5587E-05 0.25265 0 /

PVDO

250	1.369231373	0.4149082674
252.6315789	1.368426304	0.4162963776
255.2631579	1.367638294	0.4176994993
257.8947368	1.366866806	0.4191174652
260.5263158	1.366111325	0.4205501109
263.1578947	1.365371359	0.4219972744
265.7894737	1.364646435	0.4234587966
268.4210526	1.363936098	0.4249345207
271.0526316	1.363239914	0.4264242921
273.6842105	1.362557463	0.4279279587
276.3157895	1.361888343	0.4294453704
278.9473684	1.361232167	0.4309763793
281.5789474	1.360588564	0.4325208393
284.2105263	1.359957175	0.4340786064
286.8421053	1.359337656	0.4356495383
289.4736842	1.358729676	0.4372334945
292.1052632	1.358132915	0.4388303362
294.7368421	1.357547065	0.4404399261
297.3684211	1.356971831	0.4420621286
300	1.356406926	0.4436968094

/

PVDG

250	0.005307558019	0.02148857088
252.6315789	0.005260380423	0.02159486242
255.2631579	0.005214342191	0.02170127114
257.8947368	0.005169405733	0.02180778513
260.5263158	0.005125534982	0.0219143928
263.1578947	0.00508269532	0.02202108286
265.7894737	0.005040853512	0.02212784432
268.4210526	0.004999977638	0.02223466649
271.0526316	0.004960037029	0.02234153899
273.6842105	0.004921002214	0.02244845171
276.3157895	0.00488284486	0.02255539487
278.9473684	0.004845537722	0.02266235896
281.5789474	0.004809054592	0.02276933475
284.2105263	0.004773370255	0.02287631333
286.8421053	0.004738460442	0.02298328603
289.4736842	0.004704301792	0.0230902445
292.1052632	0.004670871804	0.02319718062
294.7368421	0.004638148811	0.02330408657

```
          297.3684211        0.004606111933        0.02341095479
                  300        0.004574741051        0.02351777796
  /
DENSITY
        865.05         1020.3         0.81172 /
FILLEPS
SDENSITY
 1.869 /
SOF3
-- So  Kro(o-w) Kro (o-g-wi)
0.0000          0                0
0.2000          0                0
0.2725          0.001587826      0.001353963
0.3450          0.012702604      0.010831706
0.4175          0.042871289      0.036557007
0.4900          0.101620833      0.086653646
0.5625          0.19847819       0.169245402
0.6350          0.342970313      0.292456055
0.7075          0.544624154      0.464409383
0.7800          0.812966667      0.693229167
0.8000          0.9              0.9                    /
SOF2
-- SAT_OIL KROG
0.0000          0
0.2000          0
0.2725          0.001587826
0.3450          0.012702604
0.4175          0.042871289
0.4900          0.101620833
0.5625          0.19847819
0.6350          0.342970313
0.7075          0.544624154
0.7800          0.812966667
0.8000          0.9              /
SWFN
--Sw Krw Pcw
     0.2                  0     0
    0.22                  0     0
  0.2925       0.0001953125     0
   0.365            0.003125     0
  0.4375       0.0158203125     0
    0.51               0.05     0
  0.5825       0.1220703125     0
   0.655            0.253125     0
  0.7275       0.4689453125     0
```

```
      0.8                   0.8      0
        1                     1      0     /
SGFN
-- GAS_SAT         KRG            PCOG
          0                    0        0
       0.05                    0        0
    0.11875      3.051757813E-06         0
     0.1875         0.0001953125         0
    0.25625        0.002224731445        0
      0.325                0.0125         0
    0.39375         0.04768371582        0
     0.4625         0.1423828125         0
    0.53125         0.3590362549         0
        0.6                  0.8         0
        0.8                  0.9         0         /
PMISC
1.0     0.0
100.0  0.0
150.0  0.0
200.0  0.0
335.0  0.0
335.249  0.0
450.0     0.0   /
TLMIXPAR
0.0 /
REGIONS

SOLUTION
EQUIL
            2000            275            2050              0            2000
0  0  0  0 /
RPTRST
   BASIC=3  FLOWS  /
RPTSOL
   SGAS  RESTART=2  FIP  SSOL  /
SUMMARY
FOE
GMCTP
  /
GMCTG
  /
WGIGR
  /
WAPI
  /
```

WSTAT
/
FWGR
WWGR
/
GWGR
/
FWCT
WWCT
/
GWCT
/
FRV
WTHP
/
TIMESTEP
FRS
FVPR
WVPR
/
GVPR
/
FVPT
WVPT
/
GVPT
/
FVIR
WVIR
/
GVIR
/
FVIT
WVIT
/
GVIT
/
WPI
/
FWPR
WWPR
/
GWPR
/
FOPR

WOPR
/
GOPR
/
FGPR
WGPR
/
GGPR
/
WEPR
/
FWPT
WWPT
/
GWPT
/
FOPT
WOPT
/
GOPT
/
FGPT
WGPT
/
GGPT
/
FPR
FWIP
FOIPG
FGIPL
FOIP
FOIPL
FGIP
FGIPG
FWIR
WWIR
/
GWIR
/
FOIR
WOIR
/
GOIR
/
FGIR

```
WGIR
 /
GGIR
 /
FWIT
WWIT
 /
GWIT
 /
FOIT
WOIT
 /
GOIT
 /
FGIT
WGIT
 /
GGIT
 /
FGOR
WGOR
 /
GGOR
 /
WBHP
 /
SCHEDULE
RPTSCHED
  SGAS FIP WELLS SSOL /
RPTRST
  BASIC=3 FLOWS FREQ /
WELSPECS
--'PROD_2' is the simulation well name used to describe
flow from 'Prod_2'
--'ECTION_2' is the simulation well name used to describe
flow from 'Injection_2'
  PROD_2 PRODG 10 1 1* OIL /
  ECTION_2 INJG 1 10 1* GAS /
  /
COMPDAT
  PROD_2 10 1 1 1 OPEN 1* 64.8173 0.1905 5000 0 1* Z 5.9397 /
  PROD_2 10 1 2 2 OPEN 1* 64.8173 0.1905 5000 0 1* Z 5.9397 /
  PROD_2 10 1 3 3 OPEN 1* 64.8173 0.1905 5000 0 1* Z 5.9397 /
  PROD_2 10 1 4 4 OPEN 1* 64.8173 0.1905 5000 0 1* Z 5.9397 /
  PROD_2 10 1 5 5 OPEN 1* 64.8173 0.1905 5000 0 1* Z 5.9397 /
```

```
  PROD_2 10 1 6 6 OPEN 1* 64.8173 0.1905 5000 0 1* Z 5.9397 /
  PROD_2 10 1 7 7 OPEN 1* 64.8173 0.1905 5000 0 1* Z 5.9397 /
  ECTION_2 1 10 1 1 OPEN 1* 64.8173 0.1905 5000 0 1* Z 5.9397 /
  ECTION_2 1 10 2 2 OPEN 1* 64.8173 0.1905 5000 0 1* Z 5.9397 /
  ECTION_2 1 10 3 3 OPEN 1* 64.8173 0.1905 5000 0 1* Z 5.9397 /
  /
GRUPTREE
  PRODG FIELD /
  INJG FIELD /
  /
WCONPROD
  PROD_2 OPEN BHP 5* 250 /
  /
WCONINJE
  ECTION_2 GAS OPEN RATE 60000 1* 300 /
  /
WECON
  PROD_2 2* 0.001 2* NONE /
  /
GCONPROD
  PRODG NONE 5* YES 1* INJV /
  /
DATES
  1 JAN 2025 /
  /
DATES
  1 JAN 2026 /
  /
DATES
  1 JAN 2027 /
  /
DATES
  1 JAN 2028 /
  /
DATES
  1 JAN 2029 /
  /
END
```

F. Miscible CO_2 Injection Uncertainty Parameters and Results

Table F.1 Miscible CO_2 injection uncertainty parameters and results for F2 fluid

Uncertain Parameters		***Results***
$perm_mult	*$poro_mult*	*Recovery Factor, %*
0.400346367	0.300645894	54.56353404
2.779453567	1.11325248	22.71358761
3.998131259	2.823542955	16.18640252
0.461932607	1.463222999	32.46557225
0.834336519	3.085861629	22.44453891
1.767235018	3.230948332	19.61631399
4.708331913	0.836688009	18.60645542
3.283347641	2.406440138	18.55995629
2.19232165	1.720329356	22.56365508
0.170624566	2.703054415	28.73103565
4.01461406	3.522174139	15.09060165
3.772266226	0.647490829	44.28192451
2.242368098	3.991815668	16.97303505
4.449952861	0.459169897	51.24871781
2.538320127	1.886576983	21.22934807
4.344788803	2.634612262	15.87293757
3.59130325	3.829736991	15.25185361
1.514482454	1.306722495	26.76800538
1.07352937	2.258598224	24.12896624
1.976287715	3.27471102	19.05288008
4.942551242	1.54834547	16.42696974
3.069968285	2.059870724	19.97172259
1.342569457	3.682924894	19.3967592
2.856643851	0.93424958	23.05292017

Table F.1 (Cont'd)

0.74660725	2.152739402	25.94679091
2.5005	2.15	20.88881902
0.001	0.3	39.94879617
5	0.3	60.43726388
0.001	4	2.480960362
5	4	13.4388016
0.001	2.15	5.042693617
5	2.15	15.3065761
2.5005	0.3	27.89423821
2.5005	4	16.55269166

Table F.2 Miscible CO_2 injection uncertainty parameters and results for F5 fluid

Uncertain Parameters		***Results***
$perm_mult	*$poro_mult*	*Recovery Factor, %*
0.400346367	0.300645894	51.62902417
2.779453567	1.11325248	22.54968944
3.998131259	2.823542955	15.67677425
0.461932607	1.463222999	29.99238471
0.834336519	3.085861629	20.7636529
1.767235018	3.230948332	18.22723753
4.708331913	0.836688009	19.25901598
3.283347641	2.406440138	17.74856137
2.19232165	1.720329356	21.93504983
0.170624566	2.703054415	26.66527615
4.01461406	3.522174139	14.61077747
3.772266226	0.647490829	30.43667162
2.242368098	3.991815668	15.92188139

Table F.2 (Cont'd)

4.449952861	0.459169897	44.35263785
2.538320127	1.886576983	20.78673919
4.344788803	2.634612262	15.5158143
3.59130325	3.829736991	14.65368694
1.514482454	1.306722495	25.53359019
1.07352937	2.258598224	22.88468813
1.976287715	3.27471102	17.74895811
4.942551242	1.54834547	16.63863393
3.069968285	2.059870724	19.23567752
1.342569457	3.682924894	17.92305939
0.74660725	2.152739402	24.43775329
2.856643851	0.93424958	23.03187386
2.5005	2.15	20.07161773
0.001	0.3	36.3842824
5	0.3	30.05057607
0.001	4	2.176219166
5	4	13.25502968
0.001	2.15	4.441072872
5	2.15	15.32724095
2.5005	0.3	28.76591546
2.5005	4	15.60481019

Table F.3 Miscible CO_2 injection uncertainty parameters and results for D1 fluid

Uncertain Parameters		***Results***
$perm_mult	*$poro_mult*	*Recovery Factor, %*
0.400346367	0.300645894	70.49633337
2.779453567	1.11325248	33.23751298
3.998131259	2.823542955	23.06132353
0.461932607	1.463222999	41.85299282
0.834336519	3.085861629	28.23486887
1.767235018	3.230948332	25.1363278
4.708331913	0.836688009	30.20807917
3.283347641	2.406440138	25.24822606
2.19232165	1.720329356	31.08334704
0.170624566	2.703054415	36.07846084
4.01461406	3.522174139	21.5500169
3.772266226	0.647490829	33.84898012
2.242368098	3.991815668	22.2976964
4.449952861	0.459169897	44.65814423
2.538320127	1.886576983	29.16949697
4.344788803	2.634612262	23.13833658
3.59130325	3.829736991	21.2124025
1.514482454	1.306722495	36.36985634
1.07352937	2.258598224	31.33967922
1.976287715	3.27471102	24.60935612
4.942551242	1.54834547	25.84714054
3.069968285	2.059870724	27.03966033
1.342569457	3.682924894	24.66879533
2.856643851	0.93424958	34.55693826
0.74660725	2.152739402	33.62668362
2.5005	2.15	27.81673073

Table F.3 (Cont'd)

0.001	0.3	54.35402366
5	0.3	37.36018304
0.001	4	3.874165667
5	4	19.60124326
0.001	2.15	7.746097993
5	2.15	23.58408146
2.5005	0.3	46.56954969
2.5005	4	21.95346503

Table F.4 Miscible CO_2 injection uncertainty parameters and results for M3 fluid

Uncertain Parameters		***Results***
$perm_mult	*$poro_mult*	*Recovery Factor, %*
0.400346367	0.300645894	56.35398763
2.779453567	1.11325248	27.23703951
3.998131259	2.823542955	17.70797521
0.461932607	1.463222999	32.24604625
0.834336519	3.085861629	21.15404871
1.767235018	3.230948332	18.67809464
4.708331913	0.836688009	27.87641536
3.283347641	2.406440138	19.41995228
2.19232165	1.720329356	23.86004992
0.170624566	2.703054415	25.55196081
4.01461406	3.522174139	16.20234635
3.772266226	0.647490829	31.68479548
2.242368098	3.991815668	16.53964228
4.449952861	0.459169897	34.40731753
2.538320127	1.886576983	22.4565051

Table F.4 (Cont'd)

4.344788803	2.634612262	18.0329622
3.59130325	3.829736991	15.89992885
1.514482454	1.306722495	28.01483774
1.07352937	2.258598224	23.59135237
1.976287715	3.27471102	18.27343341
4.942551242	1.54834547	22.50934951
3.069968285	2.059870724	21.02866569
1.342569457	3.682924894	18.24843089
2.856643851	0.93424958	28.78244497
0.74660725	2.152739402	25.54895742
2.5005	2.15	21.15876316
0.001	0.3	25.74450563
5	0.3	38.25276029
0.001	4	1.403358039
5	4	15.06385223
0.001	2.15	2.901060192
5	2.15	19.4400439
2.5005	0.3	43.19233079
2.5005	4	16.3043167

G. Immiscible CO_2 Injection Uncertainty Parameters and Results

Table G.5 Immiscible CO_2 Injection Uncertainty Parameters and Results for F2 fluid

Uncertain Parameters		***Results***
$perm_mult	*$poro_mult*	*Recovery Factor, %*
2.559394941	3.939639271	14.73548141
2.159287869	1.687962889	17.10295944
0.468916122	3.266288644	30.35258419
1.331118325	3.054202094	20.65662836
0.050892113	2.203501083	48.41566422
1.004432616	3.871243629	22.2319465
0.290310556	3.576775414	34.60392622
1.922457753	1.986986908	17.03917775
0.742129259	2.436704001	26.86758682
2.952930518	3.004091922	14.91145397
0.906621668	1.859526963	25.11278531
1.277429754	1.198803674	22.07718255
1.59616011	1.30908414	19.46456119
2.879794713	1.599326151	14.80298778
1.559883257	1.789139073	19.69304509
2.264618511	1.446787317	27.07592839
1.759945946	3.506486404	17.40065518
2.698487329	2.107664418	14.96084847
0.186103841	2.828634907	41.11893812
1.186380674	3.756202277	21.13610772
1.868608098	2.730055239	17.17264517
2.306837168	2.674887539	15.1109751
0.499236527	1.093119297	35.00261837
0.610552905	3.304555193	27.63401502

Table G.1 (Cont'd)

2.453064846	2.458882412	14.9450287
1.5005	2.5	19.76945627
0.001	1	3.168705671
3	1	13.89475682
0.001	4	0.769760421
3	4	13.9027854
0.001	2.5	1.143897302
3	2.5	13.89592097
1.5005	1	20.52618274
1.5005	4	18.70747092

Table G.2 Immiscible CO_2 injection uncertainty parameters and results for F5 fluid

Uncertain Parameters		***Results***
$perm_mult	*$poro_mult*	*Recovery Factor, %*
2.559394941	3.939639271	14.97176684
2.159287869	1.687962889	16.80321793
0.468916122	3.266288644	30.04124898
1.331118325	3.054202094	20.97118844
0.050892113	2.203501083	46.49994941
1.004432616	3.871243629	22.27552749
0.290310556	3.576775414	33.71507109
1.922457753	1.986986908	17.87315740
0.742129259	2.436704001	27.03309805
2.952930518	3.004091922	14.57591203
0.906621668	1.859526963	25.71835274
1.277429754	1.198803674	22.38498414
1.59616011	1.30908414	20.66945631

Table G.2 (Cont'd)

2.879794713	1.599326151	23.4954429
1.559883257	1.789139073	20.60319614
2.264618511	1.446787317	16.52690859
1.759945946	3.506486404	17.95602306
2.698487329	2.107664418	14.91033046
0.186103841	2.828634907	39.92334409
1.186380674	3.756202277	21.20937416
1.868608098	2.730055239	17.8506736
2.306837168	2.674887539	16.05546429
0.499236527	1.093119297	35.12948806
0.610552905	3.304555193	27.50514369
2.453064846	2.458882412	15.82465909
1.5005	2.5	20.38338505
0.001	1	3.092364992
3	1	28.57576601
0.001	4	0.762565273
3	4	14.43389884
0.001	2.5	1.136433922
3	2.5	18.54545328
1.5005	1	21.48885634
1.5005	4	19.09762639

Table G.3 Immiscible CO_2 injection uncertainty parameters and results for D1 fluid

Uncertain Parameters		***Results***
$perm_mult	*$poro_mult*	*Recovery Factor, %*
2.559394941	3.939639271	17.02988755
2.159287869	1.687962889	20.39054246
0.468916122	3.266288644	34.24375888
1.331118325	3.054202094	23.53336542
0.050892113	2.203501083	51.56826901
1.004432616	3.871243629	25.51491062
0.290310556	3.576775414	38.06808517
1.922457753	1.986986908	21.60289298
0.742129259	2.436704001	31.05985150
2.952930518	3.004091922	15.72668508
0.906621668	1.859526963	29.96495597
1.277429754	1.198803674	26.60228418
1.59616011	1.30908414	23.0755683
2.879794713	1.599326151	15.90375031
1.559883257	1.789139073	22.98562749
2.264618511	1.446787317	19.87929185
1.759945946	3.506486404	21.14479283
2.698487329	2.107664418	17.32587480
0.186103841	2.828634907	45.09999289
1.186380674	3.756202277	23.97876953
1.868608098	2.730055239	21.21174536
2.306837168	2.674887539	18.72835520
0.499236527	1.093119297	40.69430113
0.610552905	3.304555193	31.37080500
2.453064846	2.458882412	18.19838812
1.5005	2.5	22.93522240

Table G.3 (Cont'd)

0.001	1	5.979911740
3	1	15.85365443
0.001	4	1.295935363
3	4	15.59256525
0.001	2.5	2.037019685
3	2.5	15.71188945
1.5005	1	23.39758600
1.5005	4	22.01348695

Table G.4 Immiscible CO_2 injection uncertainty parameters and results for M3 fluid

Uncertain Parameters		***Results***
$perm_mult	*$poro_mult*	*Recovery Factor, %*
2.559394941	3.939639271	18.07509915
2.159287869	1.687962889	21.79520754
0.468916122	3.266288644	30.70148675
1.331118325	3.054202094	23.88182410
0.050892113	2.203501083	41.42523148
1.004432616	3.871243629	24.46086097
0.290310556	3.576775414	30.66783667
1.922457753	1.986986908	22.31803247
0.742129259	2.436704001	30.25981473
2.952930518	3.004091922	17.87522946
0.906621668	1.859526963	29.95141803
1.277429754	1.198803674	28.19277824
1.59616011	1.30908414	25.30352547
2.879794713	1.599326151	19.48987519
1.559883257	1.789139073	24.54362127

Table G.4 (Cont'd)

2.264618511	1.446787317	21.73896178
1.759945946	3.506486404	21.11020266
2.698487329	2.107664418	19.53094300
0.186103841	2.828634907	36.55878743
1.186380674	3.756202277	23.56967362
1.868608098	2.730055239	21.68370775
2.306837168	2.674887539	20.18930558
0.499236527	1.093119297	39.4773317
0.610552905	3.304555193	29.05672015
2.453064846	2.458882412	19.95735112
1.5005	2.5	23.73857853
0.001	1	2.160812195
3	1	19.58968478
0.001	4	0.593819152
3	4	16.96724855
0.001	2.5	0.874435344
3	2.5	18.20264949
1.5005	1	26.96795528
1.5005	4	21.53976051

Table G.5 Immiscible CO_2 injection uncertainty parameters and results for H1 fluid

Uncertain Parameters		***Results***
$perm_mult	*$poro_mult*	*Recovery Factor, %*
2.559394941	3.939639271	16.74319955
2.159287869	1.687962889	19.17299509
0.468916122	3.266288644	22.50930942
1.331118325	3.054202094	21.76193923

Table G.5 (Cont'd)

0.050892113	2.203501083	2.740189186
1.004432616	3.871243629	22.37091088
0.290310556	3.576775414	12.49660813
1.922457753	1.986986908	19.95781206
0.742129259	2.436704001	26.92492025
2.952930518	3.004091922	16.33529523
0.906621668	1.859526963	26.64017786
1.277429754	1.198803674	24.27899397
1.59616011	1.30908414	22.02751815
2.879794713	1.599326151	17.04694161
1.559883257	1.789139073	21.81455499
2.264618511	1.446787317	18.92015523
1.759945946	3.506486404	19.51369905
2.698487329	2.107664418	17.28286877
0.186103841	2.828634907	9.76676673
1.186380674	3.756202277	21.62985167
1.868608098	2.730055239	19.56783801
2.306837168	2.674887539	18.15109266
0.499236527	1.093119297	31.20925322
0.610552905	3.304555193	25.03907122
2.453064846	2.458882412	17.79467649
1.5005	2.5	21.40538168
0.001	1	0.114502044
3	1	16.96691115
0.001	4	0.034134854
3	4	15.80923313
0.001	2.5	0.051268323
3	2.5	16.38114629

H. MATLAB Code for Chatterjee Correlation Coefficient

```
function [xi, p] = xicor4(x, y, varargin)
%XICOR Computes Chaterjee's xi correlation between x and y variables
%
%   [xi, p] = xicor(x, y)
%   Returns the xi-correlation with the corresponding p-value for the pair
%   of variables x and y.
%
%   Input arguments:
%
%   'x'              Independent variable. Numeric 1D array.
%
%   'y'              Dependent variable. Numeric 1D array.
%
%   Name-value arguments:
%
%   'symmetric'      If true xi is computed as (r(x,y)+r(y,x))/2.
%                    Default: false.
%
%   'p_val_method'   Method to be used to compute the p-value.
%                    Options: 'theoretical' or 'permutation'.
%                    Default: 'theoretical'.
%
%   'n_perm'         Number of permutations when p_val_method is
%                    'permutation'.
%                    Default: 1000.
%   Output arguments:
%
%   'xi'             Computed xi-correlation.
%
%   'p'              Estimated p-value.
%
%   Notes
%   -----
%   This is an independent implementation of the method largely based on
%   the R-package developed by the original authors [3].
%   The xi-correlation is not symmetric by default.
%   Check [2] for a potential improvement over the current implementation.
%
%   References
%   ----------
%   [1]  Sourav Chatterjee, A New Coefficient of Correlation, Journal of
%   the American Statistical Association, 116:536, 2009-2022, 2021.
%   DOI: 10.1080/01621459.2020.1758115
%
%   [2] Zhexiao Lin* and Fang Han†, On boosting the power of Chatterjee's
%   rank correlation, arXiv, 2021. https://arxiv.org/abs/2108.06828
%
%   [3] XICOR R package.
%   https://cran.r-project.org/web/packages/XICOR/index.html
%
```

```
%   Example
%   ---------
%   % Compute the xi-correlation between two variables
%
%     x = linspace(-10,10,50);
%     y = x.^2 + randn(1,50);
%     [xi, p] = xicor(x,y);
%
%   David Romero-Bascones, dromero@mondragon.edu
%   Biomedical Engineering Department, Mondragon Unibertsitatea, 2022
if nargin == 1
    error('err1:MoreInputsRequired', 'xicor requires at least 2 inputs.');
end
parser = inputParser;
addRequired(parser, 'x');
addRequired(parser, 'y');
addOptional(parser, 'symmetric', false)
addOptional(parser, 'p_val_method', 'theoretical')
addOptional(parser, 'n_perm', 1000)
parse(parser,x,y,varargin{:})
x = parser.Results.x;
y = parser.Results.y;
symmetric = parser.Results.symmetric;
p_val_method = parser.Results.p_val_method;
n_perm = parser.Results.n_perm;
if ~isnumeric(x) || ~isnumeric(y)
    error('err2:TypeError', 'x and y are must be numeric.');
end
n = length(x);
if n ~= length(y)
    error('err3:IncorrectLength', 'x and y must have the same length.');
end
if ~islogical(symmetric)
    error('err2:TypeError', 'symmetric must be true or false.');
end
% Check for NaN values
is_nan = isnan(x) | isnan(y);
if sum(is_nan) == n
    warning('No points remaining after excluding NaN.');
    xi = nan;
    return
elseif sum(is_nan) > 0
    warning('NaN values encountered.');
    x = x(~is_nan);
    y = y(~is_nan);
    n = length(x);
end
if n < 10
    warning(['Running xicor with only ', num2str(n),...
             ' points. This might produce unstable results.']);
end
[xi, r, l] = compute_xi(x, y);
if symmetric
```

```
    xi = (xi + compute_xi(y, x))/2;
end
% If only one output return xi
if nargout <= 1
    return
end
if ~strcmp(p_val_method, 'permutation') && symmetric==true
    error('err2:TypeError', ...
          'p_val_method when symmetric==true must be permutation.');
end
% Compute p-values (only valid for large n)
switch p_val_method
    case 'theoretical'
        if length(unique(y)) == n
            p = 1 - normcdf(sqrt(n)*xi, 0, sqrt(2/5));
        else
            u = sort(r);
            v = cumsum(u);
            i = 1:n;

            a = 1/n^4 * sum((2*n -2*i +1) .* u.^2);
            b = 1/n^5 * sum((v + (n - i) .* u).^2);
            c = 1/n^3 * sum((2*n -2*i +1) .* u);
            d = 1/n^3 * sum(l .* (n - l));

            tau = sqrt((a - 2*b + c^2)/d^2);

            p = 1 - normcdf(sqrt(n)*xi, 0, tau);
        end
    case 'permutation'
        xi_perm = nan(1, n_perm);

        if symmetric
            for i_perm=1:n_perm
                x_perm = x(randperm(n));
                xi_perm(i_perm) = (compute_xi(x_perm, y) + ...
                                   compute_xi(y, x_perm))/2;
            end
        else
            for i_perm=1:n_perm
                xi_perm(i_perm) = compute_xi(x(randperm(n)), y);
            end
        end

        p = sum(xi_perm > xi)/n_perm;
    otherwise
        error("Wrong p_value_method. Use 'theoretical' or 'permutation'");
end

function [xi, r, l] = compute_xi(x,y)
n = length(x);
% Reorder based on x
[~, si] = sort(x, 'ascend');
```

```
y = y(si);
% Compute y ranks
[~, si] = sort(y, 'ascend');
r = 1:n;
r(si) = r;
% If no Y ties compute it directly
if length(unique(y)) == n
    xi = 1 - 3*sum(abs(diff(r)))/(n^2 - 1);
    r = nan;
    l = nan;
else
    % Get r (yj<=yi) and l (yj>=yi)
    l = n - r + 1;

    y_unique = unique(y);
    idx_tie = find(groupcounts(y)>1);

    for i=1:length(idx_tie)
        tie_mask = (y == y_unique(idx_tie));
        r(tie_mask) = max(r(tie_mask))*ones(1,sum(tie_mask));
        l(tie_mask) = max(l(tie_mask))*ones(1,sum(tie_mask));
    end

    % Compute correlation
    xi = 1 - n*sum(abs(diff(r)))/(2*sum((n - l) .* l));
end
```

This code is written by David Romero (2024) who is a MATLAB user.